NUCLEAR WASTE MANAGEMENT ORGANIZATION
SOCIÉTÉ DE GESTION DES DÉCHETS NUCLÉAIRES

Phase 2 Geoscientific Preliminary Assessment

Geological Mapping

TOWN OF BLIND RIVER, CITY OF ELLIOT LAKE AND AREA, ONTARIO

APM-REP-01332-0219

NOVEMBER 2017

For more information, please contact:
Nuclear Waste Management Organization
22 St. Clair Avenue East, Sixth Floor
Toronto, Ontario M4T 2S3 Canada
Tel 416.934.9814
Toll Free 1.866.249.6966
Email contactus@nwmo.ca
www.nwmo.ca

November 2017

PHASE 2 GEOSCIENTIFIC PRELIMINARY ASSESSMENT

GEOLOGICAL MAPPING, BLIND RIVER, ELLIOT LAKE AND AREA, ONTARIO

Submitted to:
Nuclear Waste Management Organization
22 St. Clair Ave. East, 6th Floor
Toronto, Ontario
M4T 2S3

NWMO Report: APM-REP-01332-0219

REPORT

Report Number: 1651985 (3000)

Distribution:

PDF copy - NWMO
PDF copy - Golder Associates
PDF copy - Paterson, Grant and Watson

Golder Associates

Executive Summary

This technical report documents the results of the Phase 2 Geological Mapping activity completed in 2017 as part of the Phase 2 Geoscientific Preliminary Assessment, to further assess the suitability of the Elliot Lake and Blind River area to safely host a deep geological repository. This study followed the successful completion of the Phase 1 Geoscientific Desktop Preliminary Assessment (Golder, 2014), which identified three withdrawal areas for further field studies. Geological mapping was completed within and around one of these withdrawal areas.

The purpose of the Phase 2 Geological Mapping is to advance understanding of the bedrock geology of the withdrawal area, with an emphasis on observation and analysis of bedrock structure and lithology. Information collected during Phase 2 Geological Mapping also helps to identify areas of exposed bedrock, assess overburden thickness, and identify surface constraints within and around the withdrawal areas, which might affect suitability.

Observations were made at a total of 271 select locations that were accessed using existing secondary roads, trail networks and waterbodies, as well as some off-trail hiking. The area was mapped over a total period of 32 days by two mapping teams, using a consistent workflow and standardized digital data collection system.

A digital data collection protocol was applied and observations were compiled into a GIS-compatible database. This includes information on bedrock character (lithology, magnetic susceptibility, gamma ray spectrometry, structure, and rock strength), fracture character, bedrock exposure and surface constraints. This report details the field observation for the mapped withdrawal area.

Table of Contents

TABLES

FIGURES (in order following the text)

APPENDICES

1.0 INTRODUCTION

This technical report presents the results of Phase 2 Geological Mapping conducted in the Elliot Lake and Blind River area during the spring and summer of 2017 as part of the Phase 2 Geoscientific Preliminary Assessment. The purpose of this work was to further assess the suitability of the Blind River and Elliot Lake area (Figure 1.1) to safely host a deep geological repository as part of NWMO's Adaptive Phased Management (APM) Site Selection process. Phase 2 Geological Mapping builds on the results of the Initial Screening (Geofirma, 2012), and the Phase 1 Geoscientific Desktop Preliminary Assessment (Golder, 2014) completed for the Communities of Blind River, Elliot Lake, The North Shore and Spanish.

The Phase 1 Geoscientific Desktop Preliminary Assessment (Golder, 2014) identified a number of large potentially suitable withdrawal areas warranting further assessment such as high-resolution geophysical surveys and geological mapping. Subsequent high-resolution geophysical surveys and interpretation were completed for one of the withdrawal areas, shown in Figure 1.1, and included airborne magnetic and gravity geophysical surveys (SGL, 2017), followed by a detailed lineament interpretation (SRK, 2017). Geological mapping was completed within and around the same withdrawal area.

The objective of Phase 2 Geological Mapping was to advance understanding of the bedrock geology of the withdrawal area (Figure 1.2), with an emphasis on observation and analysis of the structural geological and lithological framework. Information collected during Phase 2 Geological Mapping also helped identify areas of exposed bedrock, assess overburden thickness, and identify surface constraints affecting accessibility within the mapped withdrawal area.

The Phase 2 Geological Mapping activity was completed by Golder Associates Ltd. (Golder) and Paterson, Grant and Watson Ltd. (PGW). The observations were conducted at select locations using existing secondary roads, trail networks, overland traverses, and waterbodies.

1.1 Scope of Work

The Phase 2 Geological Mapping work was carried out in three stages as follows:

- Stage 1: Pre-mapping planning stage;
- Stage 2: Mapping stage; and
- Stage 3: Synthesis and reporting stage.

During the pre-mapping planning stage, a plan for the geological mapping was developed for the northeastern withdrawal area identified in the Phase 1 Geoscientific Desktop Preliminary Assessment (Golder, 2014) and further refined through discussion between the NWMO and the local communities. During the geological mapping activities, geological information was collected in accordance with the work plan defined during Stage 1 (See Section 4 Methodology and Appendix A) and during Stage 3 the information was analysed, compiled and is documented in this report.

The withdrawal area was investigated in the spring and summer of 2017 over a total period of 32 mapping days by two teams, each comprising two geologists and a local guide. Several GIS datasets were used as base maps for the Phase 2 geological mapping project, including predictive outcrop mapping generated by NWMO using

remote sensing data (See Appendix B), high-resolution satellite imagery and recently-acquired high-resolution geophysical data (SGL, 2017).

1.2 Qualifications of the Mapping Team

The project team was assembled and led by Golder and included subconsultants from Paterson, Grant & Watson Ltd. and several independent consultants with extensive field mapping and structural geology experience.

Golder Associates Ltd. was founded in Toronto in 1960 as a consulting firm specializing in geotechnical engineering. Since that time, Golder has expanded its range of technical services and grown to more than 7,000 employees in offices located throughout Africa, Asia, Australasia, Europe, North America and South America. Golder has a depth of experience and expertise supporting the nuclear industry including approvals and licensing, radioactive waste management, and investigations and engineering for deep geological repository studies in Canada, the United States, Sweden, Finland, France, Hungary, South Korea, Japan and the United Kingdom in addition to its work for the NWMO.

Paterson, Grant & Watson Limited was established in 1973 to provide geophysical consulting services to the mineral, petroleum and engineering sectors. PGW specializes in geophysical survey management, quality control, data processing, modelling and interpretation applied to both hard rock and sedimentary basin environments. PGW has worked extensively throughout the Canadian Shield on interpretation projects, mainly to explore for base metals, precious metals and diamonds. As a result, it is very familiar with the granite-greenstone terrains, and interpreting geophysical data for lithology and structure,

The investigations and compilation of the data presented in this report were completed by Mr. Tim Corkery, Dr. Iris Lenauer (PGW), Dr. Greg Stott, Mr. Adrian Kowalchuk (Golder), Mr. Matt Bowman (Golder), Mr. Andrey Fomenko (Golder) and Dr. Charles Mitz (Golder). The work was completed under the supervision of Mr. George Schneider (Golder). A brief description of the roles and qualifications of key professional staff is provided below.

Mr. Tim Corkery, M.Sc., P.Geo. (APGO #2586) is a Professional Geologist with over 40 years of diversified geological experience, providing geological mapping and mineral occurrence services. His work included extensive regional and detailed geological and structural mapping programs that resulted in publications of numerous reports and geological maps. Tim was employed for 38 years by the Manitoba Geological Survey and while there he provided management of multi-organizational (industry-university-Federal and Provincial Government surveys), multi-year regional studies. His projects focused on structural studies in the Archean of Manitoba. Tim led one of the two geological mapping teams for this project.

Mr. Adrian Kowalchuk, P.Geo. (APEGM 32609G) is a professional geoscientist with the Engineers Geoscientists Manitoba (EGM). Project experience has included geological field mapping, and diamond drilling programs in northern Manitoba and Saskatchewan as well as experience in the NWMO's APM project through previously completed mapping work in Ignace, Ontario. He was an active participant in the mapping as an engineering geologist.

Dr. Iris Lenauer, Ph.D., P.Geo. (APGO #2473), is a Consultant (Structural Geology) with over 8 years of experience specializing in regional mapping, structural analysis in various tectonic settings, and brittle fault analysis. She has recently completed a regional structural lineament interpretation of the Phoenix project in the Red Lake Greenstone Belt of the Superior Province, and an interpretation of fault network from aeromagnetic data from the Palmarejo project area in Mexico. Dr. Lenauer was an active participant on all phases of the NWMO's initial

(OGGF) and detailed mapping work for the community of Ignace and she was the lead author on the subsequent interpretation and reporting phase. Dr. Lenauer led one of the two mapping geological mapping teams for this project and she is a lead author of this report.

Dr. Charles Mitz, Ph.D., P.Geo. (APGO #0277), is a senior engineering geologist at Golder with expertise in fractured rock hydrogeology. He was the lead geologist for the Initial Screening and Phase 1 Geoscientific Assessments for Ignace, and several other communities that have participated in the APM site selection process. Dr. Mitz was an active participant in the NWMO's initial (OGGF) and detailed mapping work for the community of Ignace and he served as the Field Manager for the Geological Mapping in the Blind River and Elliot Lake area. He is a coauthor of this report.

Dr. Greg Stott, Ph.D., P.Geo. (APGO #0105) is a consulting geoscientist with more than 30 years of distinguished experience in the crystalline bedrock environment of northern Ontario. During his career with the OGS, Greg made significant advancements in the understanding of the tectonic evolution of the Superior Province, as well as making numerous important contributions to geochronology, economic geology and structural geology. Greg has been actively involved in a number of NWMO projects including Phase 1 Assessments of Hornepayne and Wawa, as well as providing technical review for Golder's Phase 1 Assessments of various communities in northern Ontario and Saskatchewan. Greg has also participated in the OGGF mapping and Detailed Mapping programs at NWMO's northwestern Ontario and North of Superior communities with the role of ensuring a consistent mapping approach is applied to the various communities. For this project, Greg provided oversight in the field to ensure a consistent approach was being applied by the three mapping teams.

Mr. George Schneider, M.Sc., P.Geo. (APGO #1239) is a Principal and senior geoscientist at Golder with over 25 years of experience in a wide range of geological, geophysical and hydrogeological projects, including nuclear repository site selection and characterization in Canada. He has managed a number of NWMO projects over the last several years for NWMO related to APM, including: reviews of geophysical methods for site characterization, the development of a generic approach to initial screenings for the APM site selection process, initial screenings for the APM site selection process, updates to the APM cost estimate and schedule, Phase 1 Geoscientific Desktop preliminary assessments for multiple communities in northern Ontario and Saskatchewan, and Phase 2 OGGF mapping projects in Ignace and Creighton. He is the Project Manager, responsible for senior oversight of the Blind River and Elliot Lake area geological mapping and review of this report.

1.3 Report Organization

A general description of the Blind River and Elliot Lake area, including its location, and physiography is provided in Chapter 2. Chapter 3 summarizes the regional and local geological setting for the Blind River and Elliot Lake area. The methodology employed to undertake the detailed mapping activity is provided in Chapter 4. Results are summarized in Chapter 5. A brief summary of the results is included in Chapter 6, followed by references cited in Chapter 7 and a set of figures. In addition, Appendix A provides supporting tables from the Work Plan and Appendix B describes the process that was used to undertake the remote predictive bedrock mapping exercise that was used during the planning and execution of the geological mapping.

2.0 LOCAL AREA DESCRIPTION

2.1 Location

The Blind River and Elliot Lake area is located within north-central Ontario in the highlands north of the North Channel of Lake Huron. The focus of the mapping activities described in this report (referred to herein as the "withdrawal area") is located in an area of granitic bedrock about 60 km to the north of the City of Elliot Lake and 100 km north-west of the City of Sudbury, Ontario. The withdrawal area measures approximately 16 km by 20 km in size, encompassing an area of about 320 km^2 (Figure 1.1).

2.2 Physiography

The withdrawal area in the Blind River and Elliot Lake area is covered by a discontinuous mantle of unconsolidated glacial deposits underlain by approximately 2.7 to 2.6 billion year old bedrock of the Superior Province of the Canadian Shield. The glacial deposits are generally thin and discontinuous and the topography in this area is largely bedrock-controlled with bedrock hills and ridges and structurally-controlled valleys contributing to the rugged topography and numerous lakes that characterize the area.

The land surface ranges in elevation from about 420 to 530 metres (m) above sea level, with this amount of relief being expressed over a lateral distance of about 15 km. While the present landscape predominantly reflects erosional processes associated with continental glaciation, its proximity to the contact between Archean-age granites and Proterozoic-age rocks of the Southern Province (about 30 km to the south) raises the possibility that some of the present topography represents the ancient Proterozoic topography exposed through recent glacial erosion. Glacial striae measured during the OGGF activity, with orientations of 189° to 191°, indicate glacial ice advance from the north.

The withdrawal area is drained predominantly by the Wakonassin River which flows southward to its confluence with the Spanish River some 40 km to the south. Another tributary of the Spanish River, the Mozhabong, drains a small area within the northeast part of the withdrawal area, while Rivière aux Sables drains a small portion in the southwest. Lands within the extreme northwest part of the withdrawal area drain westward to the upper Mississagi watershed. Major lakes within or bordering the withdrawal area include Lac aux Sables to the immediate southwest, and Mozhabong Lake, which borders the eastern limit of the Withdrawal area (Figure 1.1).

3.0 SUMMARY OF GEOLOGY

Details of the geology of the area were described in the Phase 1 Geoscientific Desktop Preliminary Assessment (Golder, 2014). The following sections provide brief descriptions of the geologic setting, bedrock geology, structural history and mapped structures, metamorphism and Quaternary geology of the area. The focus of the following sections are the bedrock units identified during Phase 1 as being potentially suitable to host a deep geological repository and the important structural features in the area.

3.1 Geological Setting

The area is located within the Archean Superior Province of the Canadian Shield. The Superior Province is a stable craton created from a collage of ancient plates and accreted juvenile arc terranes that were progressively amalgamated over a period of more than 2 Ga (e.g., Percival et al., 2006). The Superior Province covers an area

of approximately 1,500,000 km2 and is divided into subprovinces, including the Abitibi Subprovince within which the area is located.

The Abitibi Subprovince is bounded to the west by the Kapuskasing structural zone and Wawa Subprovince and to the north by the Opatica Subprovince. Its southern boundary is overlain by metasedimentary and metavolcanics rocks of the Huronian Supergroup of the Southern Province. The Abitibi Subprovince developed between ca. 2.8 and 2.6 Ga (Thurston, 1991) and comprises multiple units of volcanic and associated metasedimentary rocks (greenstone belts) separated by extensive granitic plutons and batholiths. These greenstone belts typically occur in elongate geometries and represent a significant percentage of the rocks in the northern portion of the subprovince, while occurring less so in the southern portion of the subprovince. The surrounding granitoid bodies are composed primarily of tonalite to granodiorite, and represent the vast majority of the rocks present throughout the area.

Six generations of Proterozoic diabase dyke swarms, ranging in age from ca. 2.473 Ga to 590 Ma intrude the bedrock units in the area (Krogh et al., 1987; Kamo et al., 1995; Buchan et al., 1996; Hamilton et al., 2002; Buchan and Ernst, 2004).

3.2 Bedrock Geology

The Abitibi Subprovince is composed of low metamorphic grade volcanic rocks and granitoid plutonic and gneiss-dominated rocks, the latter of which are predominant in the area and are represented by the Ramsey-Algoma granitoid complex (e.g., Jackson and Fyon, 1991).

The Ramsey-Algoma granitoid complex is a large heterogeneous group of granitoid bodies that intruded the older metavolcanic and subordinate metasedimentary rocks of the Whiskey Lake and Benny Lake greenstone belts. The vast majority of the area is underlain by the Ramsey-Algoma granitoid complex (shown in pink on Figure 1.2), which extends beyond the study area in all directions. Less extensive lithological unit of the area comprises a thin sliver of the westernmost portion of the Benny Lake greenstone belt (Figure 1.2).

Several generations of Proterozoic diabase dyke swarms, ranging in age from 2.473 Ga to 590 Ma, cut all bedrock units in the area. The most prominent of these dyke swarms include the northwest-trending Sudbury swarm, ca. 1.238 Ga (Krogh et al., 1987); the north-northwest-trending Matachewan swarm, ca. 2.473 Ga (Buchan and Ernst, 2004); and the north-trending Marathon dyke swarm, ca. 2.121 Ga (Buchan et al., 1996; Hamilton et al., 2002). Less numerous dykes belonging to the northeast-trending Biscotasing, ca. 2.167 Ga (Hamilton et al., 2002), west-northwest-trending North Channel, ca. 1.6 to 2.5 Ga (OGS, 2011), and east-northeast-trending Grenville, ca. 590 Ma (Kamo et al., 1995) dyke swarms also crosscut the area.

The main geological units of interest occurring in the area are further described below.

3.2.1 Ramsey-Algoma Granitoid Complex

The Ramsey-Algoma granitoid complex is a large complex of granitoid and gneissic rocks divided in three large domains: the Chapleau gneiss, Ramsey gneiss and Algoma plutonic domains (Jackson and Fyon, 1991). In the area, the granitoid complex is dominated by the Algoma plutonic domain. Although some portions of the Algoma plutonic domain have been mapped in detail (e.g., Robertson, 1965a,b,c; Robertson and Johnson, 1965; Giblin, 1976; Giblin et al.,1977), the Algoma plutonic domain remains poorly studied. The Ramsey-Algoma granitoid complex is generally described in the literature as consisting largely of a massive to foliated granite-granodiorite suite intruding a tonalite-granodiorite suite. In addition, several narrow slivers of metavolcanic rock are commonly

mapped within the gneissic tonalite portion of the Ramsey-Algoma granitoid complex. In the study area, however, these rocks are observed within the massive granodiorite to granite suite.

The Algoma plutonic domain consists of granitic and granodioritic rocks and granitic gneisses with numerous greenstone enclaves and massive to foliated granite, granodiorite, and syenite intrusions (Card, 1979). In the area of Rawhide Lake, approximately 15 km north of Elliot Lake, the Algoma plutonic domain consists generally of uniform, massive, medium to coarse-grained, equigranular granite (Ford, 1993). Approximately 45 km northwest of Elliot Lake, in the area of Kirkpatrick Lake, the plutonic complex is reported to be predominantly composed of massive to foliated biotite-bearing to hornblende-bearing granitic rock. Minor, more leucocratic phases are typically quartz monzonite to granodiorite and trondhjemite. In the Wakomata Lake area, approximately 30 km northwest of Blind River, outcrops of pink to grey, equigranular, fine- to coarse-grained trondhjemite, quartz monzonite and granodiorite have been reported, of which grey, medium- to coarse-grained, leucocratic trondhjemite predominates (Siemiatkowska, 1977). Sage (1988) described granitic rock in the Seabrook Lake area (65 km northwest of Blind River) as massive, medium- to coarse-grained, red to red-brown, leucocratic, granodiorite to quartz monzonite. In the area of East Bull Lake (25 km east-northeast of Blind River), Easton et al. (2004) reported mixtures of strongly foliated granitic gneiss and migmatitic facies enclosing mafic gneiss, whereas McCrank et al. (1989) described that area as comprising weakly to moderately foliated granodiorite and porphyritic granite. Lastly, Gordon (2012) noted massive, homogeneous syenogranite as the main plutonic phase in Otter Township, west of the study area.

Geochronology for the Algoma plutonic domain includes an age of ca. 2.716 Ga (billion years) in the Batchawana area, approximately 60 km west of Blind River and Elliot Lake (Corfu and Grunsky, 1987), and ca. 2.662 Ga for the area south of Ramsey, about 50 km north of the area (van Breemen et al., 2006). Heather et al. (1995) reported a preliminary age of ca. 2.727 Ga for biotite tonalite from immediately south of the Swayze greenstone belt approximately 60 km northeast of the area. More recently, Easton (2010) obtained preliminary dates of ca. 2.675 and 2.651 Ga for two samples of granite and granodiorite near Elliot Lake. The wide range of dates suggests that the Ramsey-Algoma granitoid complex contains distinct plutonic and gneissic lithologies emplaced over a period of 75 Ma (million years) and possibly longer. This interpretation is supported by van Breemen et al. (2006) who subdivided granitic rocks in the Swayze area, approximately 120 km north of Elliot Lake, into the following five broad categories:

- Synvolcanic diorite and hornblende tonalite intrusions ranging in age from ca. 2.740 to 2.696 Ga.
- A transitional suite of tonalite and quartz monzonite intrusions ranging from ca. 2.695 to 2.686 Ga.
- Syntectonic hornblende granodiorite intrusions ranging from ca. 2.685 to 2.686 Ga.
- A younger transitional suite of tonalite and quartz monzonite intrusions ranging from ca. 2.680 to 2.665 Ga.
- Non-foliated ca. 2.665 Ga post-tectonic granite intrusions occurring within areas of synvolcanic and syntectonic intrusions.

Although the Swayze area is located further north, it shares a similar tectonic setting to the northern part of the area. Van Breeman et al. (2006) may therefore offer an interpretative framework for the largely unmapped Ramsey-Algoma granitoid complex within the area. Heather et al. (1995) also described a large body of massive Algoma biotite granite in the area southwest of Ramsey, approximately 50 km north of the assessment area.

3.2.2 Benny Lake Greenstone Belt

The Benny Lake greenstone belt consists of Archean metavolcanic and metasedimentary rocks that form a 40 km long by 5 km wide east-striking greenstone belt extending from the Geneva Lake area to the Mink Lake area, some 70 km northeast of Elliot Lake. The greenstone belt extends only 4 km into the area (shown in green on Figure 1.2) to its mapped termination south of Mink Lake. Card and Innes (1981) described the central part of the greenstone belt as consisting of intercalated mafic flows and pyroclastic rocks with intermediate tuffs and tuff-breccia with some volcanogenic metasedimentary rocks including tuffaceous greywacke and siltstone, chert, and iron formation. The stratigraphic sequence in this part of the belt comprises cyclic repetitions of mafic, intermediate, and felsic metavolcanics, plus sulphide-bearing tuffs and tuffaceous metasedimentary rocks that commonly lie along contact zones between the metavolcanic units.

Felsic plutonic rocks are noted to surround and intrude the greenstone rocks. Card and Innes (1981) subdivided these rocks into an older gneissic, granodioritic complex that occurs mainly to the north of the greenstone belt and a younger, relatively massive, homogeneous quartz monzonite that forms most of the terrain to the south. Although there is no published information on the age of the Benny Lake greenstone belt, Easton (2010) noted that the ages obtained for the Whiskey Lake greenstone belt, located approximately 50 km to the southwest, were consistent with ca. 2.690- to 2.685 Ga volcanism in the southern part of the Abitibi Subprovince.

The greenstone sequence dips steeply to the south with a schistosity subparallel to the primary stratification. Movements on major northwest and north-northwest trending faults such as those along the Spanish River have resulted in progressive northward displacement of the Benny Lake greenstone belt from east to west (JDMA, 2014a).

3.2.3 Mafic Dykes

Six generations of Proterozoic diabase dyke swarms crosscut the area (Buchan and Ernst, 2004). The generations of dyke swarm include:

- North-northwest-trending Matachewan Suite dykes (ca. 2.473 Ga; Buchan and Ernst, 2004). This dyke swarm covers the largest area through the Canadian Shield and is predominant in the area. Individual dykes are generally up to 10 metres wide, and have vertical to subvertical dips. The Matachewan dykes comprise mainly quartz diabase dominated by plagioclase, augite and quartz (Osmani, 1991).
- Northeast-trending Biscotasing Suite dykes (ca. 2.167 Ga; Hamilton et al., 2002). The dykes form prominent northeast trending regional features, with individual dykes typically 50 to 100 metres in width. The Biscotasing dykes are quartz tholeiitic features with fine-grained chilled margins and medium- to coarse-grained interiors (Buchan et al., 1993; Halls et al., 2008), dominated by plagioclase, pyroxene and quartz with minor magnetite-ilmenite intergrowths These dykes are rare in the area.
- North-trending Marathon Suite dykes (ca. 2.121 Ga; Buchan et al., 1996; Hamilton et al., 2002). These form a fan-shaped distribution pattern around the northern, eastern, and western flanks of Lake Superior, and are relatively uncommon in the area. The dykes vary in orientation from northwest to northeast, and occur as steep to subvertical sheets, typically a few metres to tens of metres thick, but occasionally up to 75 metres thick (Hamilton et al., 2002). The Marathon dykes comprise quartz diabase (Osmani, 1991) dominated by equigranular to subophitic clinopyroxene and plagioclase.

- West-northwest-trending North Channel dykes (ca. 1.6 to 2.5 Ga; OGS, 2011). This dyke swarm may be temporally associated with the ca. 1.884 Ga Molson dyke swarm in Manitoba, and the Wabigoon dyke swarm in northwestern Ontario (OGS, 1997; Buchan and Ernst, 2004). These dykes are rare to absent in the area.
- Northwest–trending Sudbury Suite dykes (ca. 1.238 Ga; Krogh et al., 1987). Individual dykes are generally less than 10 metres wide, and appear to have intruded into older northwest-trending faults (Easton, 2009). Sudbury dykes typically range in composition from olivine diabase, amphibole diabase, diabase, magnetite-bearing diabase to lamprophyre.
- East-northeast-trending Grenville dykes (ca. 590 Ma; Kamo et al., 1995). Within the Superior Province these dykes are parallel to the Ottawa graben, and individual dykes are generally less than 15 metres in width. These dykes are rare to absent in the area.

Within an aeromagnetic data set, the dyke swarms in the area are generally distinguishable by their unique strike directions, cross-cutting relationships and, to a lesser extent, by the amplitude of the associated magnetic anomalies.

3.3 Structural History

The structural history of the area is complex. Investigations within the study area and its vicinity conclude that the region has undergone complicated polyphase deformation (e.g., Card et al., 1972; Young, 1983; Riller et al., 1999; Jackson, 2001; Easton, 2005). The most comprehensive studies on the structural geology of the area and its vicinity have been carried out by Zolnai et al. (1984), Riller et al. (1999) and Jackson (2001). These and other investigations documenting the structural geology of particular portions of the area (e.g. Easton, 2005) support the presence of up to three main deformation orogenic phases which have overprinted all bedrock lithologies, and have been assigned to the Blezardian, Penokean, and Grenville orogenies. It should be noted, however, that the occurrence of the Penokean Orogeny in the area remains controversial (e.g. Davidson et al., 1992; Piercey et al. 2003), and evidence for the Grenville Orogeny is scarce. As the aforementioned studies were performed at various scales and from various perspectives, the following summary of the structural history of the area should be considered as a best-fit model that incorporates relevant findings from all studies. The structural history of the area is described below and summarized in Table 3.3.

It is understood that there are potential problems in applying a regional deformation numbering (Dx) system into a local geological history. Nonetheless, the following summary offers an initial interpretation for the area, which may be modified in the future if site-specific information is collected.

The earliest deformation phase (D1) is associated with ca. 2.72- to 2.7 Ga penetrative deformation of rocks of the Whiskey Lake and Benny Lake greenstone belts. According to Jensen (1994), this penetrative deformation is represented by foliation closely paralleling the strike and dip of the metavolcanic and metasedimentary strata composing the greenstone belts. The foliation was likely developed concurrent with folding which is expressed by a west-northwest-trending, isoclinal syncline. Easton (2010) reported the existence of an east-trending shear zone apparently overprinting only the greenstone rocks. Later truncation of the foliation by plutonic material indicates that much of this deformation occurred prior to at least the youngest phase of emplacement of the ca. 2.716 to 2.651 Ga Ramsey-Algoma granitoid complex (Jensen, 1994).

Table 3.3: Geological and Structural History of the Blind River and Elliot Lake area

Approximate Time Period (years before present)	Geological Event
2.72 to 2.651 Ga	Kenoran Orogeny Emplacement and deformation of the ca. 2.72- to 2.68-billion-year old Whiskey Lake and Benny Lake greenstone belts and ca. 2.716- to 2.651-billion-year old Ramsey-Algoma granitoid complex. Development of folds and east-trending foliation in the greenstone belts (ca. 2.72 to 2.70 billion years ago). [D_1]
<2.651 to 2.50 Ga	Early (re)activation of NE-, ENE-, WNW- and NW-striking faults (e.g., Murray and Flack Lake faults) [D_2]
2.497 to 2.47 Ga	Onset of continental break-up [D_3]; rifting across Lake Superior. Deposition of volcanic rocks and basal sedimentary rocks of the Huronian Supergroup. Reactivation, or continued activity, of WNW- to NW- and E-striking faults. Widespread mafic magmatism, and emplacement of: Agnew Lake intrusion and East Bull Lake intrusion 2.49 to 2.47 billion years; ca. 2.473-billion-year old Matachewan dyke swarm.
2.47 to > 2.30 Ga	Blezardian Orogeny [D_4] Thick-skinned folding of Archean basement and basal rocks of the Huronian Supergroup. Initiation of Quirke Lake syncline and Chiblow anticline.
<2.3 and > 2.10 Ga	Transition of passive margin setting Continued deposition of sedimentary rocks of Huronian Supergroup. Emplacement of ca. 2.2- to 2.1-billion-year old Nipissing diabase intrusions and ca. 2.17- to 2.15-billion-year old Biscotasing dyke swarm.
2.10 to 1.89 Ga	Denudation of bedrock and formation of peneplain.
1.89 to 1.84 Ga	Penokean Orogeny [D_5] Crustal shortening and development of thrust-and-fold belt in rocks of the Huronian Supergroup, buckling and faulting of Archean basement. Subgreenschist and amphibolite grade metamorphic overprint to north and south of Murray fault, respectively. Emplacement of the Sudbury Igneous Complex ca. 1.85 billion years ago.
1.75 to 1.70 Ga	Emplacement of ca. 1.70-billion-year old Cutler pluton and metamorphic overprint south of Murray fault. Ca. 1.75 to 1.70 billion years ago, a metasomatic event of the Huronian Supergroup (Fedo et al., 1997).
1.238 to 1.235 Ga	Emplacement ago of Sudbury dyke swarm and related intrusions of unclassified olivine diabase dykes.
1.25 to 0.98 Ga	Grenville Orogeny Develop of Midcontinental Rift (ca. 1.1 billion years ago) [D_6]
<1.1 to present	ca. 1.1 to 0.54 billion years ago: denudation of bedrock, formation of peneplain (continuation of D_6). Post-0.54 billion years ago: sedimentation, erosion, ingression and regression of sea water, shallow sea, glaciations. Exhumation of peneplain.

Subsequent to emplacement of the Ramsey-Algoma granitoid complex, D2 deformation formed a series of northeast-striking sinistral strike-slip faults and shear zones, and later subvertical east-northeast-striking sinistral-oblique faults and shear zones that were formed along the margins of the greenstone belts. At least two regionally extensive east- to northeast-trending faults (the Murray and Flack Lake faults) may have initiated during D2. The Flack Lake Fault transects the southern portion of the assessment area, while the Murray Fault occurs approximately 60 km south of the assessment area along the north shore of Lake Huron and continues northeast to transect the Sudbury Igneous complex. The Flack Lake Fault has been variously interpreted as a Neoarchean thrust fault or listric-normal fault that was inverted during the Neoarchean and reactivated during the Blezardian (D4) and Penokean (D5) orogenies (Jensen, 1994 and Jackson, 2001); or as a listric normal fault that initiated in relation to rifting of the Archean continental margin during the early Proterozoic (Zolnai et al. 1984; Spray et al., 2004). Jensen (1994) suggests that south of the study area in the Whiskey Lake greenstone belt, two episodes of Archean faulting produced northeast-trending, arcuate sinistral faults and subsequent east-northeast-trending, subvertical sinistral faults.

Jolly (1978) and Zolnai et al. (1984) suggest that subsequent to D2, Archean faulting was followed by a large-scale rifting event (D3) that overprinted the area in association with the ca. 2.497- to 2.47 Ga break-up of the Superior Craton (Williams et al., 1991). This was associated with the development of east-trending rifts and overlapped in time with the earliest Proterozoic deposition of the basal volcano-sedimentary rocks of the Huronian Supergroup (Jensen, 1994); the widespread emplacement of mafic intrusions such as the Agnew Lake and East Bull Lake intrusions (Vogel et al., 1998; Easton, 2009) southeast of the study area; and emplacement of the pervasive Matachewan dyke swarm. D3 was associated with reactivation of regional D2 faults, including the Murray and Flack Lake faults, as down-to-the-south synsedimentary growth faults during the formation of the Huronian Supergroup (Zolnai et al., 1984). This event was accompanied by the initiation, or dextral reactivation, of east-southeast- to southeast-striking faults that cross-cut earlier formed structures throughout the Huronian Supergroup (Jackson, 2001). These younger faults also cut the Archean basement and the Murray fault (Jackson, 2001). Jensen (1994) indicates that the southeast-trending faults are intruded by undeformed feldspar porphyry dykes, presumably associated with the Matachewan and Sudbury dyke swarms. While typically assumed to be the youngest generation of faulting, Jensen (1994) and Jackson (2001) concede that some of the southeast-trending faults may have initiated as Late Archean (D2) structures that subsequently experienced a long history of reactivation during and post-dating the D5 Penokean Orogeny.

The Blezardian Orogeny is assigned as the fourth deformation event, D4, in the area. The Blezardian Orogeny produced steeply south-dipping reverse faults and upright, kilometre-scale folds (Zolnai et al., 1984). The timing of the Blezardian Orogeny is poorly constrained. It is thought to have occurred between ca. 2.4 Ga (possibly as early as 2.47 Ga), and 2.3 Ga (Riller et al., 1999; Raharimahefa et al., 2011).

The ca. 1.89 to 1.84 Ga Penokean Orogeny (D5) involved dextral shearing and horizontal shortening (Riller et al., 1999) in the area. Crustal shortening and fault reactivation enhanced the previously buckled (Blezardian) structure of the Archean basement and further compressed, folded and faulted rocks of the Huronian Supergroup, so that overlapping thrusted blocks stacked up to possibly 15 km in burial thickness (Zolnai et al., 1984). South of the assessment area, and south of the Murray Fault, medium to high grade metamorphic assemblages developed within Huronian Supergroup rocks, and penetrative, ductile deformation features developed that included cleavage, stretching lineation, and rotation of the tectonic fabric to a near-vertical orientation (Zolnai et al., 1984). Ductile deformation features associated with D5 are not observed in the assessment area. Northwest-trending strike-slip faults such as the Spanish River fault, Pecors Lake and Horne Lake faults that cut the Huronian

Supergroup sequence and the parallel Nook Lake fault within the Archean basement directly north of the Quirke Lake syncline (Robertson, 1968), may have been formed during the Penokean Orogeny, or they may be reactivated Archean faults as suggested by Jackson (2001). The effect that the syn-Penokean meteorite impact, which produced the Sudbury Igneous Complex, had on the geological and structural evolution of the area is unclear.

Deformation associated with the Grenville Orogeny (D6), ca. 1.250 to 0.98 Ga, is considered the final major deformation episode. In spite of the scarcity of evidence and problems of deformation overprinting and fault reactivation, it seems that the Murray fault remained active or was reactivated during this orogeny (Robertson, 1970; Card, 1978; McCrank et al., 1989; Piercey, 2006). The Midcontinent Rift (ca. 1.1 to 1.0 Ga) was developed contemporaneously with the long-lived Grenville Orogeny and is also included as part of D6, although its effect on the area is not known. There are poor constraints on any subsequent fault reactivation in the area.

3.3.1 Mapped Structures

In the area, the regional scale arcuate east-trending Flack Lake fault extends for approximately 70 km and transects the Ramsey-Algoma granitoid complex in the southern portion of the study area. The Flack Lake fault is interpreted as a north-directed listric thrust that reactivated an earlier normal fault. Its movement history may be related to the Penokean event (Bennett et al., 1991).

3.4 Metamorphism

Studies on metamorphism in Precambrian rocks across the Canadian Shield have been summarized in a few publications since the 1970s (e.g., Fraser and Heywood,1978; Kraus and Menard, 1997; Menard and Gordon, 1997; Berman et al., 2000; Easton, 2000a; 2000b; Holm et al., 2001, and Berman et al., 2005) and the thermochronological record for large parts of the Canadian Shield is documented in a number of studies (Berman et al., 2005; Bleeker and Hall, 2007; Corrigan et al., 2007; and Pease et al., 2008).

The Superior Province of the Canadian Shield largely preserves low-pressure–high-temperature Neoarchean (ca. 2.710-2.640 Ga) metamorphic rocks. The relative timing and grade of regional metamorphism in the Superior Province corresponds to the lithological composition of the subprovinces (Easton, 2000a; Percival et al., 2006). Subprovinces comprising volcano-sedimentary assemblages and synvolcanic to syntectonic plutons (i.e., granite-greenstone terranes) are affected by lower greenschist to amphibolite facies metamorphism. Subprovinces comprising both metasedimentary- and migmatite-dominated lithologies, such as English River and Quetico, and dominantly plutonic and orthogneissic domains, such as Winnipeg River, are affected by middle amphibolite to granulite facies metamorphism (Breaks and Bond, 1993; Corfu et al., 1995). Subgreenschist facies metamorphism in the Superior Province is restricted to limited areas, notably within the central Abitibi greenstone belt (e.g., Jolly, 1978; Powell et al., 1993).

In general, most of the Canadian Shield preserves a complex episodic history of Neoarchean metamorphism overprinted by Paleoproterozoic tectonothermal events culminating at the end of the Grenville orogeny ca. 950 Ma. The distribution of contrasting metamorphic domains in the Canadian Shield is a consequence of relative uplift, block rotation, and erosion resulting from Neoarchean orogenesis, subsequent local Proterozoic orogenic events and broader epeirogeny during later Proterozoic and Phanerozoic eons.

Metamorphic grade in the area is largely of subgreenschist facies north of the Murray Fault, east and north of Blind River. South of the Murray Fault (Piercey, 2006), metamorphism increases to localized lower amphibolite facies

extending eastward between Blind River, Sudbury and the Grenville Front (Riller et al., 1999). Most authors (e.g., Zolnai et al., 1984) have considered the medium grade metamorphism reached south of the Murray fault to be a product of tectonothermal burial. However, Jackson (2001) pointed out that the high temperature-low pressure metamorphism reached could not be solely the result of burial, and he advanced the alternative of a second period of crustal extension in the area. This hypothesis would not only account for the required heat for medium grade metamorphism but would also explain the emplacement of Nipissing intrusions south of the area. Holm et al. (2001) suggested that peak Penokean Orogeny metamorphism occurred ca. 1.835 Ga, based on monazite ages. More recently, Piercey (2006) showed that the Penokean Orogeny was only the first of several accretionary events that impinged on the southern Laurentide margin and presented evidence of a younger and more significant metamorphic event, possibly related to the Yavapai tectonothermal pulse at ca. 1.7 Ga. This event may have affected the metamorphic conditions in the area and possibly increased the metamorphic overprint to greenschist facies, at least in the area proximal to the Cutler pluton on the north side of the Murray fault. Fedo et al. (1997) indicated that a ca. 1.7 to 1.75 Ga metasomatic event is evident in potassic and sodic alterations of the Huronian Supergroup north of the Murray Fault. This event likely replaces most metamorphic minerals in the Huronian Supergroup with white mica and is presumably related to fluid-flow driven by post-orogenic uplift of the Penokean Orogeny. Minor contact metamorphism exists in the metavolcanic rocks of the greenstone belt near some of the large Proterozoic mafic intrusions (Rogers, 1992).

3.5 Quaternary Geology

Quaternary geology of the area is described in detail in the terrain evaluation completed as part of the Phase 1 Desktop Preliminary Assessment (JDMA, 2014b).

The Quaternary geology of the area is dominated at surface by different types of glacial deposits that accumulated with the progressive retreat of the ice sheet during the end of the Wisconsinan glaciation. This period of glaciation began approximately 115,000 years ago and peaked approximately 21,000 years ago, at which time the glacial ice front extended south of Ontario into what is now Ohio and Indiana (Barnett, 1992).

The area is dominated by exposed bedrock or bedrock having only a thin cover of unconsolidated sediments. Quaternary deposits are predominantly located in bedrock controlled valleys. Overburden deposits within this area were mapped as part of the Northern Ontario Engineering Terrain Study (NOEGTS), a program undertaken between 1977 and 1981 (Gartner, 1978a,b,c; 1980 a,b; Roed and Hallet, 1979a,b,c,d; 1980a,b; VanDine, 1979a,b,c,d; 1980a,b,c,d; Gartner et al., 1981). These studies divided the landscape into a set of distinct terrain units within which the engineering characteristics are broadly predictable.

Data on ice flow direction compiled from the literature (Karrow, 1987) reveal that glacial ice flowed in a generally southwesterly direction across the area from the Hudson Bay basin. Ford (1993) recognized two dominant orientations in glacial striations, lunate fractures, drumlinoid features, and till flutings in the Rawhide Lake area to the north of the City of Elliot Lake. These are recorded as 175° (165° to 180°) and 195° (190° to 210°). At three sites, older 100° to 120° striations were found intersecting either the 175° or 195° sets.

The most widely occurring and oldest known stratigraphic unit in the area is a silty sand to sandy silt till found overlying bedrock in low relief areas and along the flanks of topographic lows. It is typically thin and discontinuous and is coarse-textured, unsorted, and boulder-rich, although there are some areas of compact, massive to fissile and gravelly to silty and sandy till (Barnett et al., 1991). Glaciolacustrine sediments have more limited distribution and are limited to only very small mappable surficial units (Ford, 1993) largely along river valleys. These units are

typically composed of laminated silt and fine sand and silt-clay rhythmites, and may be related to the series of postglacial lakes of the Lake Huron basin.

Deposits of glaciofluvial outwash are commonly encountered along valleys in the area. Glaciofluvial outwash is common in low-lying areas and occasionally in esker ridges with the local formation of terraces related to changing lake levels in the Lake Huron basin. Thick deposits of alluvial sand and gravel are found along many of the rivers in the region. Recent swamp, lake, and stream deposits are also common throughout the area (JDMA, 2014b). A more detailed accounting of glacial deposits in the area is provided by JDMA (2014b).

4.0 METHODOLOGY

As part of the overall methodology employed in the Phase 2 Geological Mapping for the Blind River and Elliot Lake area, a Work Plan (Golder, 2017a), Project Quality Plan (Golder, 2017b) and Health, Safety and Environment Plan (Golder 2017c) were developed at the pre-mapping planning stage of the project. Key technical aspects of the methodology included the planning, implementation, and reporting of the Phase 2 Geological Mapping work are described below:

4.1 Pre-Mapping Planning

The pre-mapping planning stage of the Phase 2 Geological Mapping was completed prior to mobilizing to the Blind River and Elliot Lake area. This stage included the development of a list of available source data (Appendix A, Table A.1) and equipment requirements (Appendix A, Table A.2), for planning and implementing the various components of the geological mapping. This stage also included the development of a summary list of daily field tasks allocated to each mapping team member (Appendix A, Table A.3).

The key geological attributes to be investigated, along with the methods identified to observe and capture the relevant information at each bedrock outcrop location, are presented in Table A.4 in Appendix A. Data collection in the field was carried out using the GanFeld system which was loaded onto Trimble ruggedized tablet computers. The GanFeld system is an Ontario Geological Survey (OGS) standard system for data collection which was originally provided in an open file format by the Geological Survey of Canada (Shimamura et al., 2008). Entry of geological information into the Collector-GanFeld database follows a simple data collection protocol (Appendix A, Table A.4), which directs the observer to the appropriate digital form within the database system to capture the appropriate information for each geological characteristic being investigated. Additional guidance relevant for geomechanical characterization based on a simple field-based test of rock hardness, is provided in Table A.5 in Appendix A.

4.1.1 Predicted Outcrop Filtering and Defining Daily Traverses

The results from a remote predictive bedrock mapping exercise, provided by the NWMO, show the distribution of predicted bedrock outcrop locations within and around the withdrawal area (Figure 1.2). The process that was used to undertake the remote predictive bedrock mapping exercise is described below in Appendix B. These predicted outcrops serve as input for the task of defining traverses for the Phase 2 Geological Mapping, as they represent potential targets for direct investigation of exposed bedrock. The spatial distribution of predicted outcrop locations in relation to their distance to the existing road and trail network, and to the key geological features to be investigated was assessed.

The predicted outcrops were individually assessed for areal coverage and for their proximity to key geological features, including interpreted lineaments, interpreted geophysical anomalies and mapped geological bedrock units and their contacts. Outcrops that were coincident with, or near to, key geological features, and in close enough proximity that they could reasonably be examined during one day of mapping, were grouped together to form daily traverses.

This assessment defined the daily traverses for the geological mapping. Practical knowledge of any accessibility constraints was assessed on a daily basis during the mapping, to refine the geological mapping traverse plan. Daily traverses were assessed and adjusted to accommodate several considerations, including method(s) of access, weather and overall progress of the mapping.

4.2 Mapping Stage

The Phase 2 Geological Mapping activity followed the plan in a manner that met the technical requirements identified in the Pre-observation Planning stage. At each outcrop location in the traverse areas, the geological attributes identified in Table A.4 (Appendix A) were investigated according to the allocation of the applicable tasks listed in Table A.3 (Appendix A).

The mapping work was carried out in two campaigns: an initial campaign from June 4 to June 20th, 2017, and a second campaign from July 5 to July 19th, 2017. The initial campaign was focussed on achieving a broad spatial coverage over the withdrawal area with traverses selected primarily for areal coverage and for proximity to existing logging roads. The second campaign continued from the first but included areas with more challenging access constraints. Prior to mobilizing the teams to begin the mapping activity, a reconnaissance fly-over was done to assess the results from the remote predicted outcrop activity. In general, the outcrops observed during the fly-over corresponded well with the predicted outcrops.

An important additional aspect of the geological mapping was the non-technical workflow that was followed on a daily basis to allow the technical work to be done to meet the required objectives. This included morning safety briefings, equipment calibration checks, data quality assurance checks, and planning for the next mapping day (Appendix A, Table A.3). A telephone conference was held with NWMO every evening during the course of the mapping campaign in order to discuss all aspects of the on-going work.

This simple workflow was adhered to on a daily basis and allowed for communication between the mapping team and NWMO when field conditions resulted in changes to the proposed plans. The daily report documented the completion of the safety briefing, calibration check and data back-up (i.e. the reports served as HSE and QA records).

4.2.1 Proterozoic Mafic Dyke Scanline Fracture Mapping Exercise

Along with compiling observations on Proterozoic mafic dykes that were encountered on daily traverses, one well-exposed example of a Proterozoic mafic dyke was identified as a candidate for a scanline fracture mapping exercise. The emplacement of these Proterozoic mafic dykes, as outlined in Section 3, is understood to post-date the penetrative regional ductile deformation that is characteristic of the Superior Province. However, the relationship between dyke emplacement and the brittle deformation history of the Superior Province is less well constrained. The purpose of the scanline fracture mapping exercise is to assess both the nature and extent (if any) of the damage to the bedrock caused by dyke emplacement and the nature and extent of brittle deformation overprinting the dykes themselves. A summary of the method employed to complete the scanline fracture mapping exercise is described below.

When the suitable (i.e. well-exposed) target dyke is located, a scanline is laid out perpendicular to the strike of the dyke contact. One metre intervals were marked for reference along the strike direction, shifting the line to a parallel location where necessary (e.g. overburden cover). Observations of the type and distribution (spacing) of brittle deformation features (veins, faults, joints) were collected systematically within a 1 to 2 m wide swath parallel to the scanline line perpendicular to strike of dyke contact and extending as far as possible into the adjacent bedrock beyond the dyke contacts. Additional characteristics such as fracture infill, cross-cutting relationships and offsets were noted, if present. A sketch of the scanline was drawn, and photographs taken, to highlight key features (dyke contacts, prominent fractures, shifts in the scanline, overburden cover, etc.). Magnetic susceptibility readings were made at each 1 m interval, with five readings used to obtain an average for each measurement location. Host rock foliation on both sides of the dyke was also recorded, if present. The results from the scanline fracture mapping exercise are included in Section 5.4.2 of this report.

Note also that due to the magnetic properties of the dykes, compass readings were significantly affected when placed close to the ground surface. In order to achieve the most accurate measurements for joints within the dyke, measurements were made approximately 1.5 m above the ground, and measuring the dip with the clinometer.

4.3 Synthesis and Reporting Stage

Following the completion of the mapping stage, the team prepared this stand-alone report describing the results of the geological mapping activity, in alignment with the objective of increasing our conceptual understanding of the key geological attributes for the identified withdrawal area. This report includes the interpretation and analysis of the field observations in terms of an update on the new state of knowledge that the observations provide, specific to the potentially suitable areas. The table of contents for the report was specified by the NWMO and developed prior to the completion of the mapping stage of the geological mapping activity. This table of contents also provided guidance on the structure of a figure set, and appendices, to be included with this final report.

The reporting stage included a thorough quality assurance check of the field data and the preparation and delivery of electronic data in the form of shapefiles, digital photographs and scanned field notes in zipped folders. Shapefiles were delivered in accordance with the types of information entered into the GanFeld database. These deliverables, which align with the observed key geological attributes as described in Table A.4 (Appendix A), include:

- Station;
- Lithology;
- Structure;
- Linework;
- Samples;
- Magnetic Susceptibility;
- Gamma Ray Spectrometry; and
- Photographs.

The data delivery also included a summary calibration report that includes copies of all calibration reports provided by third-party equipment providers and summary of results from all calibration activities undertaken during the mapping activities.

Metadata accompanying each shapefile and zipped folder, along with the calibration report, was prepared according to metadata guidelines provided by the NWMO. A summary of the detailed mapping observations is presented in Section 5 of this report.

5.0 GEOLOGICAL MAPPING FINDINGS

This section summarizes the detailed field geological observations recorded in the Blind River and Elliot Lake area based on the work undertaken by Iris Lenauer and Timothy Corkery and assisted by Charles Mitz, Adrian Kowalchuk, Matthew Bowman, and Andrey Fomenko. The geological mapping activity included two mapping campaigns taking place from June 4 to 20, 2017, and from July 5 to 19, 2017. In total, this encompassed 32 days of field mapping in the Blind River and Elliot Lake area.

Geological field observations were made at a total of 271 locations within and in close proximity to the withdrawal area defined for geological mapping in the Blind River and Elliot Lake area. The results from the bedrock outcrop prediction exercise served as a guide to assessing locations to visit for detailed mapping (Figure 1.2). The predicted locations are marked with polygons on Figure 1.2 and the locations chosen to visit with coloured dots. The green dots mark those that were correctly predicted as outcrop and the red dots were those that turned out to be overburden.

Descriptions of both non-geological (e.g., accessibility) and geological observations are presented in the sections below. A summary of detailed observations relating to bedrock exposure and overburden thickness, main and minor lithological units, ductile and brittle structure and secondary mineralization/alteration is included in Section 5.1. Observations relating to Proterozoic mafic dykes and Archean felsic dykes are presented in Section 5.2, including the results from a scanline fracture mapping exercise undertaken in a traverse across one well-exposed mafic dyke. A summary of the key findings is presented in Section 6.

5.1 Mapping Observations for the Withdrawal Area

The Phase 2 Geological Mapping in the Blind River and Elliot Lake area was focussed in one withdrawal area located to the northeast of the town of Elliot Lake (See inset map on Figure 1.2). The withdrawal area is entirely within the mapped extent of the Ramsey-Algoma granitoid complex, characterized on existing bedrock geology maps as a massive granodiorite to granite. The withdrawal area is 16 km by 20 km in size, encompassing an area of about 320 km^2 (Figure 1.1).

5.1.1 Accessibility and Surface Constraints

The withdrawal area is accessible via the West Branch Road that extends in a north-south direction through its centre (Figure 1.1). This central road is well-maintained and has many secondary and tertiary logging side roads branching off of it. Several new roads were also encountered in the area. While some of the side roads were in good condition and accessible using a 4X4 vehicle, many of the older side roads were found to be washed out and completely overgrown by trees up to 10 m in height, or had culverts removed during decommissioning. More recent side roads were also often overgrown by alders or flooded by beaver activity. Multiple modes of transportation were often required in combination (e.g. ATV and foot, or canoe and foot) to access specific areas of interest. The eastern and west central parts of the withdrawal area have no road network or waterway access and so only the periphery of these areas could be accessed by foot traverse. Figure 5.1.1 shows the distribution

of station locations visited, providing an overview of the accessible versus inaccessible portions of the withdrawal area.

The Wakonassin River system provided access, by canoe, to shoreline outcrops in an otherwise inaccessible portion of the withdrawal area. It also provided a drop off and pick up point for foot traverses that allowed mapping of the Supple Lake area (Figure 5.1.1). A chain of lakes in the north central portion of the withdrawal area (Lakes from north to south: Labitiche, Armstrong, Jackson and Jeanne) provided canoe access to shoreline outcrops and foot traverses in this otherwise thickly forested and relatively inaccessible area. Airport Lake provided access into the southeastern part of the withdrawal area (Figures 5.1.1 and 5.1.2a).

The topography of the withdrawal area is a mixture of low relief areas characterized by extensive granite pavements (Figure 5.1.2b), moderate-relief topographic domes, and more rugged terrain cross-cut by steep sided valleys and scarps with up to 60 m of vertical relief (Figures 5.1.2c and 5.1.2d). Scarps often preferentially occur in the “down ice” side of uplands and may represent roches moutonées.

Forest cover is continuous except for wetlands, cutover blocks, and areas of extensive exposed bedrock. In outwash plains and upland areas, the forest cover is dominated by jack pine while a mixture of spruce, poplar, birch, maple, and alder typically dominate low-lying areas. Areas of mature forest were frequently open and presented no difficulties for foot traverses however dense successional forest cover made access difficult in older cutover areas and along the margins of lakes and wetlands.

5.1.2 Bedrock Exposure and Overburden Thickness

Many predicted locations of exposed bedrock were identified for the withdrawal area and the majority were confirmed as such through visual inspection. Out of the 292 locations visited, 261 locations were positively identified as having exposed bedrock, while ten (10) were found to be overburden covered (Figure 5.1.1). The remaining 21 locations, not shown on Figure 5.1.1, were locations where obstructions or constraints on access were encountered, including features described above in Section 5.1.1.

Visual inspection in the field suggests that the extent of bedrock outcrop is greater than the predicted extent owing to the masking effects of locally dense forest cover and the ubiquity of outcrop over some of the upland areas. Average (estimated) overburden thickness around the edges of exposed bedrock outcrop varies between 0.3 and 1.5 m. Thick overburden was generally restricted to wetland areas and to the flanks of river valleys where glaciofluvial deposits, such as outwash, are present. Three sand and gravel pits were observed within the withdrawal area, including one alongside the West Branch Road in the south-central part of the area and two others in the northwestern portion of the area. These pits exposed metre-scale sections of overburden.

5.1.3 Lithology and Physical Character

The descriptions below provide an overview of the main and minor bedrock lithological units observed in the withdrawal area, including their main physical characteristics. Main lithological units tend to occur as the predominant rock type covering at least 60% of the exposed bedrock, by area, at any individual bedrock station, and are observed at a high frequency of bedrock stations overall. Minor lithological units described below may occasionally occur as the main rock type at individual bedrock stations, but in general they occur infrequently, and represent only a small portion overall of the bedrock in the withdrawal area.

Only one main lithological unit, a medium-grained granite (with subordinate granodiorite), was identified in the withdrawal area and it is described first below. Minor lithological units, described next, often represented by

xenoliths or rafts of varying composition within the granite, may occasionally occur as the predominant rock type at an individual outcrop, however they generally represent a low percentage of exposed bedrock overall across the withdrawal area. Dykes of mafic and intermediate to felsic composition, observed in multiple locations across the withdrawal area, are discussed separately in Section 5.2.

5.1.3.1 Main Lithology: Granite

A medium-grained biotite granite was observed at 253 out of 261 bedrock stations (98%) and is the most commonly observed lithological unit across the withdrawal area (Figure 5.1.3). The granite generally covers greater than 90% of the exposed bedrock outcrop where observed suggesting that it underlies the majority of the withdrawal area. Locally, primarily in the northern to northwestern part of the withdrawal area, the proportion of minor lithological units is such that the granite covers somewhat less than 90 % of any individual outcrop, by area (see Section 5.1.3.2 below). In two locations in the extreme northwestern corner of the withdrawal area, comprising <1% of all bedrock stations, the main lithology was identified as granodiorite. These two occurrences are interpreted to represent a subtle compositional variation relative to the main granitic lithology, as opposed to a distinct and independent lithological unit. Accordingly, the few associated observations related to these granodiorite occurrences are integrated with those of the granite below. A total of 121 representative rock samples were collected of the granite.

The granite is most commonly light grey to beige or pink when weathered (Figures 5.1.4a and 5.1.4d) and predominantly pink to off white or light grey when fresh (Figure 5.1.4b). The main mineral phases within the granite are quartz, plagioclase, alkali feldspar and biotite. The main accessory mineral is magnetite.

The granite is typically only weakly foliated although it locally exhibits a moderate to strong foliation. It is also locally massive in texture. Foliation is defined by the alignment of biotite and K-feldspar laths. The matrix is typically medium-grained (1-5 mm) with local variations between fine-grained (0.5 – 1 mm) and coarse-grained (5 – 10 mm). In some locations, contrasting phases defined by grainsize variation were evident in outcrop (Figure 5.1.4c). Phenocrysts, predominantly K-feldspar, plagioclase, or quartz, were observed in about half of the locations where granite was the main lithological unit. Phenocryst grain size commonly ranged from medium- to very coarse-grained (10 to >50 mm) (Figure 5.1.4c).

Based on all the observations, different phases of granite were identifiable at the outcrop scale where differences in texture or foliation could be observed, including (in order of decreasing relative age):

1) a moderately to strongly foliated xenolith-poor phase;

2) a xenolith-bearing weakly to moderately foliated phase (the main phase of the batholith); and

3) a massive to weakly foliated phase, locally bordering on pegmatitic.

The magnetic susceptibility of the granite follows a roughly bounded normal (i.e. half-normal) distribution with a mean value of 3.53±4.40 x 10^{-3} SI (N=263). Susceptibility values range between 0.015 and 37.0 x10^{-3} SI with 50% of the readings falling between 0.46 and 5.39 x 10^{-3} SI (Figure 5.1.4e). The magnetic character of the granite appears to be principally attributable to the presence of accessory magnetite.

The gamma ray spectrometry readings (Figure 5.1.4f) for the granite, including 264 sets of measurements, show the following characteristics:

- Total count is on average 388±124 cps and ranges between 175 and 1,050 cps.
- Potassium content is on average 4.0±0.72% and ranges between 2.1 and 6.6%.
- Uranium content is on average 5.1±4.0 ppm and ranges between lower than the detection limit and 27.6 ppm.
- Thorium content is on average 36.1±18.4 ppm and ranges between 3.3 and 157.4 ppm.

A total of 271 field estimates of intact rock strength were made on the granite. In 270 instances (>99%) it exhibited a very strong (R5) character consistently classifying the granite as very strong. A single measurement (0.4%) of intact strength was recorded as R4 (strong).

5.1.3.2 Minor Lithological Unit: Xenoliths

Xenoliths of varied compositions represent the single minor lithological unit observed across the withdrawal area. Xenoliths are not evenly distributed across the withdrawal area but rather are concentrated primarily near the northwestern margin of the withdrawal area (Figure 5.1.5). Scattered additional occurrences are found through the centre, and within the southeastern corner, of the withdrawal area.

These xenoliths (and rafts), which are contained within and partially assimilated by the granite, mostly comprise mafic meta-igneous rocks (e.g., amphibolite gneiss, gabbro, diorite and other undifferentiated meta-mafic rocks) along with few instances of granitic gneiss (Figure 5.1.6). In total, xenoliths were observed at 53 out of 261 (20%) bedrock stations, with some stations showing multiple xenoliths of distinct lithologies. In 33 of the 53 (61%) observations, the xenoliths comprise less than 10% of the outcrop surface area. Xenoliths comprise between 10 to 30% of the outcrop area at 28% of the observations (15 of 53) and in about 9% of the observations (5 of 53), xenoliths make up more than 30% of the outcrop, by area (e.g. Figure 5.1.6a).

The xenoliths are typically grey to dark green when fresh and grey to green when weathered (Figure 5.1.6b). The contact between the xenoliths and the granite varies from gradational to sharp. Locally, the assimilation of the xenoliths into the granite has led to the formation of a sharp, millimetre-scale, alteration “rind” at their contact (e.g., Figure 5.1.6e). There was no clear evidence of localization of brittle deformation along the contact between the xenoliths and the surrounding granite.

The xenoliths generally exhibit a well-developed internal foliation (Figure 5.1.6c) with a highly variable equigranular to inequigranular texture. This internal foliation is variable in orientation, but commonly close to parallel with the foliation in the surrounding granite. The xenoliths themselves are also typically elongated with their long axes aligned parallel to the foliation within the granite. Plagioclase, hornblende, amphibole, biotite and quartz represent the main minerals identifiable within the xenoliths.

Magnetic susceptibility measurements for the xenoliths are highly variable and range between 0.084 and 55.0 $x10^{-3}$ SI (N=25) with an overall mean of 13.90±17.48 x 10^{-3} SI. The magnetic character of the higher susceptibility xenoliths appears to reflect accessory magnetite.

The gamma ray spectrometry readings (N=24) for the xenoliths show the following characteristics:

- Total count is on average 240±120 cps and ranges between 143 and 737 cps.
- Potassium content is on average 2.4±0.85% and ranges between 1.1 and 4.3%.
- Uranium content is on average 3.7±2.4 ppm and ranges between 0.8 and 9.8 ppm.
- Thorium content is on average 21.1±18.4 ppm and ranges between 4.2 and 113 ppm.

- Uranium/Thorium ratio is on average 28.4±20.6% and ranges from 3.3 to 76%.

5.1.4 Structure

Ductile and brittle structures observed throughout the withdrawal area are discussed below and presented in Figures 5.1.7 to 5.1.20. Ductile structures include foliation, and both ductile and brittle-ductile shear zones. Brittle structures include joints, veins, faults, and associated lineations (i.e., slickenlines). Secondary mineralization, in the form of fracture infilling minerals and alteration phases, is also discussed.

5.1.4.1 Ductile Structure

Ductile structural features observed in the withdrawal area include igneous flow foliation and tectonic foliation, and localized ductile and brittle-ductile shear zones. These structural features are described in detail below.

Orientation information is summarized in Table 5.1.4.1 for the ductile structures described below. This information is based on the analysis of the data-specific rose diagrams. A degree of confidence is provided for each orientation peak identified based on the frequency of that orientation within the dataset.

Table 5.1.4.1: Summary of Ductile Structures

Structure Type	Orientation Family	Peak (degrees)	Range (degrees)	Frequency (%)	Confidence
All Foliation	E-W	093	075-120	20.7	High
Igneous Flow Foliation	E-W	095	070-100	18.9	High
	ESE-WNW	105	100-115	17.9	High
Tectonic Foliation	E-W	095	080-105	25.4	High
	ESE-WNW	110	105-120	16	High
Shear Zones	SE-NW	140	121-152	13.8	Medium
	NNE-SSW	022	010-038	8.3	Medium-Low
	E-W	085	078-092	7.6	Medium-Low
	N-S	177	168-183	7.3	Medium-Low
	ENE-WSW	062	056-068	6.7	Medium-Low
	E-W	096	092-106	6.6	Medium-Low
	ENE-WSW	074	068-078	6.4	Medium-Low
	NE-SW	052	048-056	5.6	Medium-Low
Ductile Shear Zones	NNE-SSW	030	025-035	25.2	Medium
	N-S	000	355-005	14.6	Medium-Low
	ENE-WSW	075	070-080	14.6	Medium-Low
	E-W	085	080-090	14.6	Medium-Low
	ESE-WNW	108	103-112	14.6	Medium-Low
	SE-NW	132	127-137	14.6	Medium-Low
Brittle-Ductile Shear Zones	SE-NW	140	132-146	15.4	High
	NNE-SSW	020	012-028	8.9	Medium
	ENE-WSW	062	055-069	7.5	Medium-Low
	N-S	175	170-180	7.4	Medium-Low
	E-W	098	092-104	7.4	Medium-Low

Structure Type	Orientation Family	Peak (degrees)	Range (degrees)	Frequency (%)	Confidence
	E-W	085	080-090	6.6	Medium-Low
	NE-SW	052	047-057	6.2	Medium-Low

Foliation

The two main types of foliation recognized in the withdrawal area are igneous flow foliation and a tectonic foliation. Overall, a total of 205 measurements of foliation were made at the 261 bedrock stations (Figures 5.1.7, 5.1.8a and 5.1.8b). The combined foliation dataset is dominated by one broad orientation peak at 093° and ranges between 075° and 120° (Figure 5.1.8b). This east-trending foliation population dominantly dips at greater than 65° towards the north or south (Figure 5.1.8a).

Out of the total foliation population, 139 occurrences (68%) of igneous flow foliation were identified across the withdrawal area (Figure 5.1.7). This weakly to moderately developed igneous flow foliation represents the most common planar fabric type in the withdrawal area. The flow foliation is defined primarily by the weak alignment of feldspar phenocrysts (Figure 5.1.11a). Overall, the igneous flow foliation trends predominantly east-west, with only minor variations in the northwestern corner of the mapping area, where the dominant strike orientation of the foliation is east-southeast (Figure 5.1.7). Igneous flow foliation ranges in orientation from 070 to 115° with subpeaks at 095° and 105° (Figure 5.1.8c). The general uniformity in orientation of aligned feldspar phenocrysts throughout the mapping area may suggest that this fabric is not entirely a product of emplacement of the granite but is also influenced by tectonic processes.

Out of the total foliation population, 56 occurrences (27%) of tectonic foliation were identified across the withdrawal area (Figures 5.1.7 and 5.1.11b). Tectonic foliation is most commonly defined by aligned biotite, as well as aligned quartz eyes. The fabric intensity is primarily weakly to moderately developed, however in 11 instances it is strongly to intensely developed. Tectonic foliation strikes predominantly east (095°) or east-southeast (110°) within a broad range between 080° and 120° (Figure 5.1.8d). Tectonic foliation generally dips relatively steeply at greater than 60° (Figure 5.1.8a). Tectonic foliation observed within xenoliths is generally parallel to the east-trending foliation in the granite. No lineations were observed in association with the tectonic foliation.

Additional, less common foliation types include seven observations (3%) of gneissic layering and three observations (1%) of fracture cleavage (Figure 5.1.8a). Gneissic layering forming centimetre-thick bands of compositional variation occurs primarily within gneiss xenoliths (Figure 5.1.11c) and was observed mainly in the northwestern portion of the mapping area. A weak but penetrative fracture cleavage was recognized at two locations within granite bedrock in the northern part of the withdrawal area, and in one location within a mafic dyke in the southeastern portion of the withdrawal area.

Shear Zones

A total of 57 shear zones were measured throughout the withdrawal area, seven of which (12%) are characterized as ductile shear zones and 50 of which (88%) are described as brittle-ductile shear zones (Figures 5.1.9 and 5.1.10). The shear zones are generally evenly distributed, though clusters of shear zones were observed, including at the south end of Jeanne Lake, and in the north-central and southern portions of the withdrawal area.

The total shear zone population shows one dominant southeast-striking orientation peak at 140° that ranges between 121° and 152° (Figures 5.1.10a and 5.1.10b). Two other peak orientations are evident at 022° and 177°, as well as a series of east-northeast to east-striking minor peaks at 052°, 062°, 074°, 085°, and 096°. Shear zones predominantly dip greater than 60° (Figure 5.1.10a).

The ductile shear zones are characterized by a strong planar fabric with no evidence of associated brittle deformation. Where a tectonic foliation is well developed, this fabric is rotated in the shear zone (e.g., Figure 5.1.11d). Observed ductile shear zones are mostly between 1 and 3 centimetres in width, with one ductile shear zone wider than 3 centimetres.

Ductile shear zones exhibit one main north-northeast-striking peak orientation at 030°, ranging between 025° and 035° (Figure 5.1.10c). Other minor peaks occur at 000°, 075°, 085°, 108°, and 132° (Figure 5.1.10c). Ductile shear zones are generally steeply dipping, with 6 out of 7 shear zones (86%) dipping steeper than 65° (Figure 5.1.10a). One several centimetre-wide shear zone displays a mylonitic fabric at the margin of a northwest-striking mafic dyke.

Shear sense is interpreted for 6 of the 7 mapped ductile shear zones based on offset of markers such as gneissic layering, sigmoidal quartz veins, tension gashes, and rotation of foliation. Offset of markers is on the order of several centimetres to decimetre-scale. Horizontal dextral shear sense was observed in association with 3 west- to northwest-striking ductile shear zones and horizontal sinistral shear sense was observed in association with 3 northeast- to east-striking ductile shear zones (Figure 5.1.10e). There is some coincidence in orientation between shear zones that exhibit sinistral versus dextral offset, however, no evidence of reactivation was observed on any of the observed shear zones. No lineations were observed in association with the ductile shear zones in the withdrawal area.

Brittle-ductile shear zones are characterized by both localized ductile fabric development and brittle fracturing. The width of these shear zones ranges mostly between 1-3 cm, but they are occasionally up to 30 cm wide and with an anastomosing geometry (Figure 5.1.11e). Brittle-ductile shear zones are frequently associated with chlorite infill (21 of 50, 42%), and occasionally with epidote (14 of 50, 28%), quartz (10/50, 20%), cataclasite (8/50, 16%) and hematite (4 of 50, 8%). Two brittle-ductile shear zones are associated with an unidentified infilling mineral. No infill or alteration occurs on 9 out of 50 (18%) brittle-ductile shear zones.

Brittle-ductile shear zones exhibit one dominant southeast-striking orientation peak at 140° that ranges between 132° and 146° (Figure 5.1.10d). Two other peak orientations are evident at 020° and 175°, as well as a series of east-northeast to east-striking minor peaks at 052°, 062°, 085°, and 098° (Figure 5.1.10d). Brittle-ductile shear zones are mostly steeply dipping with 45 out of 50 (90%) exhibiting a greater than 65° dip (Figure 5.1.10a).

Shear sense is determined for 33 of the 50 mapped brittle-ductile structures based on the offset of markers, generally on the order of several centimetres to decimetres. Horizontal dextral shear sense was observed at 21 brittle-ductile shear zones and sinistral shear sense was observed at 12 brittle-ductile shear zones. Dextral and sinistral ductile shear zones occur in a broad range of strike orientations (Figure 5.1.10f). Peak orientations for dextral shear zones are broadly east-west (083° and 095°) and southeast-northwest (132°). Note that one dominant dextral shear zone orientation is roughly parallel to the orientation of the foliation in the withdrawal area. Sinistral shear zones occur in three dominant strike orientations: north-northeast (031°), east-northeast (063°) and east-southeast (122°). No linear fabrics were observed on brittle-ductile shear zones.

5.1.4.2 Brittle Structure

Fractures, including joints, veins and faults are the predominant brittle structures observed throughout the withdrawal area. A total of 916 fracture measurements were made across the 261 bedrock stations, including 660 joints, 186 faults and 70 veins. The characteristics of each of these fracture types are described below and their orientation is summarized in Table 5.1.4.2a. The secondary mineral infillings and linear structures that accompany brittle structures are also described in this section.

Table 5.1.4.2a: Summary of Brittle Structures

Structure Type	Orientation Family	Peak (degrees)	Range (degrees)	Frequency (%)	Confidence
Joints - All	ENE-WSW	058	040-073	7.6	Medium-Low
	NNE-SSW	030	020-040	7.3	Medium-Low
	SSE-NNW	152	136-163	6.7	Medium-Low
	SE-NW	125	104-136	6.3	Medium-Low
	E-W	092	086-104	5.6	Low
Joints – Shallow (<25°)	NE-SW	055	039-068	10.9	Medium
	NNE-SSW	030	018-039	10	Medium
	E-W	094	068-115	9.1	Medium
	N-S	011	003-018	6.8	Medium-Low
	SSE-NNW	158	141-167	6.1	Medium-Low
	N-S	175	167-183	6	Medium-Low
	SE-NW	130	115-141	5.7	Medium-Low
Joints – Moderate (25°-65°)	NNE-SSW	033	013-038	11	Medium
	ENE-WSW	066	054-077	10.4	Medium
	NE-SW	042	038-054	9.1	Medium
	E-W	084	077-106	8.2	Medium-Low
	N-S	005	355-013	6.9	Medium-Low
	SSE-NNW	152	138-160	5.7	Low
Joints – Steep (>65°)	SE-NW	145	136-164	7.7	Medium-Low
	ENE-WSW	058	040-069	7.6	Medium-Low
	SE-NW	125	112-136	7.2	Medium-Low
	NNE-SSW	030	020-040	6	Medium-Low
Faults - All	NE-SW	035	020-047	9.1	Medium
	E-W	087	081-114	8.5	Medium
	ENE-WSW	075	062-081	8	Medium
	SSE-NNW	147	136-164	7.9	Medium
	NE-SW	051	047-062	5.9	Medium-Low
	N-S	006	000-013	5.5	Low
Faults – Dextral	NNE-SSW	030	023-045	8.3	Medium-Low
	ENE-WSW	075	065-081	8.1	Medium-Low
	E-W	087	081-113	7.8	Medium-Low

Structure Type	Orientation Family	Peak (degrees)	Range (degrees)	Frequency (%)	Confidence
	NE-SW	055	045-065	6.8	Medium-Low
	N-S	170	158-180	6.8	Medium-Low
	N-S	005	000-012	6.2	Medium-Low
	SE-NW	145	137-158	6.1	Medium-Low
	NNE-SSW	018	012-023	5.6	Low
Faults – Sinistral	SSE-NNW	148	141-155	12	Medium
	NE-SW	040	024-060	11.1	Medium
	E-W	082	060-100	8.8	Medium-Low
	SE-NW	125	115-131	7.6	Medium-Low
	N-S	170	165-190	6.8	Medium-Low
	SSE-NNW	160	155-165	6.5	Medium-Low
Veins	N-S	000	341-015	10.6	Medium-Low
	SSE-NNW	152	145-165	9.8	Medium-Low
	SE-NW	135	128-145	8.6	Medium-Low
	NNE-SSW	023	015-045	8.2	Medium-Low
	ESE-WNW	107	098-128	8.0	Medium-Low
	E-W	086	080-098	7.0	Low
	ENE-WSW	075	072-080	5.8	Low
Secondary Mineral Infill - All	SSE-NNW	150	136-160	9.4	Medium-High
	E-W	088	061-095	8.8	Medium-High
	N-S	170	160-183	7.5	Medium
	NE-SW	037	029-061	7.4	Medium
	N-S	005	357-015	6.8	Medium
	NNE-SSW	024	015-029	6.5	Medium
	SE-NW	124	118-136	6	Medium-Low

Joints

There are 660 joint measurements recorded in the withdrawal area (Figures 5.1.12 and 5.1.13). Joints are a common structural feature at almost all bedrock observation locations and are distributed across the entire area. It is common for more than one orientation of joints to be present at any single location. The majority of these measurements were made in granite bedrock (590 of 660, 89%). The remainder included, 13 joints (1.9%) measured in xenoliths and 57 joints (9%) measured in mafic dykes. Analysis of the joint data, presented below, suggests that four main joint sets can be identified, including one shallowly-dipping set and three steeply dipping sets, trending broadly northeast, broadly southeast, and east. Based on the frequency distribution of joint dips, shallowly dipping joints are classified as <25° and steeply dipping joints with dips >65°. Intermediate dipping joints range between 25° and 65°.

The combined joint population is shown on an equal area lower hemisphere stereonet plot and rose diagram (Figures 5.1.13a and 5.1.13b). The rose diagram shows that the combined joint population is dominated by two

broad, major sets oriented striking northeast and southeast. The northeasterly set includes internal peaks at 030° and 058° and ranges between 020° and 073°. The southeasterly set has peaks at 125° and 152° and ranges between 104° and 163°. One additional, less significant, orientation peak is evident at 092° (ranging between 086° and 104°). Most of the joints in these three sets dip greater than 65° though all sets also include features that range down to sub-horizontal. The equal area lower hemisphere stereonet plot highlights the fourth, shallow-dipping (<25°), joint set by the central cluster of poles (Figure 5.1.13a).

Separating the joints into three general dip magnitude bins (shallow, <25°; moderate, 25° to 65°; steep, >65°) and re-plotting the rose diagrams individually provides a better means of defining the number of recognizable joint sets. The shallowly dipping to sub-horizontal joint set was observed in 87 instances (13%) (Figure 5.1.13c). The shallowly dipping joints with a dip magnitude <25° exhibit three main orientation peaks striking north-northeast at 030° (ranging between 018° and 039°), northeast at 055° (ranging between 039° and 068°), and east at 094° (ranging between 068° and 115°). Minor additional orientation peaks occur at 011°, 130°, 158°, and 175°.

A total of 108 joints (16%) were observed to dip at a moderate magnitude between 25 and 65 degrees (Figure 5.1.13d). The moderately dipping joints exhibit two significant orientation peaks: a broad north-northeast-striking orientation with distinct peaks at 033° and 042°, and ranging between 013° and 054°, and an east-northeast-striking peak at 066° ranging from 054° to 077°. Less significant orientation peaks occur at 084° (ranging between 077° and 106°), 005° (ranging between 355° and 013°), and 152° (ranging between 138° and 160°).

A total of 465 joints (70%) were measured with a dip magnitude greater than 65° (Figure 5.1.13e). The steeply dipping joint population is dominated by two, broad, major sets. One exhibits an east-northeast-striking peak at 058° and ranges between 040° and 069°. Another, broadly southeast-striking population, has two internal peaks at 125° and 145° and ranges between 112° and 164°. One additional, less prominent, orientation peak is evident at 030° (ranging between 020° and 040°).

Joint spacing was assessed by assigning joint sets at the outcrop scale into one of eight spacing bins as noted in Table 5.1.4.2b below. An additional category of ‘unknown’ was assigned when joint spacing could not be properly measured, for example due to small outcrop size. The results from this assessment are shown in the frequency histogram (Figure 5.1.13f) and in Table 5.1.4.2b. Table 5.1.4.2b also separates the joint spacing information by the same dip subsets described above. Rose diagrams, along with orientation peaks, for joints of each spacing class are shown in Figures 5.1.13g to 5.1.13n. It should be noted also that joint spacing was usually assessed on a subhorizontal or subvertical bedrock surface and there may therefore be minor uncertainty in spacing estimates for joint sets with moderate dips.

Looking at the distribution of spacings for the entire joint dataset, the most common spacing class of observed joints is the range between 100-500 cm (244 of 660; 37%). Considering the 188 instances of joints that exhibit 30-100 cm spacing, together with the 244 instances of joints that exhibit 100-500 cm spacing, more than 50% of all joint spacings measured in the withdrawal area range from 30-500 cm (432 of 660; 65%). Nineteen joints (3%) exhibited spacing of 10 cm or less. Joint spacing of 500 cm or greater was observed in 113 (17%) instances.

All spacing bins exhibit a similar variability in joint peak orientation to that of the total joint set. The north-northeast orientation peak at 030° is most prominent in the 10-30 cm joint spacing class (Figure 5.1.13i), whereas the east-northeast-striking orientation peaks at 060° and 055° dominate the 30-100 cm and 100-500 cm joint spacing classes (Figures 5.1.13j and 5.1.13k). The southeast and south-southeast orientation peaks evident from the combined joint data sets are evident as peaks in almost all of the joint spacing classes. Tightly spaced joints (1-3

cm) are oriented mostly north and east-northeast (Figure 5.1.13g). The 3-10 cm joint spacing class is dominated by east-northeast-, east-southeast-, and south-southeast-striking joints (Figure 5.1.13h). Joints spaced 500-1000 cm are mostly oriented north-south with peaks at 162° and 170° and east-west with a peak at 083° (Figure 5.1.13l), which notably are less evident peaks in the combined joint orientation. Joints spaced >1000 cm show orientation peaks striking east-southeast at 105° and 120°, as well as south-southeast at 155° (Figure 5.1.13m). The one joint with unknown spacing strikes north-south (Figure 5.1.13n).

Table 5.1.4.2b: Joint Spacing

	All Joints		Steep Dip		Moderate Dip		Shallow Dip	
Spacing Bins (cm)	# of joints	% of joints	# of joints	% of all joints	# of joints	% of all joints	# of joints	% of all joints
<1	0	0	0	0	0	0	0	0
1–3	3	0.45	2	0.43	1	0.93	0	0
3–10	16	2.42	14	3.01	1	0.93	1	1.15
10–30	95	14.4	67	14.4	17	15.7	11	12.6
30–100	188	28.5	123	26.5	29	26.9	36	41.4
100–500	244	37.0	166	35.7	41	38.0	37	42.5
500–1000	71	10.8	60	12.9	11	10.2	0	0
>1000	42	6.4	32	6.88	8	7.41	2	2.30
Unknown	1	0.15	1	0.22	0	0	0	0
Total # Joints	660	100	465	100	108	100	87	100

The frequency distributions of joint spacing classes are also presented for shallow, moderate and steep joint dip subsets (Table 5.1.4.2b), with stated percentages calculated using the total number of 660 joints. The majority of shallowly dipping joints (73 of 87; 83.9%) fall into the 30–500 cm range in spacing, with few examples exhibiting tighter spacing. Joint spacing for shallowly dipping joints greater than 500 cm are rare due to the scarcity of vertical exposure that would allow the assessment of such wide joint spacing. The most common joint spacing range of moderately dipping joints is between 100-500 cm (41 of 108; 38%). The steeply dipping joints also predominantly exhibit spacing of 100-500 cm, occurring in 166 out of 465 (35.7%) instances.

Overall, the majority of joints are sub-vertical. A sub-horizontal set is observed locally, where vertical relief is present, and is commonly spaced 100-500 cm apart (Figure 5.1.14a). While most joints are spaced between 30 and 500 cm, several locations in the central portion of the withdrawal area exhibit joint spacing greater than 1000 cm (Figure 5.1.14b). Joint spacing under 30 cm occurs locally throughout the withdrawal area (Figure 5.1.14c). Multiple, tightly-spaced, joint sets are commonly observed at individual bedrock locations (Figure 5.1.14d). Instances of two orthogonal joint sets and three sets at 60° to each other occur throughout the mapping area.

Faults

One hundred and eighty-six faults were observed throughout the withdrawal area. The faults are generally evenly distributed, though clusters of faults occur in the northwestern and northeastern portions of the withdrawal area, especially around Jackson and Jeanne Lakes (Figure 5.1.15). Of the 186 fault observations made, 175 (94%) are located within granite bedrock and five (3%) within gneissic xenoliths. The remaining six faults (3%) occur within mafic dykes.

Poles to the fault planes and the corresponding fault rose diagrams are shown on Figure 5.1.16. The majority of faults dip relatively steeply with few dipping less than 65° (Figure 5.1.16a). The combined fault population exhibits three main orientation peaks: one striking northeast with a peak at 035° and ranging between 020° and 062°, including a smaller subpeak at 051°, one striking east with subpeaks at 075° and 087° ranging from 062° to 114°, and one striking south-southeast at 147° ranging between 136° and 164° (Figure 5.1.16b). One additional minor fault orientation peak strikes north at 006°.

Damage zones of faults range from millimetre-scale, single slip surfaces (Figures 5.1.17a and 5.1.17b), to zones several tens of centimetres wide comprising an anastomosing network of joints and fault planes (Figure 5.1.17c). The majority of the observed faults (136 of 186, 73%) are less than 1 cm in width, and 32 (17%) are between 1-3 cm wide. The remaining 18 faults (10%) were described with a width of greater than 3 cm, which accounts for a damage zone around the fault core. These wider faults are commonly associated with moderate amounts of brecciation and cataclasite development (Figure 5.1.17d).

Slip sense on faults was inferred from the geometry of curviplanar splaying fractures and steps on slickensided surfaces, and more confidently interpreted by offset of markers (e.g., veins) and the presence of extensional jogs (e.g., Figures 5.1.17a and 5.1.17b). Out of the 186 faults observed in the withdrawal area, 73 exhibit dextral horizontal offset and 63 exhibit sinistral horizontal offset (Figures 5.1.16c and 5.1.16d). Four reverse faults and one normal fault were also recorded (Figure 5.1.16e). An additional 45 faults of unknown slip sense were also observed.

Where observed, displacement of markers ranged from 0.2 to 5 cm. Slickenlines were observed on individual, isolated, fault planes and in fault zones characterized by multiple parallel surfaces (Figures 5.1.17e and 5.1.17f). They range from sub-horizontal to moderately-plunging suggesting a combination of strike-slip and oblique- to dip-slip fault movement (Figure 5.1.16e).

The dextral fault population covers a wide range of strike orientations (Figure 5.1.16c). This includes, one north-northeast-striking orientation peak at 030° and ranging from 023° to 045° and a broad east-northeast- to east-striking population ranging from 065° to 111° with internal peaks at 075° and 087°. Several additional less prominent peaks occur at 005°, 018°, 055°, 145° and 170°. The sinistral fault population is dominated by narrow northeast- and southeast-striking orientation peaks (Figure 5.1.16d). The northeastern peak at 040° ranges from 024° to 060° and the southeastern peak at 148° ranges from 141° to 155°. An east-striking sinistral fault population displays a peak at 082° and has a range from 060° to 100°. Additional minor orientation peaks occur at 125°, 160° and 170°.

Fault cross-cutting relationships observed at seven locations provided a means of separating the dextral and sinistral faults into three conjugate sets, including: (1) east-striking (087°) dextral faults with south-southeast-striking (148°) sinistral faults, (2) south-striking (170°) dextral faults with northeast-striking (040°) sinistral faults, and (3) north-northeast-striking (030°) dextral faults with east-striking (082°) sinistral faults.

Faults are commonly coated with chlorite, epidote, quartz, and hematite. Cataclasite, breccia, pseudotachylite, and gouge are locally encountered as fault core fillings. Minor mineral infills on faults include magnetite and feldspar. Secondary minerals associated with fault zones are described in detail in Section 5.1.4.8 below.

Veins

There are 61 observations of veins in the withdrawal area (Figure 5.1.18). Veins are generally evenly distributed, though there is a slight increase in occurrences in the southwestern and north-central parts of the withdrawal area and the central part of the withdrawal area exhibits a much lower density of veins.

The vein population is dominated by two adjacent orientation sets (Figures 5.1.19a and 5.1.19b). One ranges between 341° and 015° with a peak striking north at 000°. The other ranges between 015° and 043° with a peak striking north-northeast at 023°. Another dominant vein orientation peak is evident striking east-southeast at 107° and four additional minor peaks are evident at 152°, 135°, 086°, and 075° (Figure 5.1.19b). Veins are mostly steeply dipping, with only few occurrences of veins dipping less than 65° (Figure 5.1.19a).

The majority of observed veins are narrow, up to 3 cm in width (46 of 61; 75%). Fourteen veins (23%) are between 3 and 30 cm in width. One vein greater than 30 cm wide was recorded. In 58 instances (58 out of 61, 95%), the observed vein was interpreted as extensional in nature (Figure 5.1.19c). The three (5%) observed shear veins range between 1-3 cm in width (Figure 5.1.19d) and are located in the southwestern and northwestern corners of the Withdrawal area (Figure 5.1.18).

Almost all of the observed veins (56 of 61; 92%) were quartz filled. Other mineral infills are feldspar, biotite, chlorite, magnetite, calcite, epidote, pyrite and hematite. Mineral infill in veins is described in more detail below in Section 5.1.4.3.

5.1.4.3 Secondary Minerals, Fault Rocks and Alteration

Evidence of secondary mineral infilling within, and alteration of, fractures was documented during geological mapping (Figure 5.1.20). Out of the total population of all fracture types (660 joints + 186 faults + 61 veins; N = 907), 222 fractures (24%) exhibited at least one infilling mineral phase, alteration type or fault rock type, with the remaining 76% of fractures (685 out of 907) displaying no mineral infill. The most common secondary minerals observed across all fracture types include quartz (91 occurrences; 10%), epidote (62 occurrences; 6.8%), chlorite (56 occurrences; 6.4%), hematite (45 occurrences; 5.0%), cataclasite (32 occurrences; 3.5%), feldspar (12 occurrences, 1.3%), and magnetite (seven occurrences, 0.8%) (Table 5.1.4.3a). Lesser biotite (four occurrences), carbonate, pseudotachylite, pyrite, and gouge (two occurrences each) as well as breccia (one occurrence), and two unknown mineral infills represent the remaining secondary mineral types and are collectively referred to as ‘other’ (N=15, 1.5%) in Table 5.1.4.3a and on Figure 5.1.20. Note that in some instances more than one infilling mineral was identified within a single fracture. Common mineral associations are quartz and epidote, quartz and chlorite, epidote and chlorite, as well as chlorite and hematite.

Occurrences of quartz, epidote, and chlorite infilling are evenly distributed across the entire withdrawal area (Figure 5.1.20). Hematite infilling occurs in the south as well as in the northwestern corner of the withdrawal area, and in a cluster around Jackson Lake in the northeast. Cataclasite was observed mainly in the northeastern and southeastern parts of the withdrawal area. Feldspar mineral infilling was documented in the northcentral portion of the withdrawal area. Magnetite mineral infill occurs in isolated locations throughout the Withdrawal area.

Table 5.1.4.3a: Joints, Faults and Veins (Combined) - Secondary Mineral Infills and Alteration

Mineral Phase/ Alteration	All Occurrences	% of total
Quartz	91	10.0

Mineral Phase/ Alteration	All Occurrences	% of total
Epidote	62	6.8
Chlorite	56	6.2
Hematite	45	5.0
Cataclasite	32	3.5
Feldspar	12	1.3
Magnetite	7	0.8
Other	15	1.7
None	685	75.5
Total # of Fractures	**907**	

The orientations of all infilled fractures (N=222) is summarized in Figure 5.1.21. The majority of filled fractures are steeply dipping, with only few dipping less than 65° (Figure 5.1.21a). The combined filled fracture population is dominated by two main orientation peaks striking southeast at 150° and east at 088°. Both are narrow peaks displaying ranges from 136° to 160°, and from 061 to 095°, respectively (Figure 5.1.21b). Less prominent are a broad northeast-striking peak ranging from 015° to 061° with internal peaks at 024° and 037°, as well as a narrow peak at 170° ranging from 160° to 183°. Additional minor peaks occur at 005° and 124°.

The fracture population infilled by quartz (Figure 5.1.21c) is dominated by two main peaks oriented south-southeast at 150° and north at 005°, both of which are narrow peaks ranging between from 130° to 164°, and from 354° to 018°, respectively. An additional peak strikes east at 088° and ranges from 081° to 098°. Less prominent peaks are oriented at 023°, 108°, and 122°. The population of epidote filled fractures (Figure 5.1.21d) is dominated by two main orientations: a broad northeast-striking peak ranging from 016° to 062° with peaks at 035° and 048°, and a narrow south-striking peak at 170° ranging from 161° to 182°. Additional minor peaks are evident at 003° and 152°. For chlorite, the dominant orientation peaks are at 130° and a broad east-striking population ranging from 065° to 094° with internal peaks at 075° and 085°. Additional peaks are evident at 032°, 150° and 170° (Figure 5.1.21e). The orientation distribution for fractures infilled with hematite is dominated by a narrow southeast-striking peak at 148°, ranging from 141° to 153° (Figure 5.1.21f). Other peaks are at 080° and 045°, and statistically less significant peaks occur at 026°, 170°, and 115°. For cataclasite-filled fractures the main orientation peak is east-striking at 088° with additional peaks at 006°, 015°, 032°, 058°, 074°, 108°, 150° and 167° (Figure 5.1.21g). For fractures filled with feldspar, orientation peaks are northeast at 040° and 052°, east at 088°, and east-southeast at 107° and 125° (Figure 5.1.21h). Magnetite-filled fracture show dominant orientation peaks trending north-northeast with peaks at 013° and 028°, with minor peaks at 040°, 123°, and 136° (Figure 5.1.21i).

Table 5.1.4.3b provides an overview of the types and number of joints with secondary mineral infilling and alteration. The majority of observed joints (616 of 660; 93%) are unfilled. For the remaining 7% of filled joints, the predominant infill mineral is hematite with18 occurrences (2.7%), followed by epidote which occurs as infill in 17 joints (2.6%), quartz in 6 joints (0.9%) and chlorite in 5 joints (0.8%). One feldspar and one cataclasite filled joint are also documented. Mineral infill is most common in joints with a steep dip. Epidote, hematite and chlorite occur on joints of moderate dip and three shallowly dipping joints with hematite infill were noted.

Table 5.1.4.3b: Joints - Secondary Mineral Fills and Alteration

Mineral Phase / Alteration	All Occurrences	% of total	Steep Dip (>65°)	Moderate Dip (25°-65°)	Shallow Dip (<25°)
Hematite	18	2.7	14	1	3
Epidote	17	2.6	15	2	0
Quartz	6	0.9	6	0	0
Chlorite	5	0.8	4	1	0
Feldspar	1	0.2	1	0	0
Cataclasite	1	0.2	1	0	0
Unknown	2	0.3	2	0	0
None	616	93.3	428	104	84
Total # of Joints	**660**		**596**	**156**	**43**

Table 5.1.4.3c provides an overview of the types and number of fault rock or fault infill occurrences encountered in the withdrawal area. The majority of faults displayed mineral infill, with unfilled faults occurring only in 37% (69 out of 186) of instances where faults were observed. The most common fault mineral infills identified were chlorite and epidote. Chlorite was observed in 47 (25%) faults and epidote in 43 (23%) faults. Other common fault infills are cataclasite in 31 (17%) faults (see also Figure 5.1.17d), along with quartz in 29 (16%) and hematite in 26 (14%) instances (see also Figure 5.1.17c). Three faults (1.6%) were recorded with feldspar as infill and two instances (1%) with magnetite infill. Four faults (3.2%) are associated with 'other' infill, which includes pseudotachylite, breccia, and gouge. Chlorite, epidote, and hematite are observed mostly as pervasive coatings on and around fault surfaces (Figures 5.1.22a, 5.1.22b and 5.1.22c).

Table 5.1.4.3c: Faults - Secondary Mineral Fills and Alteration

Mineral Phase/ Alteration	All Occurrences	% of total
Chlorite	47	25.3
Epidote	43	23.1
Cataclasite	31	16.7
Quartz	29	15.6
Hematite	26	14.0
Feldspar	3	1.6
Magnetite	2	1.1
Other	4	2.2
None	69	37.1
Total # of Faults	**186**	

Evidence of secondary mineral infilling and alteration of veins was also documented during mapping. Table 5.1.4.3d below provides an overview of the types and number of vein infill occurrences encountered in the withdrawal area. The most common infill in veins is quartz, occurring in 56 out of 61 (92%) instances (Figures

5.1.19c and 5.1.19d). Eight veins (13%) are infilled with feldspar, six (9.8%) with chlorite, five (8.2%) with magnetite (Figure 5.1.22d), two (2.9%) epidote, and one (1.4%) with hematite. Carbonate, pyrite (Figure 5.1.22f), and biotite, collectively referred to as 'other' in Table 5.1.4.3d, were observed in eight instances (13%). Note that the carbonate veins occur within a mafic dyke (Figure 5.1.22e). One vein (1.6%) has an unknown infilling mineral.

Table 5.1.4.3d: Veins - Secondary Mineral Fills and Alteration

Mineral Phase/ Alteration	All Occurrences	% of total
Quartz	56	91.8
Feldspar	8	13.1
Chlorite	6	9.8
Magnetite	5	8.2
Epidote	2	3.3
Hematite	1	1.6
Other	8	13.1
Unknown Fill	1	1.6
Total # of veins	**61**	

5.2 Dykes in the Blind River and Elliot Lake Area

This section summarizes the observations made regarding mafic and felsic dyke occurrences documented during the geological mapping activity in the withdrawal area. Proterozoic mafic dykes are described in Section 5.2.1 below, including the presentation of results from one detailed scanline fracture mapping exercise undertaken across one well-exposed mafic dyke of the Matachewan swarm (Section 5.2.1.1). A summary of lithological and physical properties for each of the Proterozoic mafic dyke sets is included in Table 5.2.1. Felsic dykes are described in Section 5.2.2.

Table 5.2.1: Summary of Proterozoic Mafic Dyke Characteristics

Mafic Dyke Swarm	Number of Bedrock Station Occurrences	Width (m)	Orientation	Peaks (°)	Magnetic Susceptibility (average SI)	Gamma (average K, U, Th)	Strength (range)
Matachewan	29	0.2 – 40	NW-NNW	315 345	35.6 x10^{-3}	K = 1.31 % U = 1.52 ppm Th = 7.65 ppm	R3-R6
Sudbury	8	0.2 - 20	W	265	23.4 x10^{-3}	K = 1.46 % U = 1.38 ppm Th = 10.84 ppm	R5
Biscotasing	1	10	NNE	035	38.5 x 10^{-3}	K = 0.5 % U = 0.7 ppm Th = 1.6 ppm	R5

Mafic Dyke Swarm	Number of Bedrock Station Occurrences	Width (m)	Orientation	Peaks (°)	Magnetic Susceptibility (average SI)	Gamma (average K, U, Th)	Strength (range)
North Channel	1	5	ENE	-	0.98×10^{-3}	K = 0.62 % U = 0.20 ppm Th = 2.89 ppm	R5

5.2.1 Mafic Dykes

Mafic dykes and intrusions of diabase and gabbroic composition are widespread in and around the Blind River and Elliot Lake area, including:

- Northwest-trending, ca. 2.473 billion year old, Matachewan dykes (Buchan and Ernst, 2004);
- North-trending Marathon swarm dykes (ca. 2.121 Ga; Buchan et al., 1996; Hamilton et al., 2002)
- Northeast-trending, ca. 2.167 billion year old, Biscotasing dykes (Buchan et al., 1993);
- West-northwest-striking North Channel dykes, poorly constrained to a ca. 1.6 to 2.5 billion year age of emplacement (OGS, 2011).
- West-northwest-trending, ca. 1.238 to 1.235 billion year old, Sudbury dykes (Krogh et al., 1987); and
- East-northeast-trending Grenville dykes (ca. 590 Ma; Kamo et al., 1995)

In the withdrawal area, a total of 42 bedrock observation locations included observations of mafic dykes (Figure 5.2.1.1). This included a total of 29 observed mafic dykes attributed to the northwest-striking Matachewan dyke swarm (Section 5.2.1.1), a total of eight (8) observed mafic dykes attributed to the west-northwest- to northwest-striking Sudbury dyke swarm (Section 5.2.1.2), a single mafic dyke attributed to the northeast-striking Biscotasing dyke swarm (Section 5.2.1.3), and a single mafic dyke attributed to the west-northwest-striking North Channel dyke swarm (Section 5.2.1.4). In addition, a scanline fracture mapping exercise was completed across one, well-exposed, Matachewan mafic dyke. The results from this exercise are presented at the end of Section 5.2.1.1.

Described separately from the mafic dykes and not included in the total count of 42, are two (2) additional observations of diatreme breccia dykes, which are presented in Section 5.2.1.5.

5.2.1.1 Matachewan Mafic Dyke Swarm

A total of 29 mafic dyke observations are attributed to the Matachewan mafic dyke swarm and occur throughout the Withdrawal area (Figure 5.2.1.1). The Matachewan mafic dykes were interpreted to be distinct from other dyke swarms based primarily on orientation, colour and, where evident, the plagioclase phenocrysts. Dykes of the Matachewan swarm generally strike northwest to north-northwest.

Matachewan mafic dykes occupy anywhere between less than 10% to up to 100% of the outcrop by area at any single bedrock observation location. In several instances, these mafic dykes were observed at multiple locations along the same dyke. Twenty-four representative Matachewan mafic dyke rock samples were collected. The mafic dykes are dark grey to black when fresh and grey to dark grey when weathered (Figures 5.2.1.2a, 5.2.1.2b, and

5.2.1.2c). They are mostly massive in texture. At one location the dyke displays a strong east-west striking cleavage or tightly-spaced joint set.

The groundmass of these mafic dykes generally varies from very fine- to medium-grained, with one location displaying pods of coarse grained texture. Medium to very coarse grained plagioclase phenocrysts occur locally within the finer grained groundmass (Figure 5.2.1.2b). There is a common transition from very fine grain size at chilled margins adjacent to the bedrock host transitioning to increasingly coarser grainsize towards the centre of the dyke. The coarsest grains were consistently observed at the greatest distance from the bedrock contact (i.e., towards the middle of the dyke). The primary mineral phases observed within the Matachewan mafic dykes include pyroxene, plagioclase, magnetite with minor occurrences of pyrrhotite and biotite (Figure 5.2.1.2b). Plagioclase phenocrysts, typical of Matachewan mafic dykes, were observed at six of the locations.

The Matachewan mafic dykes predominantly exhibit a sharp and mm- to cm-width chilled margin with the surrounding bedrock host. Four of the observed Matachewan mafic dykes, including the dyke described for the scanline fracture mapping exercise, were broken and faulted at their contact with the adjacent granite host rock. However, most observed dyke-host contacts do not display evidence of brittle reactivation along the contact horizon and are intact adjacent to the host rock.

A total of 29 field estimates of intact rock strength were undertaken on the Matachewan mafic dykes. The results include one instance (1 out of 29; 3%) of medium strong (R3) character, two instances (2 out of 29; 7%) of a strong (R4) character, twenty-four instances (24 out of 29; 83%) of a very strong (R5) character and two instances (2 out of 29; 7%) of an extremely strong (R6) character.

Matachewan mafic dykes observed in the withdrawal area range from 5 cm to approximately 40 m in width, with the majority of dykes (15 out of 29, 52%) between 10 and 40 m wide (Figure 5.2.1.2d). Ten out of the 29 observations (34%) are greater than 20 m in width. In some cases, the reported width is a minimum estimate, where only one contact is exposed. In 7 instances (24%) neither contact was exposed and the width of the dyke could not be determined. Small mafic dyke apophyses, up to 50 cm wide, and oriented both at high angles and parallel to the main dyke trend are commonly observed in close proximity to the main dyke segments. At one location, the exposed Matachewan mafic dyke displays an oblong shape with contacts to the surrounding granite exposed on all four sides.

Magnetic susceptibility values for the Matachewan mafic dykes range between 0.66 and 145.3 $x10^{-3}$ SI with an overall mean of 35.6±32.6 $x\ 10^{-3}$ SI (N=28) (Figure 5.2.1.2e). The magnetic susceptibility is distinctly bimodal with one cluster having a modal peak of approximately 1 $x\ 10^{-3}$ SI and the other with a peak at approximately 40 $x10^{-3}$ SI.

The gamma ray spectrometry readings (Figure 5.2.1.2f) for the Matachewan mafic dykes, including 27 sets of measurements, show the following characteristics:

- Total count is on average 145.6±56.0 cps and ranges between 93 and 337 cps..
- Potassium content is on average 1.31±0.66% and ranges between 0.5 and 3.9%.
- Uranium content is on average 1.52±1.19 ppm and ranges between 0.0 and 4.4 ppm.
- Thorium content is on average 7.65±5.67 ppm and ranges between 2.8 and 24.1 ppm.
- Uranium/Thorium ratio is on average 15.8±11.0% and ranges from 7.8 to 35.0%.

Twenty-four of the Matachewan mafic dyke observations are coincident with, or very close to, dyke segments that were previously identified in the lineament analysis (note that only twelve of these lineaments are attributed to Matachewan mafic dykes, ten of these coincide with Sudbury mafic dyke swarm lineaments, and one with a Marathon dyke swarm lineament, and one with a North Channel swarm lineament). In the five other observation locations, mafic dykes were not previously identified in the lineament analysis. These latter five occurrences of mafic dykes display a wide range of widths between 10 and 40 m and magnetic susceptibility values between 0.9 and 145 $x10^{-3}$ SI.

The Matachewan mafic dyke contact orientation to the granite host rock was visible and was measured at 22 of the 29 locations of Matachewan mafic dyke observations (Figures 5.2.1.3a and 5.2.1.3b). The orientations of Matachewan mafic dyke contacts are dominated by two main peaks oriented southeast at 135° and south-southeast at 165°, with a small subpeak between these at 150°. The range encompassing these peaks extends from 128° to 170° (Figure 5.2.1.3b). All dyke contacts are uniformly steeply dipping (Figure 5.2.1.3a).

Within the Matachewan mafic dykes, 49 joints, 2 faults, and 2 veins were measured during geological mapping. The two faults strike south-southwest and west, respectively, the latter of which is a reverse fault with hematite and chlorite on the slip surface. At one station, one calcite vein (strike/dip = 314/74) and one calcite-quartz (strike/dip = 022/74) vein occur within the mafic dyke. In addition to the veins, the dyke at this location is also associated with epidote alteration and brecciated contacts with the adjacent granite. Joints within the Matachewan mafic dykes are mostly vertical, but include a smaller number of inclined and sub-horizontal joints (Figure 5.2.1.3c). The orientations of joints show two main peaks, one trending northeast at 040° and another south-southeast at 150° (Figure 5.2.1.3d), orthogonal and parallel to the main dyke contact orientations (Figure 5.2.1.3b). The northeastern orientation peak includes two subpeaks at 023° and 060°, and the southeastern orientation peak includes two subpeaks at 122° and 135°. A lesser orientation peak strikes east at 095°.

Overall, the average joint spacing within the mafic dykes is smaller compared to joints in the granite host rock. The most common spacing class for joints within Matachewan mafic dykes (16 out of 49, 33%) is between 10 and 30 cm (Figure 5.2.1.3e). More than half of the joints (34 out of 49, 69%) are spaced under 100 cm apart (see also Figure 5.2.1.2c). In the granite host rock of stations with Matachewan mafic dyke observations, the dominant joint spacing class (12 out of 38, 32%) is between 100 and 500 cm (Figure 5.2.1.3f). Approximately half (21 out of 38, 55%) of the joints are spaced under 100 cm apart. Both mafic dykes and granite at dyke observation stations show a proportionally greater number of tightly spaced joints than the average joint spacing for the whole area (Figure 5.1.13f).

Matachewan Mafic Dyke Scanline Fracture Mapping Exercise

A detailed scanline fracture mapping exercise was performed along a single, northeast-trending, 40 m long transect across one 20 m wide west-northwest to northwest trending Matachewan mafic dyke located in the southwestern portion of the withdrawal area. The orientation of the mafic dyke, and its physical characteristics, such as the presence of plagioclase phenocrysts, indicates that this dyke is part of the Matachewan dyke swarm. The main purposes of the fracture mapping exercise were to attempt to increase the general understanding the character of the fractures both within and in the vicinity of mafic dykes and to investigate the character of the dyke-host bedrock contact zone.

The selected location (Station 17TC0136; Figure 5.1.1) provided good exposure of the dyke, including both its southwestern and northeastern contacts with the adjacent granite bedrock. Almost continuous bedrock exposure

was available for examination over the total scanline length of 40 m except for a 4 m section between 30 and 34 m, and the last metre of the section, that were both covered by vegetation and soil (Figure 5.2.1.4a).

The scanline, shown in Figure 5.2.1.4a, crosses a Matachewan dyke that is typical of this swarm of mafic dykes observed in the withdrawal area (Figure 5.2.1.5a). The profile is oriented NE-SW and is orthogonal to the dyke contacts. The northeastern contact between the mafic dyke and the granite is well exposed and is oriented 311/87 (Figure 5.2.1.5b). The well exposed southern contact is oriented 108/89 (Figure 5.2.1.5c). Irregular fingers of dyke and granite, indicative of a failed en echelon propagating dyke tip, occur along the southwestern contact (Figure 5.2.1.4g and 5.2.1.5d).

Across the scanline, 51 fracture measurements, including 41 joints and 10 faults, were recorded (Figures 5.2.1.4b and 5.2.1.4c). Of these, a total of 45 fractures, composed of 36 joints and 9 faults, were measured within the dyke itself and the remaining 6 fractures, 5 joints and 1 fault, were measured in the granite. This includes locations in the granite both northeast and southwest of the dyke. Both the northeastern and the southwestern dyke-granite contacts are broken and exhibit evidence of dextral faulting. The fault at the northeastern contact is a 5-mm wide dextral strike-slip fault with hematite and epidote mineral infill (Figure 5.2.1.5b). Slickenlines on the fault plane plunge 04° towards 323°. The two faults at the southwestern dyke contact are also dextral and exhibit an infill of cataclasite (Figure 5.2.1.5c). Within the dyke, three additional dextral faults and one sinistral fault were observed. No ductile structures or veins were identified in the mapped scanline area.

All the observed faults are steeply dipping (Figure 5.2.1.4d). The fault population is dominated by a series of east-southeast- to southeast-striking orientation peaks ranging from 101° to 141°, with peaks at 108°, 117° and 133° (Figure 5.2.1.4d). These orientations are parallel to northeastern and southwestern mafic dyke-granite contacts (see also Figure 5.2.1.5f). Additional narrow peaks occur at 152° and 054°, which together form an orthogonal set (Figure 5.2.1.4d).

Joints are mostly steep, with a small number of moderately dipping joint sets measured within in the dyke and two shallowly dipping joint sets measured in granite (Figures 5.2.1.4b and 5.2.1.4c). The joint population in the mafic dyke is dominated by a broad southeast-striking orientation peak ranging from 103° to 140°, with peaks at 112° and 133° (Figure 5.2.1.4b). These orientations are parallel to northeastern and southwestern mafic dyke-granite contacts (see also Figures 5.2.1.5b and 5.2.1.5c). Additional peaks occur at 157° and 057°, which together form an orthogonal set (Figure 5.2.1.5e). Less significant orientation peaks strike north-northeast at 015° and northeast at 038°. Within the granite, one dominant orientation peak is evident at 138°, parallel to the northeastern dyke-granite contact (Figure 5.2.1.4c).

The frequency of fractures measured along the scanline is significantly higher within the mafic dyke than within the adjacent granite (Figure 5.2.1.4e). A total of 6 fractures were observed in the 16 m of granite observations (average of 0.4 fractures per 1 m interval), highlighting its generally unfractured character away from the dyke contact (Figure 5.2.1.5f). Within the 20 m of dyke, a total of 45 fractures were documented, forming an average of 2.3 fractures per 1 m interval. The section with the most abundant number of fractures (10 fractures per 1 m) occurs at the 5 to 6 m interval within the mafic dyke near to its northeastern contact with the granite. Throughout the remainder of the dyke, fractures are evenly distributed with most 1 m intervals exhibiting 1 to 4 fractures.

Hematite, epidote, and cataclasite are documented as infill of the faults forming the dyke contacts. Breccia infill occurs on one west-striking fault within the mafic dyke. Six of the measured faults display dextral sense-of-slip and one faults displays sinistral slip. The south-southeast-striking sinistral fault is offset by the east-southeast-striking

dextral fault. Cross-cutting evidence is documented by the termination of joints of one orientation on joints of another orientation. For example, northeast-striking joints limit the extent of joints of all other strike orientations.

A series of magnetic susceptibility measurements taken along the scanline shows that the susceptibility values of the dyke are about an order of magnitude higher than the granite host rock (Figure 5.2.1.4f). Magnetic susceptibility values for the granite range from 0.015 to 0.50 $x10^{-3}$ SI and are on average 0.14 $x10^{-3}$ SI. These values are consistent with what is expected for granite in the withdrawal area (see Section 5.1.3.1 above). Susceptibility values for the dyke range from 0.11 to 25.0 $x10^{-3}$ SI and are on average 7.25 $x10^{-3}$ SI. Magnetic susceptibility values within the dyke are generally higher within its northern half than within its southern half. The magnetic susceptibility in the granite is lower northeast of the mafic dyke than southwest of the dyke contact. Elevated susceptibility values occur locally in the granite adjacent to the overburden covered segment between 30 and 34 m (Figure 5.2.1.4f).

In summary, the detailed mapping transect across the Matachewan mafic dyke was useful in characterizing lithology and structures of the mafic dyke-granite contact zone. The granite displayed a small number of fractures. Mostly dextral southeast-striking faults occur within the Matachewan mafic dyke and along both the northern and southern contact between the dyke and the granite. The Matachewan mafic dyke exhibited an abundance of joints, with two main joint orientations parallel to the each of the dyke contacts. A third dominant joint set is oriented at a low angle to the dyke contact. Most joints were steeply dipping. The frequency distribution of fractures shows that more joints per metre occur within the dyke than within the granite. The Matachewan mafic dyke near its northern contact to the granite displays the highest frequency of joints. Several sections of the granite contain no fractures. The magnetic susceptibility of the Matachewan mafic dyke is one order of magnitude higher than the surrounding granite host rock. Within the Matachewan mafic dyke, the magnetic susceptibility is higher near its northern contact than near the southern contact to the granite.

5.2.1.2 Sudbury Mafic Dyke Swarm

Mafic dykes were attributed to the Sudbury dyke swarm based on the following criteria: (1) proximity to a lineament interpreted as a Sudbury mafic dyke, (2) green fresh and weathered colour, and (3) west-northwest strike orientation. Based on this criteria, a total of eight (8) observed, west-northwest- to northwest-striking, mafic dykes are attributed to the Sudbury swarm of mafic dykes (Figure 5.2.1). Sudbury mafic dykes are green to brown colour when fresh and rusty-coloured when weathered (Figures 5.2.1.6a and 5.2.1.6b). Although no occurrences of olivine, a mineral typically occurring in the Sudbury swarm of dykes, were recognized, these dykes were interpreted to be examples of the Sudbury swarm based primarily on their orientation and colour.

Sudbury mafic dykes occupy anywhere between less than 10% to up to 100% of the outcrop by area at any single bedrock observation location. In several instances, Sudbury mafic dykes were observed at multiple locations along the same dyke segment. Seven representative Sudbury mafic dyke rock samples were collected. The Sudbury mafic dykes are dark grey to green when fresh and light green to grey when weathered (Figures 5.2.1.6a, 5.2.1.6b, and 5.2.1.6c). They are mostly massive in texture. The groundmass of the Sudbury mafic dykes generally varies from very fine- to medium-grained and equigranular texture (Figure 5.2.1.6c). The primary mineral phases observed within the Sudbury mafic dykes include pyroxene and plagioclase, with minor occurrences of biotite and magnetite (Figure 5.2.1.6b).

Most observed Sudbury dyke-granite contacts are intact adjacent to the granite and do not display evidence of brittle reactivation along the contact horizon. A chilled margin was observed at one of the Sudbury mafic dyke

locations. A total of 8 field estimates of intact rock strength were undertaken on the Sudbury mafic dyke exposures. The results all exhibit a very strong (R5) character.

Sudbury mafic dykes observed in the withdrawal area range from 20 cm to approximately 20 m in width, with the majority of dykes (5 out of 8, 63%) between 10 and 20 m wide (Figure 5.2.1.6d). One dyke greater than 20 m in width, and two dykes are under 5 m wide were observed. In some cases, the reported width is a minimum estimate, if only one contact is exposed.

Magnetic susceptibility values for the Sudbury mafic dykes range between 0.51 and 86.6 $x10^{-3}$ SI with an overall mean of 23.4±27.9 x 10^{-3} SI (N=8) (Figure 5.2.1.6e).

The gamma ray spectrometry readings (Figure 5.2.1.6f) for the Sudbury mafic dykes, including 5 sets of measurements, show the following characteristics:

- Total count is on average 159.6±60.0 cps and ranges between 127 and 246 cps.
- Potassium content is on average 1.46±0.31% and ranges between 1.2 and 2.0%.
- Uranium content is on average 1.38±0.54 ppm and ranges between 0.7 and 2.2 ppm.
- Thorium content is on average 10.84±5.84 ppm and ranges between 4.0 and 17.9 ppm.
- Uranium/Thorium ratio is on average 19.6±11.2% and ranges from 0 to 44.0%.

Four of the eight (50%) Sudbury mafic dyke observations are coincident with, or very close to, dyke segments that were previously identified in the lineament analysis and classified as Sudbury swarm dykes. In the four other observation locations, Sudbury mafic dykes were not previously identified in the lineament analysis. These latter four occurrences of Sudbury mafic dykes are either under 3 m wide, or have a low magnetic susceptibility between 0.8 and 0.8$x10^{-3}$ SI.

The dyke contact orientation to the granite host rock was visible and measured at 6 of the 8 locations of Sudbury mafic dyke observations (Figures 5.2.1.7a and 5.2.1.7b). The orientation of Sudbury mafic dyke contacts is dominated by an east-trending peak at 085°, oblique to the strike of the lineaments at which these dykes were observed and their expected west-northwest trend. All Sudbury mafic dyke contacts are uniformly steeply dipping (Figure 5.2.1.7a).

Within the Sudbury mafic dykes, 8 joints and 4 faults were measured during geological mapping. The faults are strike-slip faults striking northwest-southeast and are partly filled with hematite, chlorite, and epidote. Joints within the Sudbury mafic dykes are mostly vertical, but include a smaller number of inclined joints (Figure 5.2.1.7c). The orientation of joints shows two main peaks, one trending east at 088° and another south-southeast at 168° (Figure 5.2.1.7d), orthogonal and parallel to the main Sudbury mafic dyke contact orientations.

The two most common spacing class for joints (3 out of 8, 38%, respectively) within Sudbury mafic dykes are between 3 and 10 cm, and between 30 and 100 cm (Figure 5.2.1.7e). The majority of the joints (7 out of 8, 88%) are spaced under 100 cm apart. In the granite host rock of stations with Sudbury mafic dyke observations, the dominant joint spacing class (5 out of 14, 36%) is between 500 and 1000 cm (Figure 5.2.1.7f). More than half (10 out of 14, 71%) of the joints are spaced over 100 cm apart. Overall, average joint spacing is smaller within the mafic dykes compares to the granite host rock. Additionally, joints within Sudbury mafic dyke rocks show a greater relative number of tightly spaced joints than the average joint spacing for the whole area (Figure 5.1.13f).

5.2.1.3 Biscotasing Mafic Dyke Swarm

At one location (Station 17TC0140) at the shore of Jeanne Lake in the northeast of the withdrawal area, a northeast-trending deformed mafic dyke was observed (Figure 5.2.1.1). The dyke was tentatively attributed to the Biscotasing dyke swarm due to the northeastern strike of its contact to the granite host rock and its vicinity to a dyke lineament interpreted as a Biscotasing mafic dyke. The dyke forms 60-90% of the outcrop and, where observed, its contacts with the surrounding granite host rock are consistently sharp and intact.

The Biscotasing mafic dyke is dark grey when fresh and weathered (Figure 5.2.1.8a). It exhibits a medium-grained gabbro texture with equigranular pyroxene, plagioclase, biotite, and magnetite (Figure 5.2.1.8b). The one field estimate of rock strength of the Biscotasing mafic dyke showed a very strong character (R5). One sample of the Biscotasing mafic dyke was collected.

The contact of the Biscotasing mafic dyke with the granite is oriented 045/90. This dyke is also folded around a northwest-trending (325°) fold axis. The dyke contains 20 to 30 cm spaced joints that form a pair of cylindrical folds in fault contact with a pair of z-type asymmetrical folds (Figure 5.2.1.8a). The contacts between the fold segments are narrow brittle ductile shear zones oriented 320/88, the strike of which is parallel to the strike of the fold axis in the dyke structures. The shear zones are filled with epidote and are less than 1 cm in width and extend into the granite host rock. No slip sense was determined on these structures. An additional northeast-striking brittle-ductile shear zone occurs within the granite, has a width of 1-3 cm and shows dextral sense of slip. One joint set with a spacing greater than 10 m was observed within the granite.

The measurements of magnetic susceptibility of the Biscotasing mafic dyke are 1.100, 0.990, 1.100, 1.100 and 0.630×10^{-3} SI, reflecting a moderate to low magnetic susceptibility. The one gamma ray spectrometry reading for the Biscotasing mafic dyke has a total count of 64.0 cps, potassium content of 0.5%, uranium content of 0.7 ppm, and thorium content of 1.6 ppm.

5.2.1.4 North Channel Mafic Dyke Swarm

In the southeast of the withdrawal area (Station 17IL0150), an irregularly shaped mafic dyke intrudes the granite host rock (Figure 5.2.1.1). The dyke is tentatively attributed to the North Channel swarm based on the proximity to a dyke lineament interpreted as a North Channel mafic dyke. This dyke forms 30-60% of the outcrop and, where observed, its contacts with the surrounding granite host rock are irregular. The outcrop size of 5 x 5 m delimits the minimum width of the dyke, however the dominant strike orientation of the dyke body could not be determined due to the irregular contact geometry. The North Channel mafic dyke is dark green when fresh and grey when weathered (Figures 5.2.1.8c and 5.2.1.8d). The dyke is composed of a very fine grained equigranular matrix surrounding rounded clasts ranging in size from millimetres to one metre (Figures 5.2.1.8c and 5.2.1.8d). The clasts are composed mostly of granite as well as minor amounts of rounded clasts of an unknown lithology. The one field estimate of rock strength of the mafic dyke showed a very strong character (R5). One sample of a North Channel mafic dyke was collected.

The North Channel mafic dyke displays a moderately well-developed foliation oriented 296/88. No joints were observed within this dyke itself. The granite host rock is fractured by north-northeast striking and steeply dipping joints spaced 10 – 30 cm.

The measurements of magnetic susceptibility of the North Channel mafic dyke are 47.4, 17.2, 48.0, 22.7 and 57.2×10^{-3} SI, reflecting a very high magnetic susceptibility. The one gamma ray spectrometry reading for the North

Channel mafic dyke has a total count of 273 cps, potassium content of 1.5%, uranium content of 5.0 ppm, and thorium content of 25.4 ppm. As the dyke contains abundant lithic clasts, the gamma ray spectrometry likely reflects the influence of both the dyke matrix and the granitic clasts.

5.2.1.5 Diatreme Breccia

At two locations (Stations 17TC0067 and 17TC0115) in the centre and north-central part of the withdrawal area, discontinuous patches of diatreme breccia were observed. The diatreme breccia bodies are up to several tens of centimetres wide, matrix supported, and have irregularly shaped and fractured contacts to the granite host rock (Figure 5.2.1.8e) with indications of brittle fracture of the wall rock. The diatreme breccia bodies are composed of a wide variety of lithic clasts, including angular granite host rock fragments and rounded allochthonous clasts (Figure 5.2.1.8f). The granite host rock is notably fractured by the intrusions of the diatreme breccia. No magnetic susceptibility or gamma-ray spectrometry measurements were made on these diatreme breccia bodies. The matrix of the diatreme breccia displays a strong hardness (R4), whereas the granite host rock is very strong (R5).

The diatreme breccia shows an overall west-striking orientation at 258° and is bounded by northeast- and northwest-striking joints within the granite. Joints in the granite host rock at stations of diatreme breccia occurrences are spaced 30 to 500 cm. The matrix of the diatreme breccia displays no internal fabric.

5.2.2 Felsic Dykes

Felsic dykes and veins, including pegmatite and aplite were documented at 21 bedrock observation locations (Figure 5.2.2.1). The majority of the felsic dykes were observed in the central, southern, and northwestern portions of the withdrawal area. This section provides a brief overview of the geological characteristics of these felsic dyke occurrences. Felsic dyke orientation information, and some field examples, are shown on Figure 5.2.2.2.

Felsic dykes represent a very small component of the bedrock in the withdrawal area. In these documented occurrences, felsic veins primarily occupy much less than 10% of the outcrop by area. They range in width between 3 and 30 cm (e.g., Figures 5.2.2.2c and 5.2.2.2d). They are observed to transect the bedrock as single, linear dykes. Often these dykes are observed to be hosted by fractures that are parallel to unfilled joints. The surrounding granite bedrock consistently shows no increase in fracturing adjacent to, or along the contact with, these emplaced felsic dykes. Pegmatite dykes often occur at stations with gneissic xenoliths and are observed to cross-cut or form a margin, or rind, around these xenoliths (Figure 5.2.2.2d).

The felsic dykes are primarily beige or pink when fresh and pink to off-white when weathered (Figures 5.2.2.2c and 5.2.2.2d). Variations in grainsize are evident between occurrences. Felsic dykes are characterized as aplitic when finer-grained, with grainsize varying between 0.1 to 5 mm, and pegmatitic when coarse-grained, with grainsize up to 50 mm. Most felsic dykes are equigranular, although in few cases coarse-grained K-feldspar phenocrysts up to 50 mm were observed within a finer-grained matrix. The main matrix minerals include plagioclase, quartz, K-feldspar and biotite. Felsic dykes are uniformly observed as massive.

Where there is a clear grainsize or colour difference between the felsic dyke and the surrounding bedrock the contact is sharp. In some instances, negligible colour or grainsize differences highlight a gradational contact. In all instances the observed contacts between felsic dykes and the surrounding bedrock are intact. There is no evidence of brittle deformation localized along these contacts.

The majority of the felsic dykes are steeply-dipping (Figure 5.2.2.2a). The total felsic dyke population exhibit three dominant orientation peaks trending south at 175° and ranging between 167° and 181°, trending east- southeast-

at 087° and ranging between 082° and 109°, as well as trending north-northeast with peaks at 012° and 025° (Figure 5.2.2.2b). These peaks are roughly orthogonal and parallel to the main east-trending orientation of foliation in the Withdrawal area. An additional prominent peaks is evident trending southeast at 140° (Figure 5.2.2.2b).

The one field estimate of rock strength of the felsic dykes showed a very strong character (R5). No felsic dyke samples were collected.

6.0 SUMMARY OF FINDINGS

6.1 Elliott Lake and Blind River Area

The withdrawal area is accessible via a network of logging roads, some of which were accessible using a 4X4 vehicle. The balance of the logging roads were overgrown or contained washouts requiring ATV of foot traverses for access. Other areas lacked any form of road or trail network and were accessed by overland foot traverse or by canoe. Multiple modes of transportation were often required to access specific areas of interest. Topography is a mixture of low relief areas characterized by extensive granite pavements (Figures 5.1.2a and 5.1.2b), moderate-relief topographic domes, and more rugged terrain cross-cut by steep sided valleys and scarps with up to 60 m of vertical relief (Figures 5.1.2c and 5.1.2d). In general, the steep valleys appear to be largely structurally controlled and to coincide with mapped dykes and/or interpreted faults. Scarps often preferentially occur in the “down ice” side of uplands and may represent roches moutonées.

Forest cover is continuous except for wetlands, cutover blocks, and areas of extensive exposed bedrock. In outwash plains and upland areas, the forest cover is dominated by jack pine while a mixture of spruce, poplar, birch, maple, and alder typically dominate low-lying areas. Areas of mature forest were frequently open and presented no difficulties for foot traverses however dense successional forest cover made access difficult in older cutover areas and along the margins of lakes and wetlands.

6.1.1 Lithology of the Withdrawal Area

Only one main lithological unit, a medium-grained granite, was identified in the withdrawal area and it is described first below. Minor lithological units locally occur in the form of xenoliths of varying composition within the granite. Dykes of mafic and felsic composition were observed in multiple locations across the withdrawal area.

The granite is most commonly light grey to beige or pink when weathered and predominantly pink to off white or light grey when fresh. The main mineral phases within the granite are quartz, plagioclase, alkali feldspar and biotite. The main accessory mineral is magnetite. The granite is typically weakly foliated although moderate to strong foliation is developed locally. Xenoliths are not evenly distributed but rather appear to be concentrated in an approximately 4 km wide east-northeast-trending band along the northern margin of the withdrawal area. The presence of distinct linear trends of xenolith-rich granite suggests that the batholith may have intruded locally along planes in mafic gneissic host rock.

The majority of mafic dykes in the withdrawal area strike northwest to north-northwest and are attributed to the Matachewan mafic dyke swarm. Dykes are generally several tens of meters wide and have a diabase composition. Several mafic dykes are attributed to the Sudbury dyke swarm. One northeast-striking mafic dyke is attributed to the Biscotasing mafic dyke swarm. A west-northwest-striking mafic dyke with rounded granitic clasts is tentatively attributed to the North Channel mafic dyke swarm. Two occurrences of diatreme breccia with a soft epidote-chlorite

matrix and allochthonous rounded clasts together with angular granite fragments were documented in the Withdrawal area. Felsic dykes, mostly aplite and pegmatite, occur locally throughout the withdrawal area.

6.1.2 Structure of the Withdrawal Area

The most common ductile structure measured in the withdrawal area is weakly to moderately well-developed igneous flow foliation, which predominantly trends east-west and is steeply dipping. Tectonic foliation is weakly to moderately-developed throughout the area and also strikes east-west, parallel to the igneous flow foliation.

Ductile shear zones are uncommon in the withdrawal area, with only seven occurrences mapped. Fifty-seven brittle ductile shear zones occur mainly in the northwest and south-central portion of the withdrawal area. Brittle-ductile shear zones strike dominantly northwest and dip steeply. The width of these shear zones ranges mostly between 1-3 cm, but they are occasionally up to 0.3 m wide and with an anastomosing geometry. Brittle-ductile shear zones are associated with chlorite infill (42%), and occasionally with epidote (28%), quartz (20%), cataclasite (16%) and hematite (8%).

Joints, faults, and veins are the main brittle structure types documented during the geological mapping. Most of the measured joints are sub-vertical, with dominant joint orientations north-northeast to east-northeast and northwest to north-northwest. Infilling was observed on approximately 7% of joint surfaces. Joint spacing is variable, ranging from <1 cm to several tens of meters, with most of the joints falling into the 100 to 500 cm spacing class. Overall, widely spaced (500–1000 cm) joints were observed in the central portion of the Withdrawal area. Sub-horizontal joints make up 13% of the overall joint population and are generally spaced several meters apart.

A total of 186 fault measurements were collected throughout the withdrawal area, with lesser faults occurring in the centre of the withdrawal area. The majority of the measured faults were steeply dipping, with the dominant strike north-northeast and east-northeast, as well as a lesser population of northwest-striking faults. Damage zones of faults range from thin, single slip surfaces to metre wide zones parallel to the fault plane. Faults display mineral infill in the majority of occurrences (63%), the most common minerals are chlorite (25%) and epidote (23%). Cataclasite (17%), quartz (16%), and hematite (14%) are additional mineral infills observed on faults.

Veins occur rarely in the withdrawal area. The majority of veins are extensional and filled with quartz, with lesser occurrences of chlorite and magnetite veins. The majority of observed veins are less than 3 cm in width. Veins strike mostly north to north-northeast and east-southeast and are primarily steeply-dipping.

6.2 Structural History of the Blind River and Elliot Lake Area

A brief synthesis of lithological and structural observations from the outcrop mapping activity is provided below as a general summary of the geological history of the area:

The oldest fabric is a relict tectonic gneissosity observed in some of the xenolith occurrences. A younger igneous flow foliation is weakly developed in the granite throughout the withdrawal area and may reflect the geometry of the magma chamber as it occurs in an orientation parallel to zones of xenolith abundance. Tectonic foliation is oriented parallel to the igneous flow foliation and may have locally realigned the earlier fabric.

Ductile shear zones occur rarely. Brittle-ductile shear zones generally display a minor ductile character to what are predominantly brittle features. These shear zones strike predominantly northwest-southeast. They may have formed at the same time as emplacement of northwest-trending mafic dykes, or they may represent discontinuities along which northwest-trending mafic dykes were emplaced. Brittle reactivation documented by faults and breccia

at some margins of northwest-trending dykes indicate tectonic activity post-dating the emplacement of Matachewan dykes at 2.473 Ga.

It is difficult to assign mapped structures to different tectonic events that occurred during the Proterozoic as the different mafic dyke swarms followed generally similar northwesterly trending orientations and northeast-trending dyke swarms are only sparsely represented within the Withdrawal area.

The majority of brittle faults are associated with mineral infill, commonly chlorite and epidote, indicating that these faults were located at depth during fault activity. The occurrence of cohesive cataclasite in several faults provide additional evidence for deformation at a minimum depth.

While many of the brittle joints are undoubtedly of comparatively recent origin related to erosional and/or glacial unloading, at least some of the brittle joints are ancient features as they locally are observed to contain mafic dyke infill. Erosional unloading would have occurred at several periods since the Archaean notably during the Paleoproterozoic when Huronian sedimentary deposition occurred on an erosional paleosurface. The presence of short centimetre-scale hematite-coated fractures in many locations suggests the influence of glacial unloading from Pleistocene-age glacial events predating the most recent late Wisconsinan glaciation.

7.0 REFERENCES

Barnett, P.J., A.P. Henry and D. Babuin, 1991. Quaternary geology of Ontario, east-central sheet; Ontario Geological Survey, Map 2555, scale 1:1,000,000.

Barnett, P.J., 1992. Quaternary Geology of Ontario; *in* Geology of Ontario, Ontario Geological Survey, Special Volume 4, Part 2, p. 1010–1088.

Bennett G, B.O. Dressler and J.A. Robertson, 1991. The Huronian Supergroup and Associated Intrusive Rocks. *in* Geology of Ontario. Ontario Geological Survey, Special Volume 4, Part 1, p. 549-591.

Berman, R.G., R.M. Easton and L. Nadeau, 2000. A New Tectonometamorphic Map of the Canadian Shield: Introduction. The Canadian Mineralogist **38**, p. 277-285.

Berman, R.G., M. Sanborn-Barrie, R.A. Stern and C.J. Carson, 2005. Tectonometamorphism at ca. 2.35 and 1.85 Ga in the Rae Domain, western Churchill Province, Nunavut, Canada: Insights from structural, metamorphic and in situ geochronological analysis of the southwestern Committee Bay Belt. The Canadian Mineralogist **43**, p. 409-442.

Bleeker, W. and B. Hall, 2007. The Slave Craton: Geology and metallogenic evolution; *in* Mineral deposits of Canada: A synthesis of major deposit-types, district metallogeny, the evolution of geological provinces, and exploration methods. Geological Association of Canada, Mineral Deposits Division, Special Publication No. 5, p. 849-879.

Breaks, F.W. and W.D. Bond, 1993. The English River Subprovince-An Archean Gneiss Belt: Geology, Geochemistry and associated mineralization; Ontario Geological Survey, Open File Report 5846, v.1, p. 1-483.

Buchan, K.L., J.K. Mortensen and K.D. Card, 1993. Northeast-trending Early Proterozoic dykes of southern Superior Province: multiple episodes of emplacement recognized from integrated paleomagnetism and U - Pb geochronology. Can. J. Earth Sci. **30**, p. 1286-1296.

Buchan, K.L., H.C. Halls, and J.K. Mortensen, 1996. Paleomagnetism, U–Pb geochronology, and geochemistry of Marathon dykes, Superior Province, and comparison with the Fort Frances swarm. Can. J. Earth Sci. **33**, p. 1583-1595.

Buchan, K.L. and R.E. Ernst, 2004. Diabase dyke swarms and related units in Canada and adjacent regions. Geological Survey of Canada, Map 2022A, scale 1:5,000,000.

Card, K.D., 1978. Geology of the Sudbury-Manitoulin area, districts of Sudbury and Manitoulin. Ontario Geological Survey, Report 166, 238 p.

Card, K.D., 1979. Regional geological synthesis, Central Superior Province. Geological Survey of Canada, Paper 79-1A, p. 87-90.

Card, K. D., W.R. Church, J.M. Franklin, M.J. Frarey, J.A. Robertson, G.F. West, and G.M. Young, 1972. The Southern Province; *in* Variations in Tectonic Styles in Canada. Geological Association of Canada, Special Paper No. 11. P. 335-380.

Card, K.D., and D.G. Innes, 1981. Geology of the Benny Area, District of Sudbury. Ontario Geological Survey Report 206, 117 p.

Corfu, F. and E.C. Grunsky, 1987. Igneous and tectonic evolution of the Batchawana greenstone belt, Superior Province: a U-Pb zircon and titanite study. Journal of Geology **95**, p. 87-105.

Corfu, F., G.M. Stott and F.W. Breaks, 1995. U-Pb Geochronology and evolution of the English River Subprovince, an Archean low P-highT metasedimentary belt in the Superior Province. Tectonics **14**, p. 1220-1233.

Corrigan, D., A.G. Galley and S. Pehrsson, 2007. Tectonic evolution and metallogeny of the southwestern Trans-Hudson Orogen; *in* Mineral deposits of Canada: A synthesis of major deposit-types, district metallogeny, the evolution of geological provinces, and exploration methods. Geological Association of Canada, Mineral Deposits Division, Special Publication No. 5, p. 881-902.

Cowan, W.R., 1976. Quaternary Geology of the Sault Ste. Marie Area, District of Algoma; *in* Summary of Fieldwork, 1976. Geological Branch, Ontario Division of Mines, Miscellaneous Paper 67, p. 134-136.

Cowan, W. R., 1985. Deglacial Great Lakes Shorelines at Sault Ste. Marie, Ontario; *in* Quaternary Evolution of the Great Lakes. Geological Association of Canada Special Paper 30, p. 33-37.

Cowan, W. R., and G. Bennett, 1998. Urban Geology: City of Sault Ste. Marie, Ontario; *in* Urban Geology of Canadian Cities. Geological Association of Canada Special Paper 42, p. 197-205.

Cruden, A.R., 2006. Emplacement and growth of plutons: implications for rates of melting and mass transfer in continental crust; *in* Evolution and Differentiation of the Continental Crust. Cambridge University Press, Cambridge, UK, p. 455-519.

Davidson, A., O. van Breeman, R.W. Sullivan, 1992. Circa 1.75 Ga ages for plutonic rocks of the Southern Province and adjacent Grenville Province: what is the expression of the Penokean orogeny? *in* Radiogenic Age and Isotopic Studies: Report 6, Geological Survey of Canada, Paper 92-2, p.107-118.

Easton, R.M., 2000a. Metamorphism of the Canadian Shield, Ontario, Canada. I. The Superior Province. The Canadian Mineralogist **38**, p. 287-317.

Easton, R.M., 2000b. Metamorphism of the Canadian Shield, Ontario, Canada. II. Proterozoic metamorphic history. The Canadian Mineralogist **38**, p. 319-344.

Easton, R. M., 2005, Geology of Porter and Vernon townships, Southern Province; *in* Summary of Field Work and Other Activities, 2005. Ontario Geological Survey, Open File Report 6172, p. 13–1 to 13–20.

Easton, R.M. 2009. Compilation Mapping, Pecors–Whiskey Lake Area, Southern and Superior Provinces; *in* Summary of Field Work and Other Activities 2010. Ontario Geological Survey, Open File Report 6240, 254 p.

Easton, R.M. 2010. Compilation Mapping, Pecors–Whiskey Lake Area, Southern and Superior Provinces; *in* Summary of Field Work and Other Activities 2010. Ontario Geological Survey, Open File Report 6260, p. 8-1 to 8-12.

Easton, R.M., L.S. John-Bevans and R.S. James, 2004. Geological Guidebook to the Paleoproterozoic East Bull Lake Intrusive Suite Plutons at East Bull Lake, Agnew Lake and River Valley, Ontario. Ontario Geological Survey, Open File Report 6315, 84 p.

Eschman, D. F. and P. F. Karrow, 1985. Huron Basin Glacial Lakes: A Review; *in* Quaternary Evolution of the Great Lakes. Geological Association of Canada Special Paper 30, p. 79-93.

Fedo, C.M., G.M. Young, H.W. Nesbitt, and J.M. Hanchar, 1997. Potassic and sodic metasomatism in the Southern Province of the Canadian Shield: evidence from the Paleoproterozoic Serpent Formation, Huronian Supergroup, Canada. Precambrian Research **84**, p. 17-36.

Ford, M.J., 1993. The Quaternary Geology of the Rawhide Lake area, District of Algoma. Ontario Geological Survey, Open File Report 5867, 10 p.

Fraser, J.A. and W.W. Heywood (editors), 1978. Metamorphism in the Canadian Shield. Geological Survey of Canada, Paper 78-10, 367p.

Gartner, J.F., 1978a. Northern Ontario Engineering Geology Terrain Study, data base map, Cartier, NTS 41I/NW. Ontario Geological Survey, Map M5000, scale 1:100,000.

Gartner, J.F., 1978b. Northern Ontario Engineering Geology Terrain Study, data base map, Espanola, NTS 41I/SW. Ontario Geological Survey, Map M5002, scale 1:100,000.

Gartner, J.F., 1978c. Northern Ontario Engineering Geology Terrain Study, general construction capability map, Cartier, NTS 41I/NW. Ontario Geological Survey, Map M5004, scale 1:100,000.

Gartner, J.F., 1980a. Cartier Area (NTS 41I/NW), Districts of Algoma and Sudbury. Ontario Geological Survey, Northern Ontario Engineering Geology Terrain Study 94, 18 p.

Gartner, J.F., 1980b. Espanola Area (NTS 41I/SW), Districts of Manitoulin and Sudbury. Ontario Geological Survey, Northern Ontario Engineering Geology Terrain Study 99, 14 p.

Gartner, J.F., J.D. Mollard and M.A. Roed, 1981. Ontario Engineering Geology Terrain Study User's Manual. Ontario Geological Survey, Northern Ontario Engineering Geology Terrain Study 1.

Geofirma, 2012a. Initial Screening for Siting a Deep Geological Repository for Canada's Used Nuclear Fuel, City of Elliot Lake, Ontario; Document ID: 10-214-5_Initial Screening Blind River_R0, August 24, 2012

Geofirma, 2012b. Initial Screening for Siting a Deep Geological Repository for Canada's Used Nuclear Fuel, Town of Blind River, Ontario; Document ID: 10-214-5_Initial Screening Elliot Lake_R0, August 24, 2012

Giblin, P.E., 1976. Report of the Northeastern Regional Geologist and Sault Ste. Marie Resident Geologist; p. 91-99 in Annual Report of the Regional and Resident Geologist, 1975, edited by C.R. Kustra, Ontario Division of Mines, MP64, 146p.

Giblin, P.E., E.J. Leahy and J.A. Robertson, 1977. Geological Compilation of the Blind River-Elliot Lake Sheet, Districts of Algoma and Sudbury. Ontario Geological Survey Preliminary Map P.304, scale 126,720.

Golder, 2014. Phase 1 Desktop Geoscientific Preliminary Assessment of Potential Suitability for Siting a Deep Geological Repository for Canada's Used Nuclear Fuel, City of Elliot Lake, Town of Blind River,

Township of The North Shore, and Town of Spanish, Ontario. Report for the Nuclear Waste Management Organization (NWMO). NWMO report number: APM-REP-06144-009

Golder, 2017a. Work Plan: Observation of General Geological Features (OGGF) and Detailed Outcrop Mapping – North of Huron, 30p.

Golder, 2017b. Project Quality Plan: North of Huron Communities OGGF and Detailed Outcrop Mapping, 105p.

Golder, 2017c. Health Safety and Environment Plan: OGGF and Detailed Outcrop Mapping – North of Huron, 30p.

Gordon C.A., 2012 Preliminary Results from the Otter–Morin Townships Bedrock Mapping Project, Southern and Superior Provinces; *in* Summary of Field Work and Other Activities 2012. Ontario Geological Survey, Open File Report 6280, p. 17-1 to 17-10.

Halls, H.C., D.W. Davis, G.M. Stott, R.E. Ernst, and M.A. Hamilton, 2008. The Paleoproterozoic Marathon Large Igneous Province: New evidence for a 2.1 Ga long-lived mantle plume event along the southern margin of the North American Superior Province. Precambrian Research **162**, p. 327-353.

Hamilton, M.A, D.W. Davis, K.L. Buchan, and H.C. Halls,, 2002. Precise U-Pb dating of reversely magnetized Marathon diabase dykes and implications for emplacement of giant dyke swarms along the southern margin of the Superior Province, Ontario., *in* Current Research, Geological Survey of Canada, 2002-F6, p. 1-8.

Heather, K. B., G.T. Shore, and O. van Breeman, 1995. The convoluted “layer cake”, an old recipe with new ingredients for the Swayze greenstone belt, southern Superior Province, Ontario; *in* Current Research, Geological Survey of Canada, 1995-C, p. 1-10.

Holm, D.K., D.A. Schneider, C. O'Boyle, M. A. Hamilton, M.J. Jercinovic and M. L. Williams, 2001. Direct timing constraints on Paleoproterozoic metamorphism, southern Lake Superior region: results from SHRIMP and EMP U-Pb dating of metamorphic monazites; Geological Society of America, Abstracts with Program, v.33, no.6, p.A-401.

JDMA (J.D. Mollard and Associates Ltd.), 2014a. Phase 1 Geoscientific Desktop Preliminary Assessment, Terrain and Remote Sensing Study, City of Elliot Lake, Town of Blind River, Township of The North Shore, Town of Spanish, Ontario. Prepared for Nuclear Waste Management Organization (NWMO). NWMO Report Number: APM-REP-06144-0092.

JDMA (J.D. Mollard and Associates Ltd.), 2014b. Phase 1 Geoscientific Desktop Preliminary Assessment, Lineament Interpretation, City of Elliot Lake, Town of Blind River, Township of The North Shore, Town of Spanish, Ontario. Prepared for Nuclear Waste Management Organization (NWMO). NWMO Report Number: APM-REP-06144-0094.

Jackson, S.L. and J.A. Fyon, 1991. The Western Abitibi Subprovince in Ontario; *in* Geology of Ontario. Ontario Geological Survey, Special Volume 4, Part 1, p. 405-482Jackson, S.L., 2001. On the structural geology of the Southern Province between Sault Ste. Marie and Espanola, Ontario. Ontario Geological Survey, Open File Report 5995, 55 p.

Jensen, L.S., 1994. Geology of the Whiskey Lake Greenstone Belt (West Half), Districts of Sault Ste. Marie and Sudbury. Ontario Geological Survey, Open File Report 5883, 101 p.

Jolly, W.T., 1978. Metamorphic history of the Archean Abitibi Belt; *in* Metamorphism in the Canadian Shield. Geological Survey of Canada, Paper 78-10, p. 63-78.

Karrow, P.F., 1987. Glacial and glaciolacustrine events in northwestern Lake Huron, Michigan and Ontario Geological Society of America Bulletin **98**, p. 113-120.

Kamo, S.L., T.E. Krogh, and P.S. Kumarapelli, 1995. Age of the Grenville dyke swarm, Ontario–Quebec: implications for the timing of lapetan rifting. Can. J. Earth Sci., **32** (3): 273-280,

Kraus, J. and T. Menard, 1997. A thermal gradient at constant pressure: Implications for low- to medium-pressure metamorphism in a compressional tectonic setting, Flin Flon and Kisseynew domains, Trans-Hudson Orogen, Central Canada. The Canadian Mineralogist **35**, p. 1117-1136.

Krogh, T.E., F. Corfu, D.W. Davis, G.R. Dunning, L.M. Heaman, S.L. Kamo, N. Machado, J.D. Greenough and E. Nakamura, 1987. Precise U-Pb isotopic ages of diabase dykes and mafic to ultramafic rocks using trace amounts of baddeleyite and zircon; *in* Mafic dyke swarms. Geological Association of Canada, Special Paper 34, p. 147-152.

McCrank, G.F.D., D.C. Kamineni, R.B. Ejeckam and R. Sikorsky, 1989. Geology of the East Bull Lake gabbro-anorthosite pluton, Algoma District, Ontario. Can. J. Earth Sci. **26**, p. 357-375.

Menard, T. and T.M. Gordon, 1997. Metamorphic P-T paths from the Eastern Flin Flon Belt and Kisseynew Domain, Snow Lake, Manitoba. The Canadian Mineralogist **35**, p. 1093-1115.

OGS (Ontario Geological Survey), 1997. Bedrock geology of Ontario, explanatory notes and legend, Ontario Geological Survey, Map 2545.

OGS (Ontario Geological Survey), 2011. Mineral Deposit Inventory-2011. Ontario Geological Survey.

Osmani, I.A., 1991. Proterozoic mafic dyke swarms in the Superior Province of Ontario; *in* Geology of Ontario, Ontario Geological Survey, Special Volume 4, Part 1, p. 661-681.

PGW (Paterson, Grant and Watson Limited), 2014. Phase 1 Geoscientific Desktop Preliminary Assessment, Processing and Interpretation of Geophysical Data, City of Elliot Lake, Town of Blind River, the Township of The North Shore, Town of Spanish, Ontario. Prepared for Nuclear Waste Management Organization (NWMO). NWMO Report Number: APM-REP-06144-0093.

Palmer, H.C., R.E. Ernst and K.L. Buchan, 2007. Magnetic fabric studies of the Nipissing sill province and Senneterre dykes, Canadian Shield, and implications for emplacement, Can. J. Earth Sci. **44**, p. 507-528.

Pease, V., J. Percival, H. Smithies, G. Stevens and M. Van Kranendonk, 2008. When did plate tectonics begin? Evidence from the orogenic record; *in* When Did Plate Tectonics Begin on Earth? Geological Society of America Special Paper 440, p. 199-228.

Percival, J.A., M. Sanborn-Barrie, T. Skulski, G.M. Stott, H. Helmstaedt and D.J. White, 2006. Tectonic evolution of the western Superior Province from NATMAP and Lithoprobe studies. Can. J. Earth Sci. **43**, p. 1085-1117.

Piercey, P., D.A. Schneider and D.K. Holm, 2003. Petrotectonic evolution of Paleoproterozoic rocks across the 1.8 Ga Central Penokean orogen, northern MI & WI. Geological Society of America, Abstracts **35**, 554 p.

Piercey, P., 2006. Proterozoic Metamorphic Geochronology of the Deformed Southern Province, Northern Lake Huron Region, Canada: unpublished M.Sc. Thesis, Ohio University, 67 p.

Powell, W.G., D.M. Carmichael and C.J. Hodgson, 1993. Thermobarometry in a subgreenschist to greenschist transition in metabasites of the Abitibi greenstone belt, Superior Province, Canada. J. Metamorphic Geology **11**, p.165-178.

Raharimahefa, T., D.K. Tinkham and B. Lafrance, 2011. New U-Pb Geochronological Constraints on the Structural Evolution of the Southern Province, Sudbury, Canada. Paper No. 101-10. 2011 GSA Annual Meeting in Minneapolis. 9-12 October 2011.

Riller, U., W.M Schwerdtner, H.C Halls, and K.D Card, 1999. Transpressive tectonism in the eastern Penokean orogen, Canada: Consequences for Proterozoic crustal kinematics and continental fragmentation. Precambrian Research **93**, p. 51–70.

Robertson, J.A., 1965a. Ontario Department of Mines Preliminary Geology Map No P318, Shedden Township Part IR No 7.

Robertson, J.A., 1965b. Ontario Department of Mines Preliminary Geology Map No P319, IR No 7 East and Offshore, District of Algoma.

Robertson, J.A., 1965c. Ontario Department of Mines Preliminary Geology Map No P320, IR No 5 West and Offshore Islands, District of Algoma.

Robertson, J.A. 1968. Geology of Township 149 and Township 150, District of Algoma. Ontario Department of Mines, Geological Report 57, 162 p.

Robertson, J.A., 1970. Geology of the Spragge area, District of Algoma. Ontario Department of Mines, Geological Report Number 76, 109 p.

Robertson, J.A., and J.M. Johnson, 1965. Ontario Department of Mines Preliminary Geology Map No P317, Deagle Township, District of Algoma.

Roed, M.A. and D.R. Hallett,. 1979a. Northern Ontario Engineering Geology Terrain Study, data base map, Biscotasing, NTS 41O/SE. Ontario Geological Survey, Map M5017, scale 1:100,000.

Roed, M.A. and D.R. Hallett, 1979b. Northern Ontario Engineering Geology Terrain Study, data base map, Wenebegon Lake, NTS 41O/SW. Ontario Geological Survey, Map M5016, scale 1:100,000.

Roed, M.A. and D.R. Hallett, 1979c. Northern Ontario Engineering Geology Terrain Study, data base map, Westree, NTS 41P/SW. Ontario Geological Survey, Map M5022, scale 1:100,000.

Rogers, M.C., 1992. Geology of the Whiskey Lake Area, East Half. Ontario Geological Survey, Open File Report 5834, 109 p.

SGL, 2017. Phase 2 Geoscientific Preliminary Assessment, Acquisition, Processing and Interpretation of High-Resolution Airborne Geophysical Data, Elliot Lake and Blind River Area, Ontario. APM-REP-01332-0217.

SRK, 2016. Data Collection System for Outcrop Mapping: Overview, Procedures and Guidance. SRK Consulting (Canada) Inc., 27p.

SRK, 2017. Phase 2 Geoscientific Preliminary Assessment, Lineament Interpretation, Elliot Lake and Blind River Area, Ontario. APM-REP-01332-0218

Sage, R.P., 1988. Geology of Carbonatite Alkalic Rock Complexes in Ontario: Seabrook Lake Carbonatite Complex, District of Algoma. Ontario Geological Survey, Study 31, 45 p.

Shimamura, K., Williams, S. P. and Buller, G. 2008. Ganfeld user guide: a map-based field data capture system for geoscientists. Geological Survey of Canada, Open File 5912, 90 p.

Siemiatkowska, K.M., 1977. Geology of the Wakomata Lake area. Ontario Division of Mines, Geological Report 151, 57p. Accompanied by map 2350, scale 1 inch to 1/2 mile (1:31,680).

Spray, J.G., H.R Butler, and L.M. Thompson, 2004. Tectonic influences on the morphometry of the Sudbury impact structure: Implications for terrestrial cratering and modeling. Meteoritics and Planetary Science 39, 2, p. 287-301.

Thurston, P.C., 1991. Geology of Ontario: Introduction; *in* Geology of Ontario, Special Volume No. 4, Part 1, p. 3-26.

van Breemen, O., K.B. Heather, and J.A. Ayer, 2006. U-Pb geochronology of the Neoarchean Swayze sector of the southern Abitibi greenstone belt. Current Research 2006 F1, Geological Survey of Canada.

VanDine, D.F., 1979a. Northern Ontario Engineering Geology Terrain Study, database map, Bark Lake, NTS 41J/NE. Ontario Geological Survey, Map 5006, scale 1:100,000.

VanDine, D.F., 1979b. Northern Ontario Engineering Geology Terrain Study, database map, Blind River, NTS 41J/SE. Ontario Geological Survey, Map 5008, scale 1:100,000.

VanDine, D.F., 1979c. Northern Ontario Engineering Geology Terrain Study, database map, Thessalon, NTS 41J/SW. Ontario Geological Survey, Map 5007, scale 1:100,000.

VanDine, D.F., 1979d. Northern Ontario Engineering Geology Terrain Study, database map, Wakomata Lake, NTS 41J/NW. Ontario Geological Survey, Map 5005, scale 1:100,000.

VanDine, D.F., 1980a. Bark Lake Area (NTS 41J/NE), Districts of Algoma and Sudbury. Ontario Geological Survey, Northern Ontario Engineering Geology Terrain Study 93, 12 p.

VanDine, D.F., 1980b. Blind River Area (NTS 41J/SE), Districts of Algoma, Manitoulin, and Sudbury. Ontario Geological Survey, Northern Ontario Terrain Study 98, 14 p.

VanDine, D.F., 1980c. Thessalon Area (NTS 41J/SW), District of Algoma. Ontario Geological Survey, Northern Ontario Engineering Geology Terrain Study 97, 16 p.

VanDine, D.F., 1980d. Wakomata Lake Area (NTS 41J/NW), District of Algoma. Ontario Geological Survey, Northern Ontario Engineering Geology Terrain Study 92, 13 p.

Vogel D.C., R.S. James and R.R. Keays, 1998. The early tectono-magmatic evolution of the Southern Province: implications from the Agnew Intrusion, central Ontario, Canada. Can. J. Earth Sci. **35**, p. 854-870.

Williams, H., P.F. Hoffman, J.F. Lewry., J.W.H. Monger and T. Rivers, 1991. Anatomy of North America: thematic portrayals of the continent. Tectonophysics **187**, p. 117–134.

Zolnai, A.l., R.A. Price and H. Helmstaedt, 1984. Regional cross section of the Southern Province adjacent to Lake Huron, Ontario: implications for the tectonic significance of the Murray Fault Zone. Can. J. Earth Sci. **21**, p. 447-456.

Report Signature Page

GOLDER ASSOCIATES LTD.

Iris Lenauer, Ph.D., P.Geo.
Senior Structural Geologist, PGW

Charles Mitz, Ph.D., P.Geo.
Senior Engineering Geologist, Golder

George Schneider, M.Sc., P.Geo.
Senior Geoscientist – Principal, Golder

IL/CM/GWS/

c:\users\cmitz\downloads\1651985 noh mapping report 24nov2017.docx

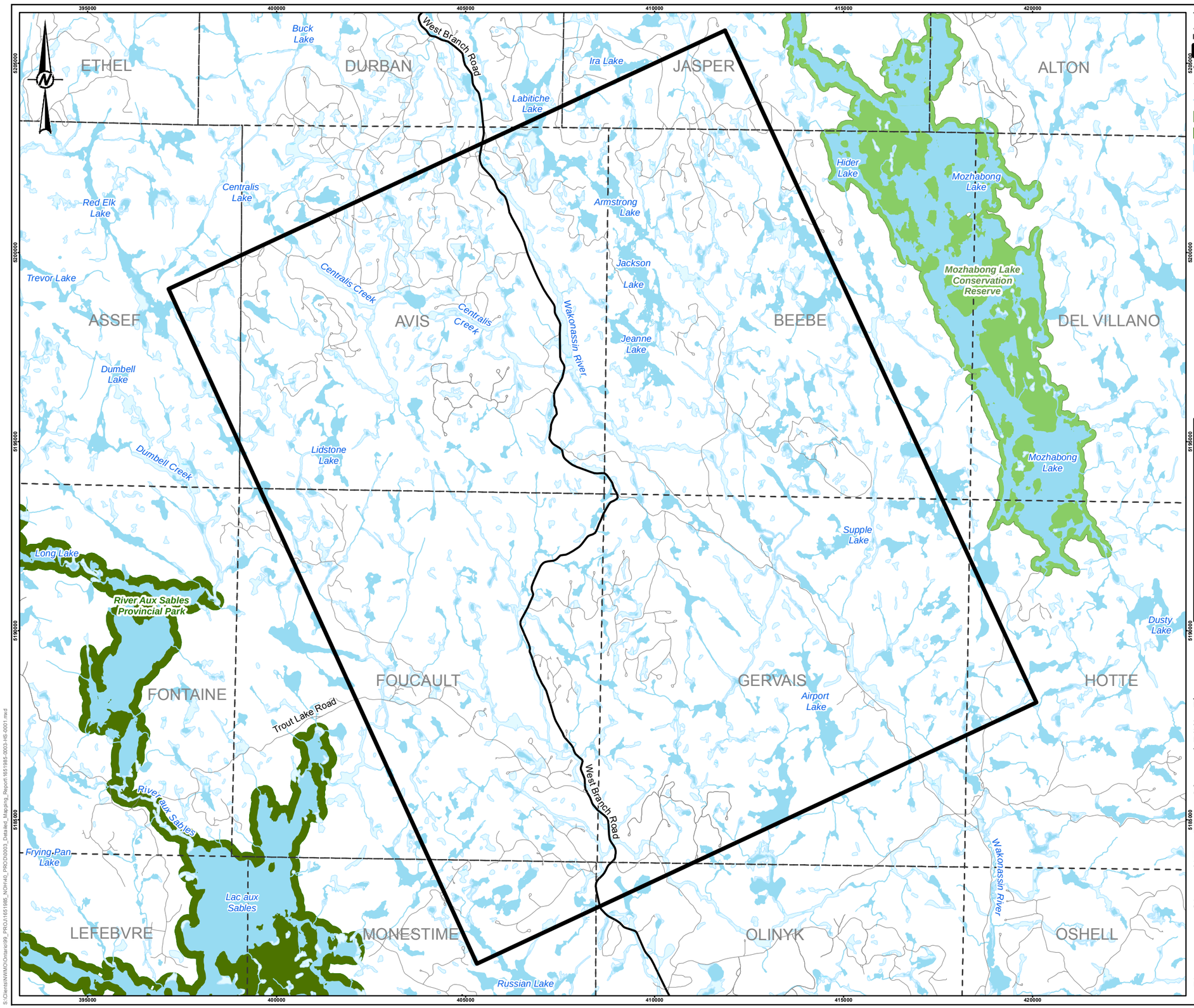

LEGEND

- Geographic Township
- Withdrawal Area
- Main Road
- Local Road
- Watercourse
- Conservation Reserve
- Provincial Park
- Waterbody
- Wetland

INDEX MAP

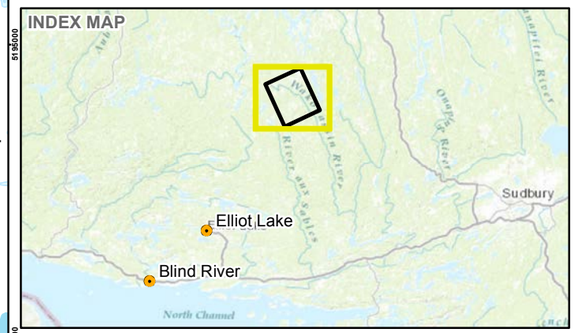

0 4 8

1:100,000 KILOMETRES

REFERENCE(S)

1. LIO (2017).
2. BEDROCK GEOLOGY, MRD126 REV-1, OGS (2011).
3. PRODUCED BY GOLDER ASSOCIATES LTD UNDER LICENCE FROM ONTARIO MINISTRY OF NATURAL RESOURCES AND FORESTRY, © QUEENS PRINTER 2017
4. PROJECTION: TRANSVERSE MERCATOR DATUM: NAD 83 COORDINATE SYSTEM: UTM ZONE 17

CLIENT
NWMO
BLIND RIVER, ELLIOT LAKE AND AREA, ONTARIO

PROJECT
BLIND RIVER, ELLIOT LAKE AND AREA GEOLOGICAL MAPPING REPORT

TITLE
BLIND RIVER AND ELLIOT LAKE AREA - STUDY AREA

CONSULTANT
Golder Associates

YYYY-MM-DD	2017-11-23
DESIGNED	JB
PREPARED	JB
REVIEWED	CM
APPROVED	GWS

PROJECT NO. 1651985 | CONTROL | REV. | FIGURE **1.1**

IF THIS MEASUREMENT DOES NOT MATCH WHAT IS SHOWN, THE SHEET SIZE HAS BEEN MODIFIED FROM: 25mm 0

S:\Clients\NWMO\Ontario\99_PROJ\1651985_NOH\40_PROD\0003_Data\ecl_Mapping_Report\1651985-0003-HS-0001.mxd

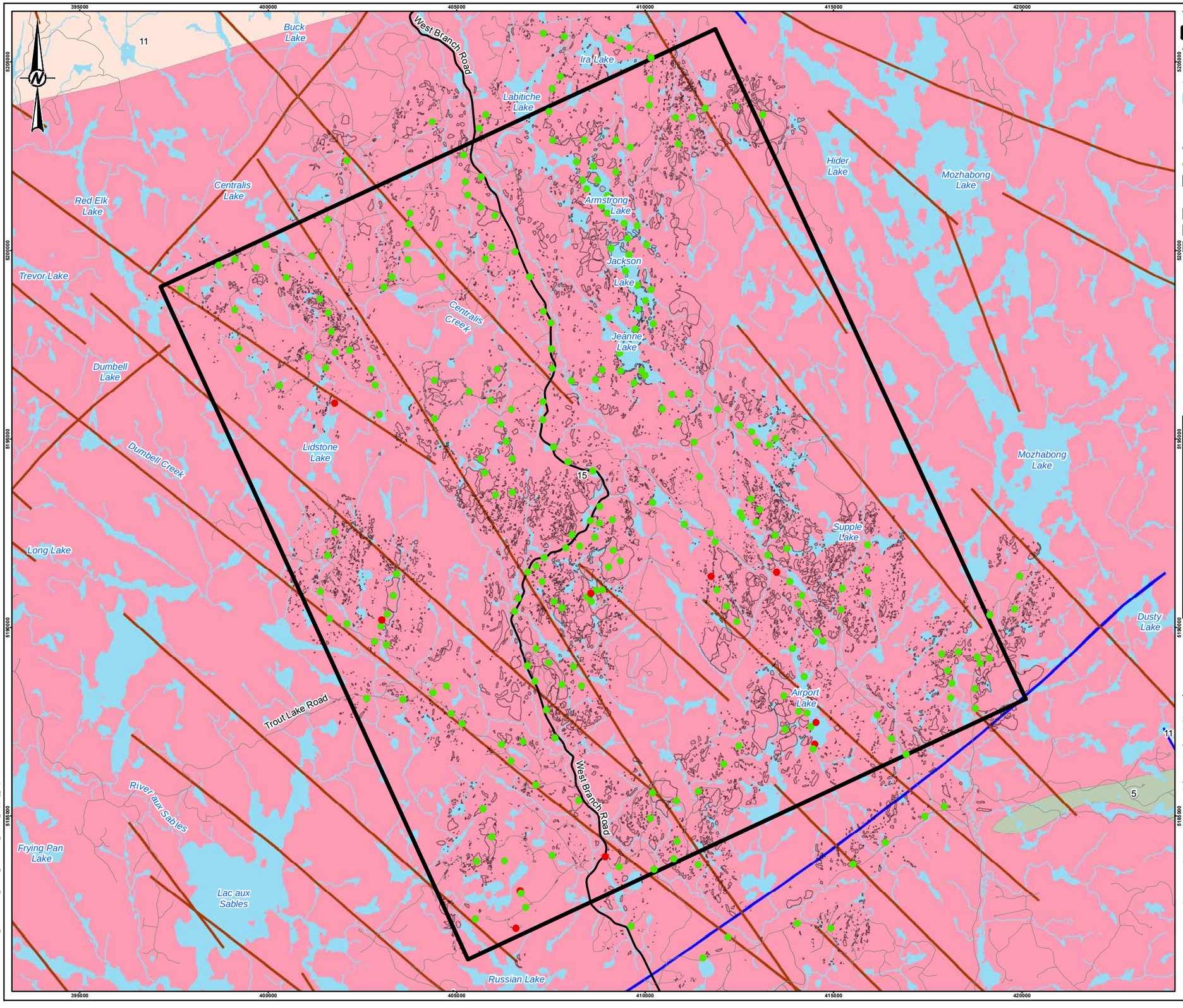

LEGEND

- Withdrawal Area
- Main Road
- Local Road
- Watercourse
- Waterbody
- Overburden (10)
- Outcrop (261)
- Geologic Fault
- OGS Mapped Dyke
- Predicted Outcrop

Bedrock Geology

- 15 Massive granodiorite to granite
- 11 Gneissic tonalite suite
- 5 Mafic to intermediate metavolcanic rocks

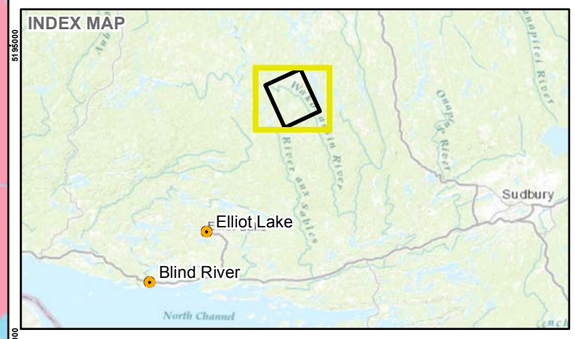

0 4 8

1:100,000 KILOMETRES

REFERENCE(S)

1. LIO (2017).
2. BEDROCK GEOLOGY, MRD126 REV-1, OGS (2011).
3. PRODUCED BY GOLDER ASSOCIATES LTD UNDER LICENCE FROM ONTARIO MINISTRY OF NATURAL RESOURCES AND FORESTRY, © QUEENS PRINTER 2017
4. PROJECTION: TRANSVERSE MERCATOR DATUM: NAD 83 COORDINATE SYSTEM: UTM ZONE 17

CLIENT
NWMO
BLIND RIVER, ELLIOT LAKE AND AREA, ONTARIO

PROJECT
BLIND RIVER, ELLIOT LAKE AND AREA GEOLOGICAL MAPPING REPORT

TITLE
BLIND RIVER AND ELLIOT LAKE AREA - BEDROCK GEOLOGY

CONSULTANT
Golder Associates

YYYY-MM-DD	2017-11-23
DESIGNED	JB
PREPARED	JB
REVIEWED	CM
APPROVED	GWS

PROJECT NO. 1651985 | CONTROL | REV. | FIGURE **1.2**

IF THIS MEASUREMENT DOES NOT MATCH WHAT IS SHOWN, THE SHEET SIZE HAS BEEN MODIFIED FROM: 25mm 0

S:\Clients\NWMO\Ontario\99_PROJ\1651985_NOH40_PROD\0003_Detailed_Mapping_Report\1651985-0003-HS-0002.mxd

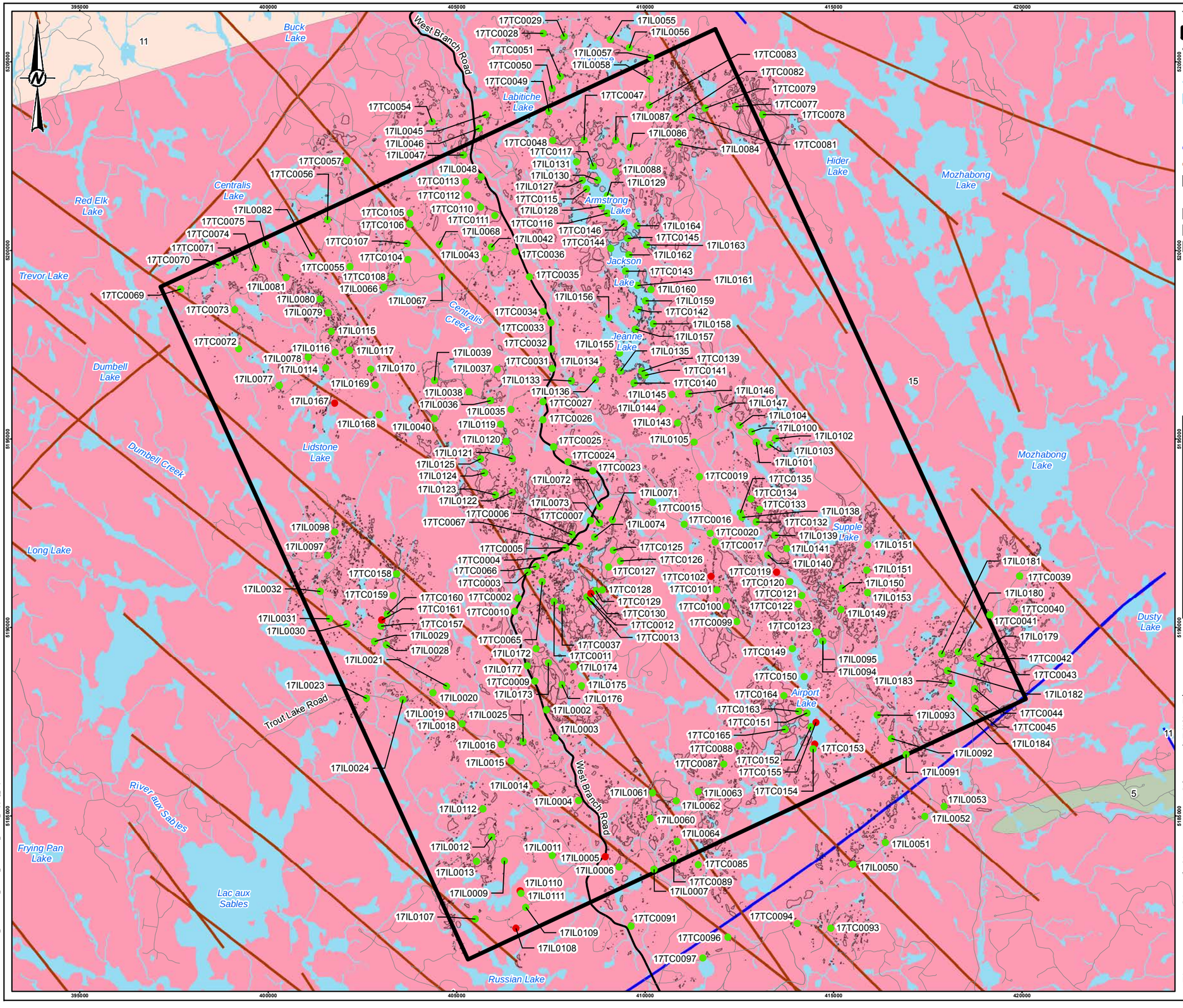

LEGEND

- Withdrawal Area
- Main Road
- Local Road
- Watercourse
- Waterbody
- Overburden (10)
- Outcrop (261)
- Geologic Fault
- OGS Mapped Dyke
- Predicted Outcrop

Bedrock Geology

- 15 Massive granodiorite to granite
- 11 Gneissic tonalite suite
- 5 Mafic to intermediate metavolcanic rocks

INDEX MAP

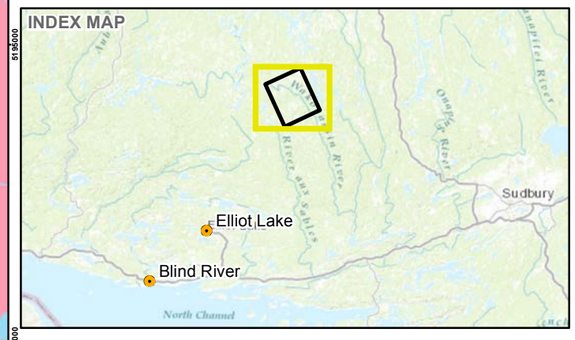

0 4 8

1:100,000 KILOMETRES

REFERENCE(S)

1. LIO (2017).
2. BEDROCK GEOLOGY, MRD126 REV-1, OGS (2011).
3. PRODUCED BY GOLDER ASSOCIATES LTD UNDER LICENCE FROM ONTARIO MINISTRY OF NATURAL RESOURCES AND FORESTRY, © QUEENS PRINTER 2017
4. PROJECTION: TRANSVERSE MERCATOR DATUM: NAD 83 COORDINATE SYSTEM: UTM ZONE 17

CLIENT
NWMO
BLIND RIVER, ELLIOT LAKE AND AREA, ONTARIO

PROJECT
BLIND RIVER, ELLIOT LAKE AND AREA GEOLOGICAL MAPPING REPORT

TITLE
WITHDRAWAL AREA - MAPPING OBSERVATION LOCATIONS

CONSULTANT
Golder Associates

YYYY-MM-DD	2017-11-23
DESIGNED	JB
PREPARED	JB
REVIEWED	CM
APPROVED	GWS

PROJECT NO. 1651985 | CONTROL | REV. | FIGURE **5.1.1**

IF THIS MEASUREMENT DOES NOT MATCH WHAT IS SHOWN, THE SHEET SIZE HAS BEEN MODIFIED FROM: 25mm 0

S:\Clients\NWMO\Ontario\99_PRO\1651985_NOH40_PRO\D0003_Detailed_Mapping_Report\1651985-0003-H8-0013.mxd

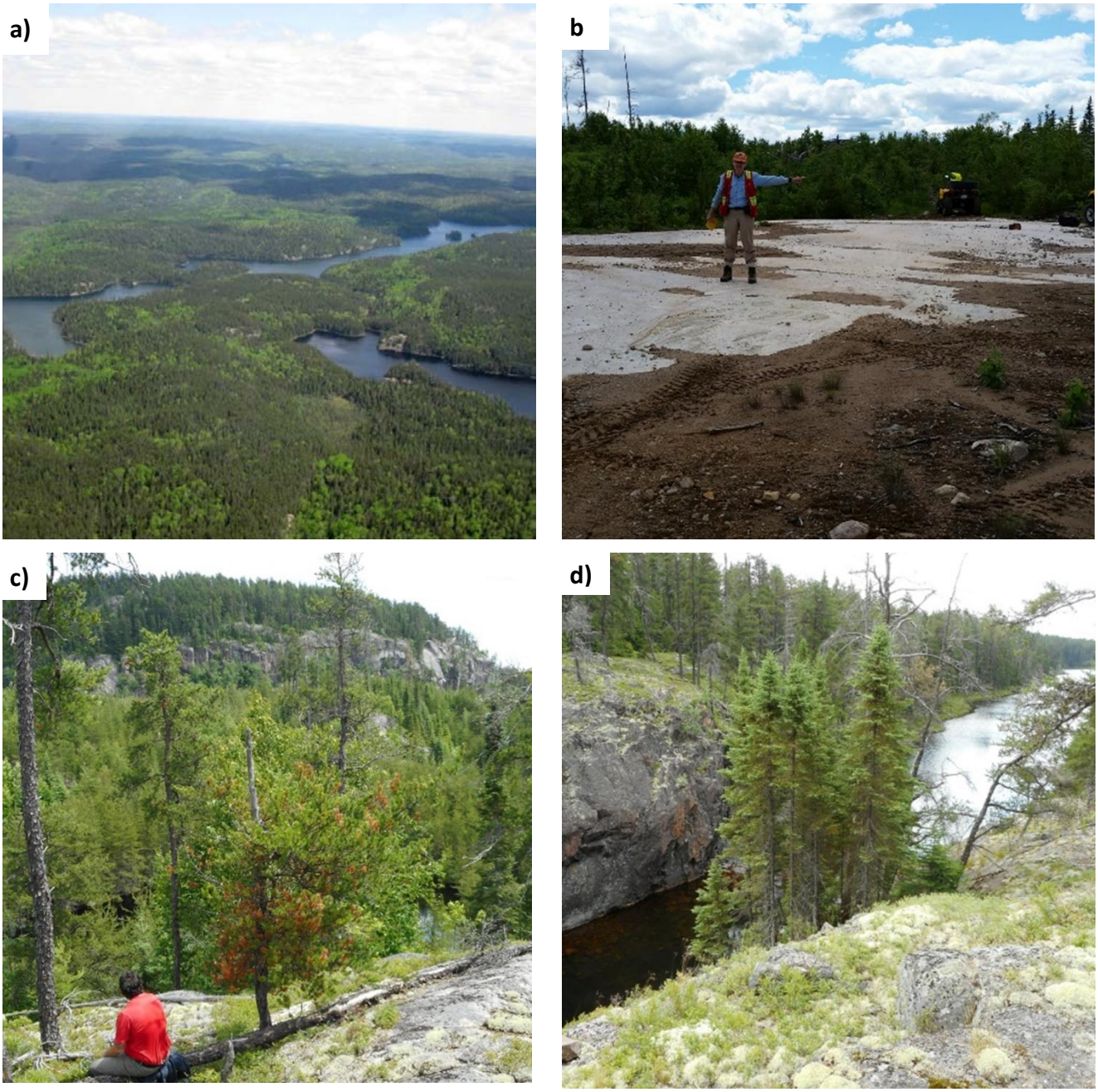

Figure 5.1.2: Field Examples of Accessibility and Bedrock Exposure

a - Typical landscape of the southeastern quadrant of the Withdrawal Area. Airport Lake in the foreground. Lakeshores provide excellent bedrock exposure. View to the southeast.

b - Typical secondary forestry road used for access are poorly maintained and largely overgrown. Primary access to secondary forestry roads was via ATV. View to the southwest, ATV for scale (Station 17TC0088).

c - Example of the degree of bedrock exposure and vertical relief in the northwest part of the Withdrawal Area. View to the east, person for scale (Station 17IL0078).

d - Topographic lineament formed by steep-sided creek. View to the southeast (Station 17IL0119).

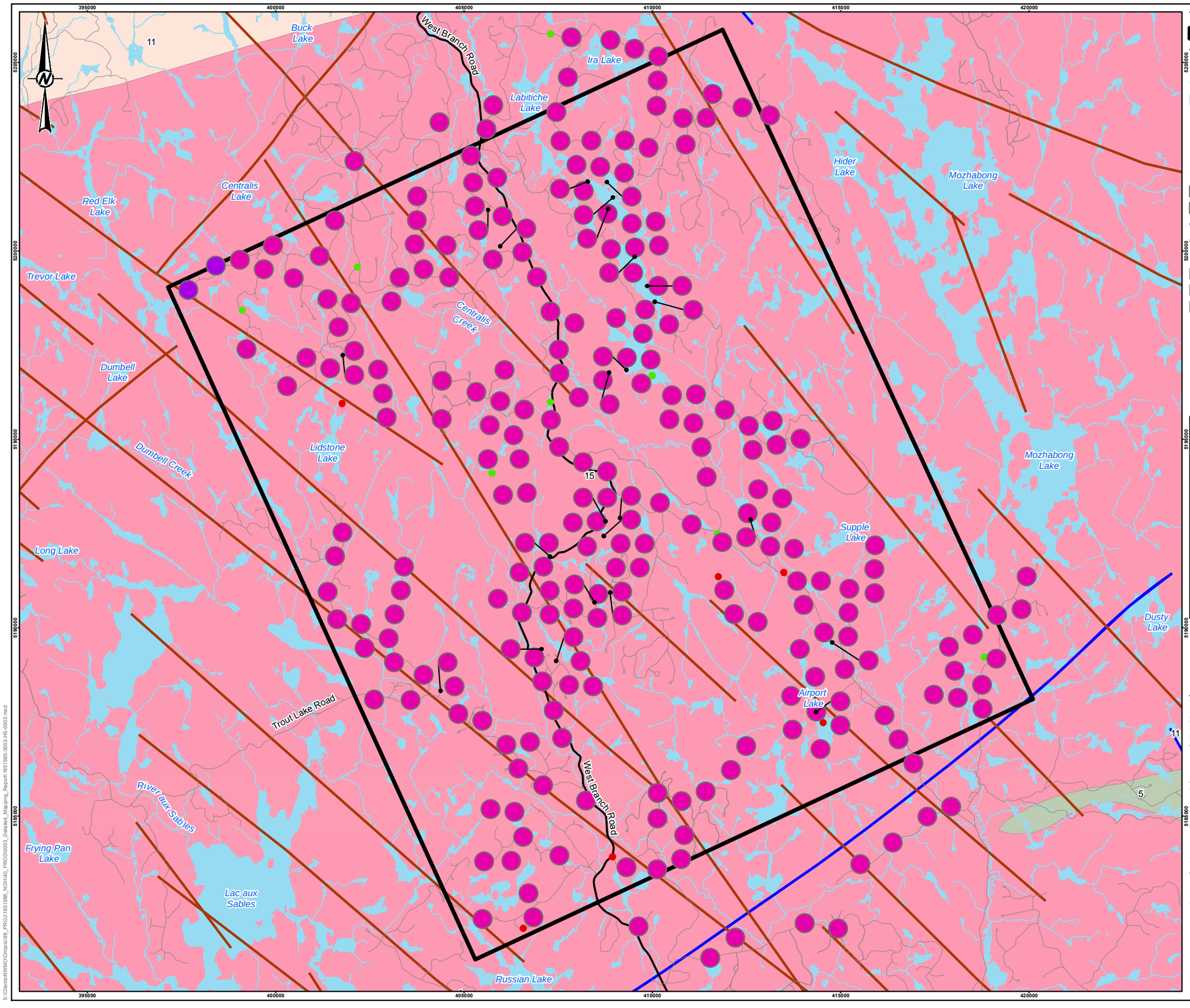

LEGEND

- Withdrawal Area
- Main Road
- Local Road
- Watercourse
- Waterbody
- Outcrop (8)
- Overburden (8)

Major Lithology

- Granite (253)
- Granodiorite (2)
- Geologic Fault
- OGS Mapped Dyke

Bedrock Geology

- 15 Massive granodiorite to granite
- 11 Gneissic tonalite suite
- 5 Mafic to intermediate metavolcanic rocks

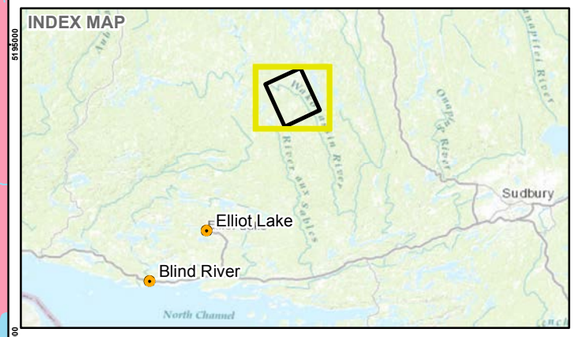

0 4 8

1:100,000 KILOMETRES

REFERENCE(S)

1. LIO (2017).
2. BEDROCK GEOLOGY, MRD126 REV-1, OGS (2011).
3. PRODUCED BY GOLDER ASSOCIATES LTD UNDER LICENCE FROM ONTARIO MINISTRY OF NATURAL RESOURCES AND FORESTRY, © QUEENS PRINTER 2017
4. PROJECTION: TRANSVERSE MERCATOR DATUM: NAD 83 COORDINATE SYSTEM: UTM ZONE 17

CLIENT
NWMO
BLIND RIVER, ELLIOT LAKE AND AREA, ONTARIO

PROJECT
BLIND RIVER, ELLIOT LAKE AND AREA GEOLOGICAL MAPPING REPORT

TITLE
WITHDRAWAL AREA - MAIN LITHOLOGICAL UNIT: GRANITE

CONSULTANT
Golder Associates

YYYY-MM-DD	2017-11-23
DESIGNED	JB
PREPARED	JB
REVIEWED	CM
APPROVED	GWS

PROJECT NO. 1651985 | CONTROL | REV. | FIGURE **5.1.3**

S:\Clients\NWMO\Ontario\99_PROJ\1651985_NOH140_PROJ\0003_Detailed_Mapping_Report\1651985-0003-HS-0003.mxd

IF THIS MEASUREMENT DOES NOT MATCH WHAT IS SHOWN, THE SHEET SIZE HAS BEEN MODIFIED FROM:
25mm
0

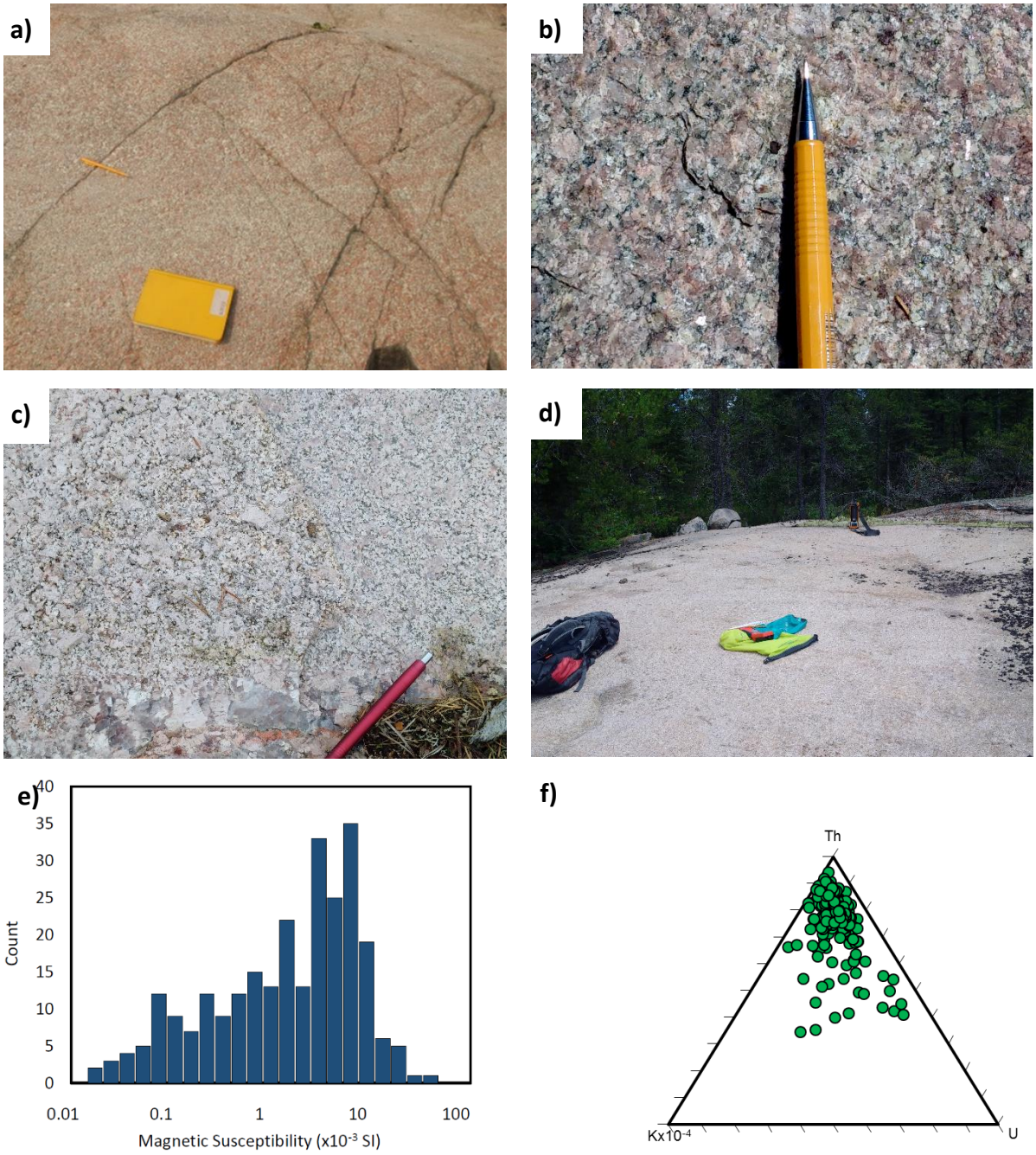

Figure 5.1.4: Field Examples of Main Lithology – Granite

a - Field example of granite at outcrop scale. View to the southeast, book for scale (Station 17TC0143).

b - Close-up of granite showing mineral composition and texture. View to the north, pencil for scale (Station 17TC004).

c - Close-up of granite outcrop showing contrasting phases defined by grainsize variation (Station 17IL0046)

d - Field example of massive intact granite outcrop, backpack for scale (Station 17IL0133)

e - Logarithmic plot of magnetic susceptibility for granite (N=263).

f - Ternary plot of gamma ray spectrometer data for granite (N=264).

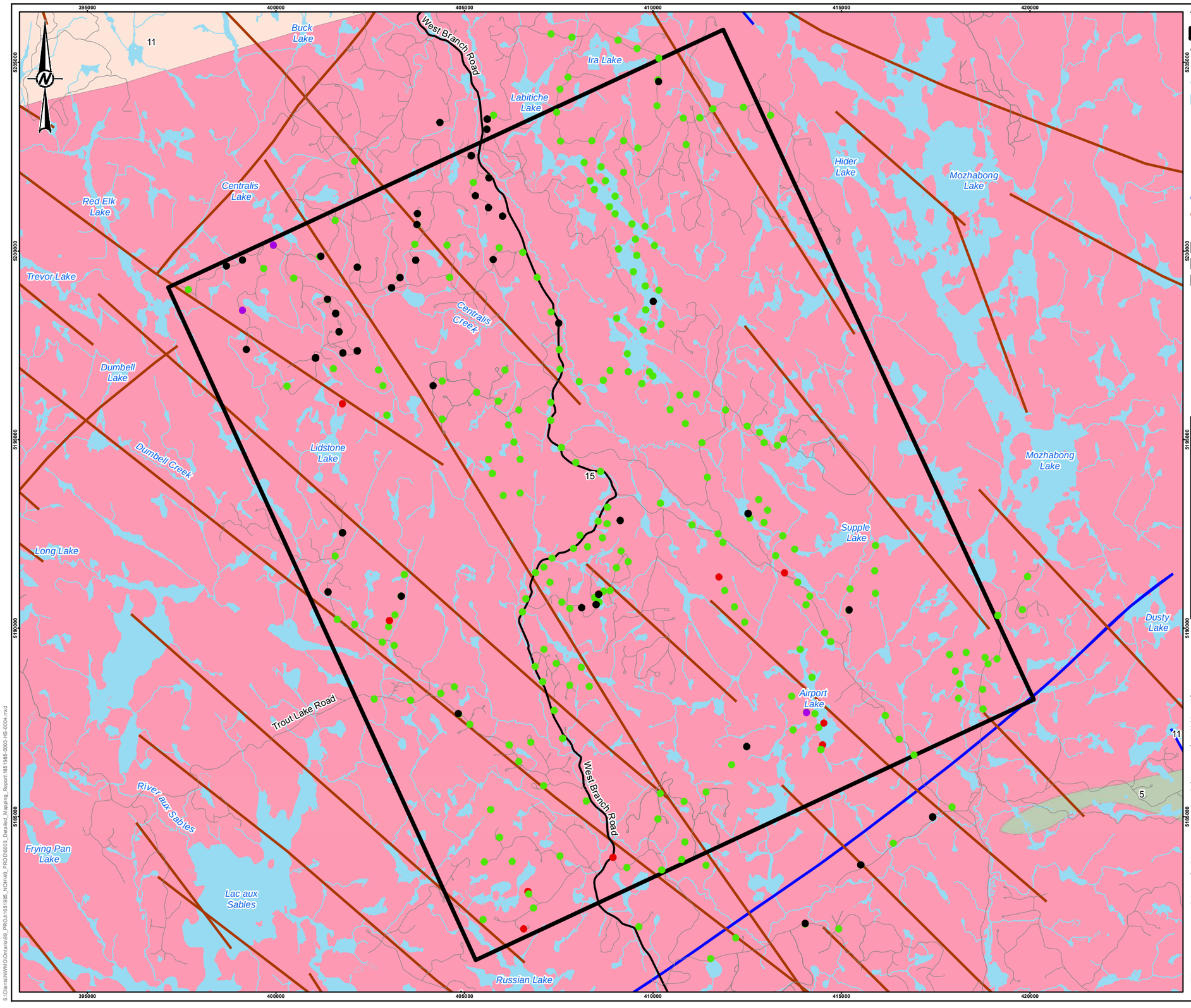

LEGEND

- Withdrawal Area
- Main Road
- Local Road
- Watercourse
- Waterbody
- Outcrop (219)
- Overburden (10)

Minor Lithologies (Occurrence as Xenoliths)

- Xenolith: Mafic Protolith (50)
- Xenolith: Granite or Tonalite Protolith (3)
- Geologic Fault
- OGS Mapped Dyke

Bedrock Geology

- 15 Massive granodiorite to granite
- 11 Gneissic tonalite suite
- 5 Mafic to intermediate metavolcanic rocks

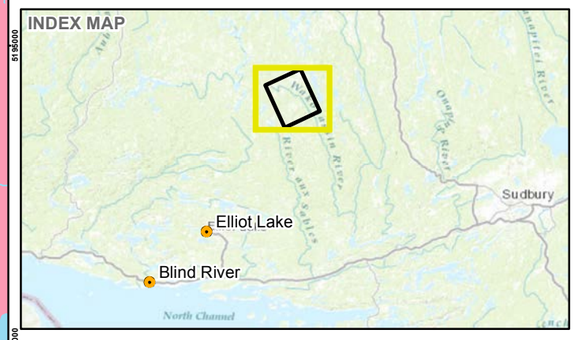

0 4 8

1:100,000 KILOMETRES

REFERENCE(S)

1. LIO (2017).
2. BEDROCK GEOLOGY, MRD126 REV-1, OGS (2011).
3. PRODUCED BY GOLDER ASSOCIATES LTD UNDER LICENCE FROM ONTARIO MINISTRY OF NATURAL RESOURCES AND FORESTRY, © QUEENS PRINTER 2017
4. PROJECTION: TRANSVERSE MERCATOR DATUM: NAD 83 COORDINATE SYSTEM: UTM ZONE 17

CLIENT
NWMO
BLIND RIVER, ELLIOT LAKE AND AREA, ONTARIO

PROJECT
BLIND RIVER, ELLIOT LAKE AND AREA GEOLOGICAL MAPPING REPORT

TITLE
WITHDRAWAL AREA - MINOR LITHOLOGICAL UNITS

CONSULTANT
Golder Associates

YYYY-MM-DD	2017-11-23
DESIGNED	JB
PREPARED	JB
REVIEWED	CM
APPROVED	GWS

PROJECT NO. 1651985 CONTROL REV. FIGURE **5.1.5**

IF THIS MEASUREMENT DOES NOT MATCH WHAT IS SHOWN, THE SHEET SIZE HAS BEEN MODIFIED FROM: 25mm 0

S:\Clients\NWMO\Ontario\99_PRO\1651985_NOH40_PRO\0003_Detailed_Mapping_Report\1651985-0003-HS-0004.mxd

Figure 5.1.6: Field Examples of Minor Lithological Units

a - Photo of gneissic xenoliths at outcrop scale. View to the south, person for scale (Station 17TC0071).
b - Photo of separated fragments of a fine-textured mafic xenolith, knife for scale (Station 17TC0071).
c - Photo of amphibolite gneiss xenolith. View to the south, pencil for scale (Station 17IL0080).
d - Photo of granite gneiss xenolith. View to the north, hammer for scale (Station 17IL0082).
e - Photo of gabbro xenolith. View to the west, pencil for scale (Station 17IL0078).
f - Photo of meta-volcanic xenolith. View to the southwest, pencil for scale (Station 17IL0119).

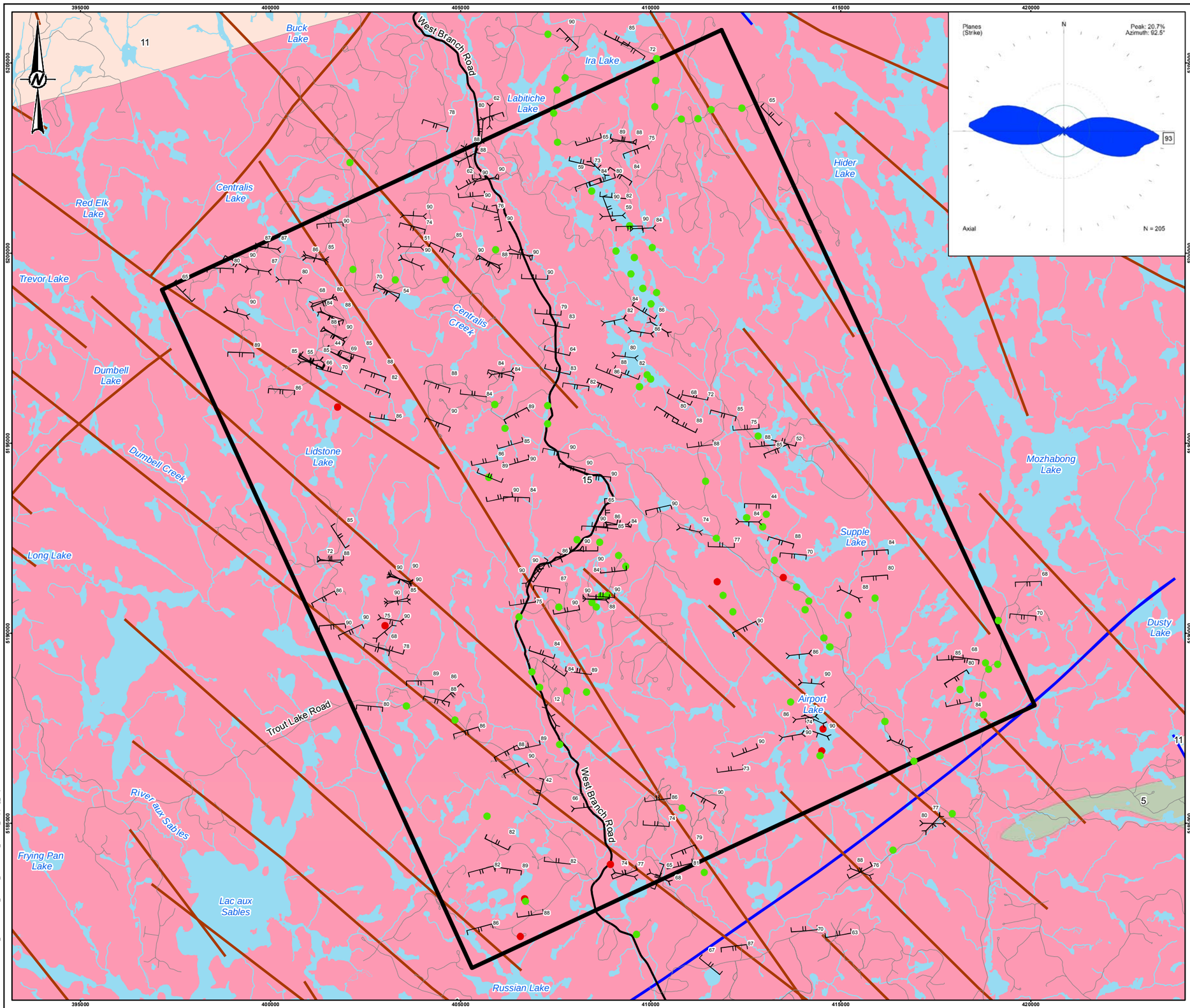

LEGEND

- Withdrawal Area
- Main Road
- Local Road
- Watercourse
- Waterbody
- Outcrop (86)
- Overburden (9)
- Cleavage (3)
- Foliation (56)
- Gneissic Layering (7)
- Igneous Flow Foliation (139)
- Geologic Fault
- OGS Mapped Dyke

Bedrock Geology

- 15 Massive granodiorite to granite
- 11 Gneissic tonalite suite
- 5 Mafic to intermediate metavolcanic rocks

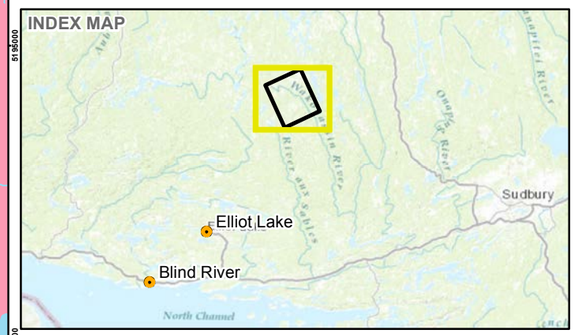

0 4 8

1:100,000 KILOMETRES

REFERENCE(S)

1. LIO (2017).
2. BEDROCK GEOLOGY, MRD126 REV-1, OGS (2011).
3. PRODUCED BY GOLDER ASSOCIATES LTD UNDER LICENCE FROM ONTARIO MINISTRY OF NATURAL RESOURCES AND FORESTRY, © QUEENS PRINTER 2017
4. PROJECTION: TRANSVERSE MERCATOR DATUM: NAD 83 COORDINATE SYSTEM: UTM ZONE 17

CLIENT
NWMO
BLIND RIVER, ELLIOT LAKE AND AREA, ONTARIO

PROJECT
BLIND RIVER, ELLIOT LAKE AND AREA GEOLOGICAL MAPPING REPORT

TITLE
WITHDRAWAL AREA - FOLIATION

CONSULTANT
Golder Associates

YYYY-MM-DD	2017-11-23
DESIGNED	JB
PREPARED	JB
REVIEWED	CM
APPROVED	GWS

PROJECT NO. 1651985 | CONTROL | REV. | FIGURE **5.1.7**

IF THIS MEASUREMENT DOES NOT MATCH WHAT IS SHOWN, THE SHEET SIZE HAS BEEN MODIFIED FROM: 25mm

S:\Clients\NWMO\Ontario\99_PROJ\1651985_NOH140_PROJ\D\0003_Detailed_Mapping_Report\1651985-0003-HS-0007.mxd

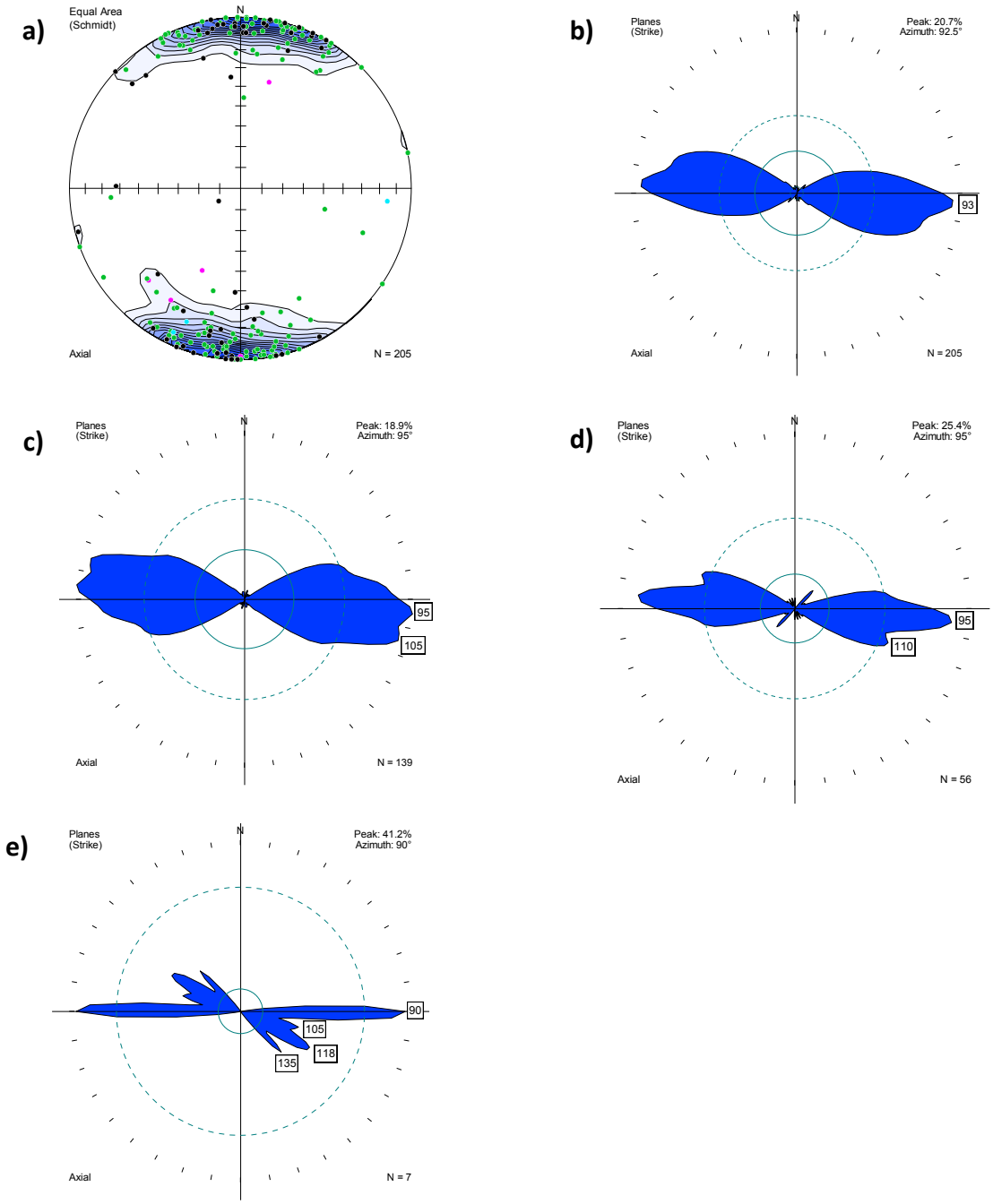

Figure 5.1.8: Foliation Orientation Data

a - All foliation data (N=205) displayed as equal area lower hemisphere stereonet plot of poles to foliation planes. Igneous flow foliation: green circles (N=139). Tectonic foliation: black circles (N=56). Gneissic layering: pink circle (N=7). Fracture cleavage: blue circle (N=3). Contours show multiples of the standard deviation S above the expectant count E calculated using Gaussian K-100.

b - All foliation data displayed as rose diagram of trends of foliation planes (N=205). Bins for rose diagrams are 10°.

c - Igneous flow foliation data displayed as rose diagram of trends of foliation planes (N=139). Bins for rose diagrams are 10°.
d - Tectonic foliation data displayed as rose diagram of trends of foliation planes (N=56). Bins for rose diagrams are 10°.
e – Gneissic layering data displayed as rose diagram of trends of foliation planes (N=7). Bins for rose diagrams are 10°.

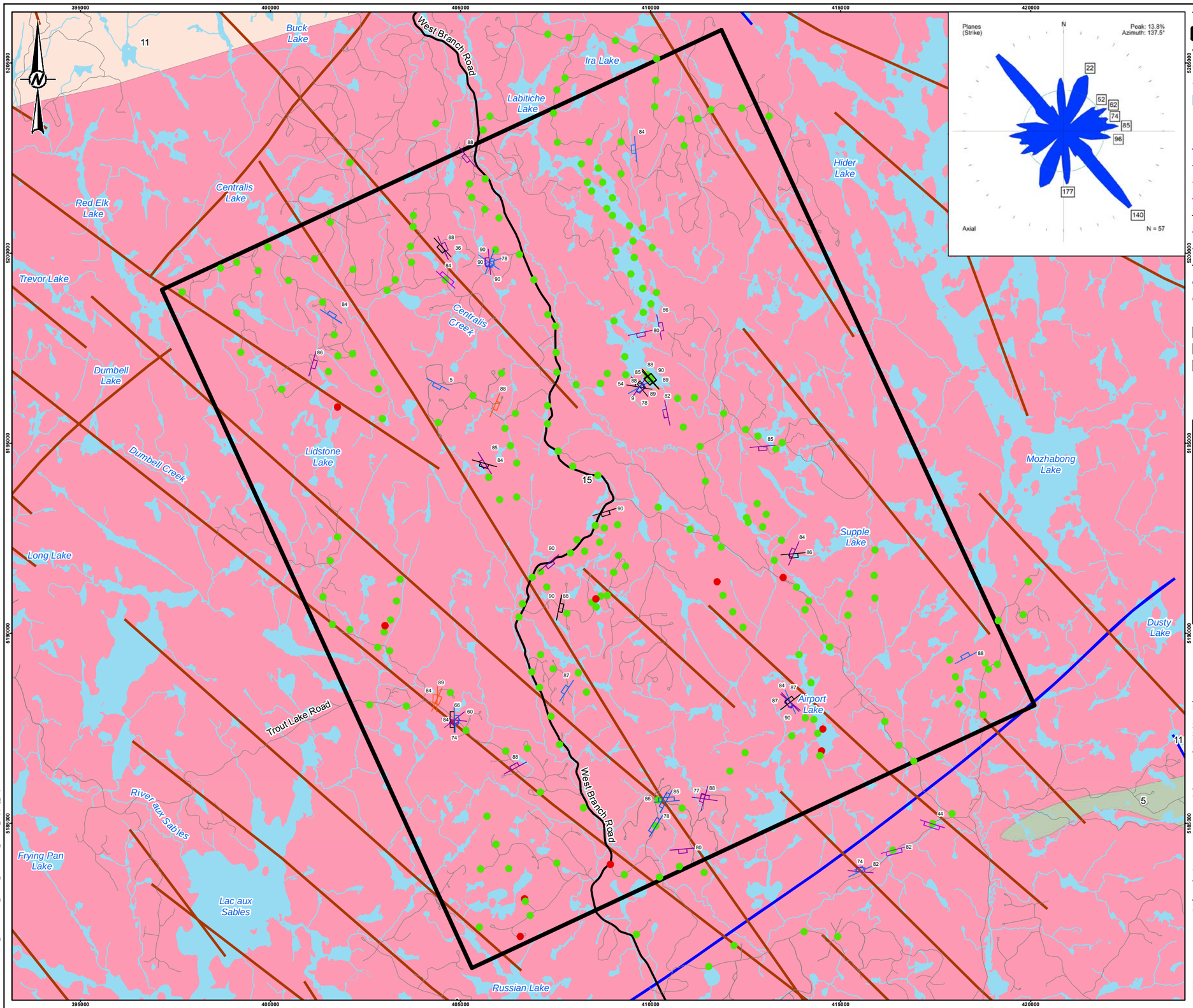

LEGEND

- Withdrawal Area
- Main Road
- Local Road
- Watercourse
- Waterbody
- Outcrop (234)
- Overburden (10)
- Brittle-ductile shear zones - Dextral (21)
- Brittle-ductile shear zones - Sinistral (12)
- Brittle-ductile shear zones - Dip Slip (3)
- Brittle-ductile shear zones - Strike Slip (1)
- Brittle-ductile shear zones - Unknown Slip (13)
- Ductile shear zone - Dextral (3)
- Ductile shear zone - Sinistral (3)
- Ductile shear zone - Unknown Slip (1)
- Geologic Fault
- OGS Mapped Dyke

Bedrock Geology

- 15 Massive granodiorite to granite
- 11 Gneissic tonalite suite
- 5 Mafic to intermediate metavolcanic rocks

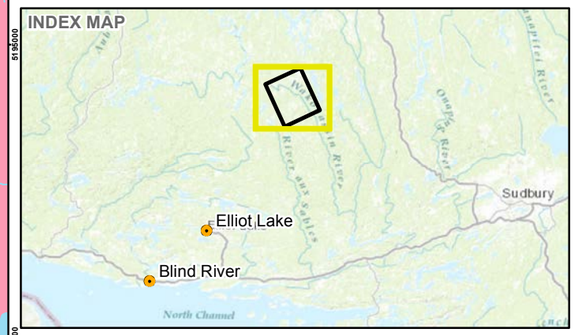

0 4 8

1:100,000 KILOMETRES

REFERENCE(S)

1. LIO (2017).
2. BEDROCK GEOLOGY, MRD126 REV-1, OGS (2011).
3. PRODUCED BY GOLDER ASSOCIATES LTD UNDER LICENCE FROM ONTARIO MINISTRY OF NATURAL RESOURCES AND FORESTRY, © QUEENS PRINTER 2017
4. PROJECTION: TRANSVERSE MERCATOR DATUM: NAD 83 COORDINATE SYSTEM: UTM ZONE 17

CLIENT
NWMO
BLIND RIVER, ELLIOT LAKE AND AREA, ONTARIO

PROJECT
BLIND RIVER, ELLIOT LAKE AND AREA GEOLOGICAL MAPPING REPORT

TITLE
WITHDRAWAL AREA - DUCTILE AND BRITTLE-DUCTILE SHEAR ZONES

CONSULTANT
Golder Associates

YYYY-MM-DD	2017-11-23
DESIGNED	JB
PREPARED	JB
REVIEWED	CM
APPROVED	GWS

PROJECT NO. 1651985 | CONTROL | REV. | FIGURE **5.1.9**

S:\Clients\NWMO\Ontario\99_PRO\A1651985_NOH140_PRO\Dli\0003_Detailed_Mapping_Report\1651985-0003-HS-0008.mxd

IF THIS MEASUREMENT DOES NOT MATCH WHAT IS SHOWN, THE SHEET SIZE HAS BEEN MODIFIED FROM: 25mm

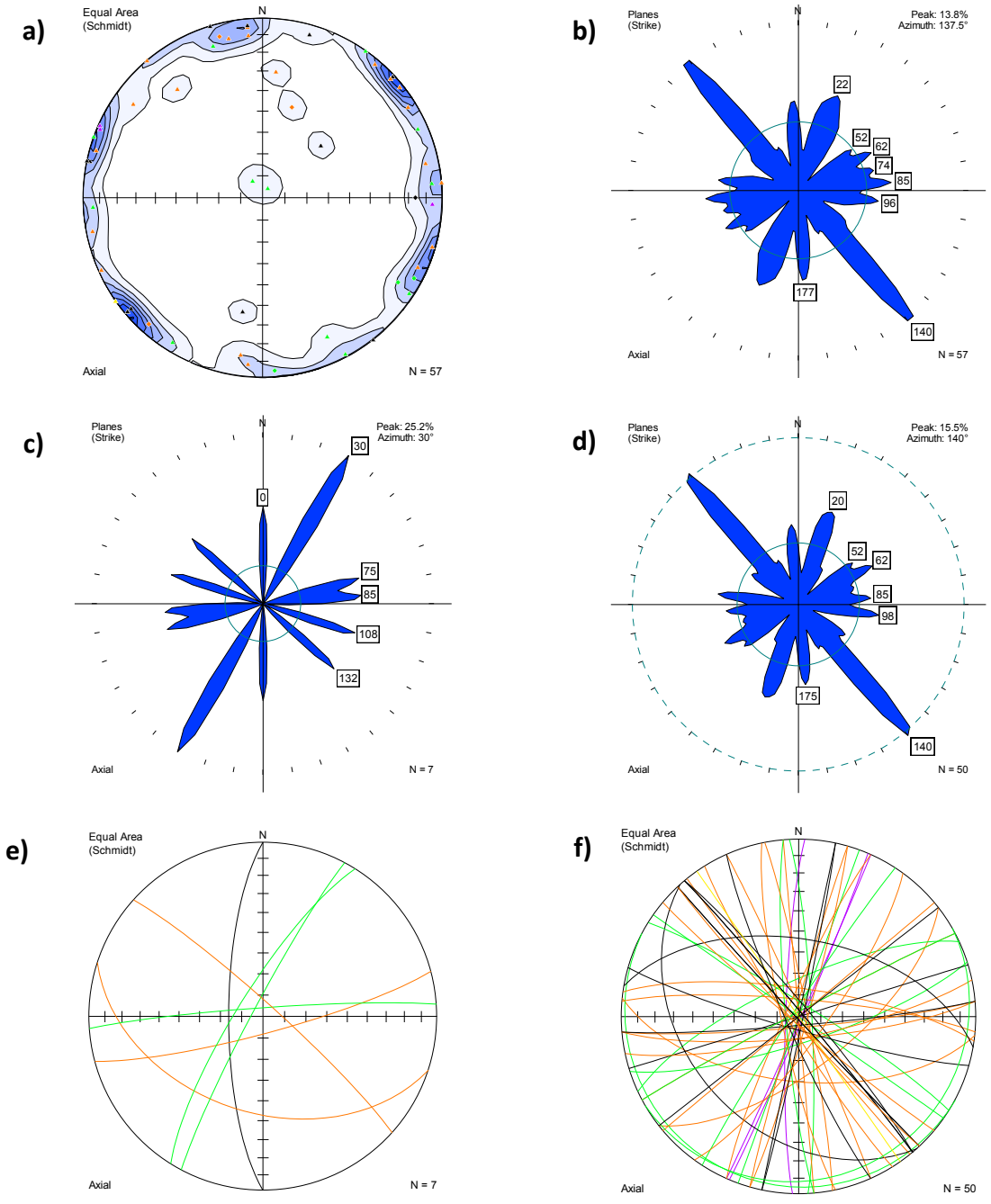

Figure 5.1.10: Ductile and Brittle-Ductile Shear Zone Orientation Data

a - All shear zones (N=57) displayed as equal area lower hemisphere stereonet plot of poles to shear planes. Ductile shear zones are displayed as diamonds, brittle ductile shear zones as triangles. Dextral ductile shear zones: orange diamonds (N=3). Sinistral ductile shear zones: green diamonds (N=3). Ductile shear zones with unknown slip: black diamonds (N=1). Dextral brittle-ductile shear zones: orange triangles (N=21). Sinistral brittle-ductile shear zones: green triangles (N=12). Dip-slip brittle-ductile shear zones: purple triangles (N=3). Strike-slip brittle-ductile shear zones: yellow triangles (N=1). Brittle-ductile

shear zones with unknown slip: black triangles (N=13). Contours show multiples of the standard deviation S above the expectant count E calculated using Gaussian K-100.
b - All shear zone data displayed as rose diagram of trends of shear planes (N=57). Bins for rose diagrams are 10°.
c - Ductile shear zone data displayed as rose diagram of trends of shear planes (N=7). Bins for rose diagrams are 10°.
d - Brittle-ductile shear zone data displayed as rose diagram of trends of shear planes (N=50). Bins for rose diagrams are 10°.
e - Ductile shear zones displayed as equal area lower hemisphere stereonet plot of great circles (N=7). Dextral structures: orange lines (N=3). Sinistral structures: green lines (N=3). Structures with unknown slip sense: black (N=1).
f - Brittle-ductile shear zones displayed as equal area lower hemisphere stereonet plot of great circles (N=50). Dextral structures: orange lines (N=21). Sinistral structures: green lines (N=12). Dip-slip structures: purple (N=3). Strike-slip structures: yellow (N=1). Structures with unknown slip sense: black (N=13).

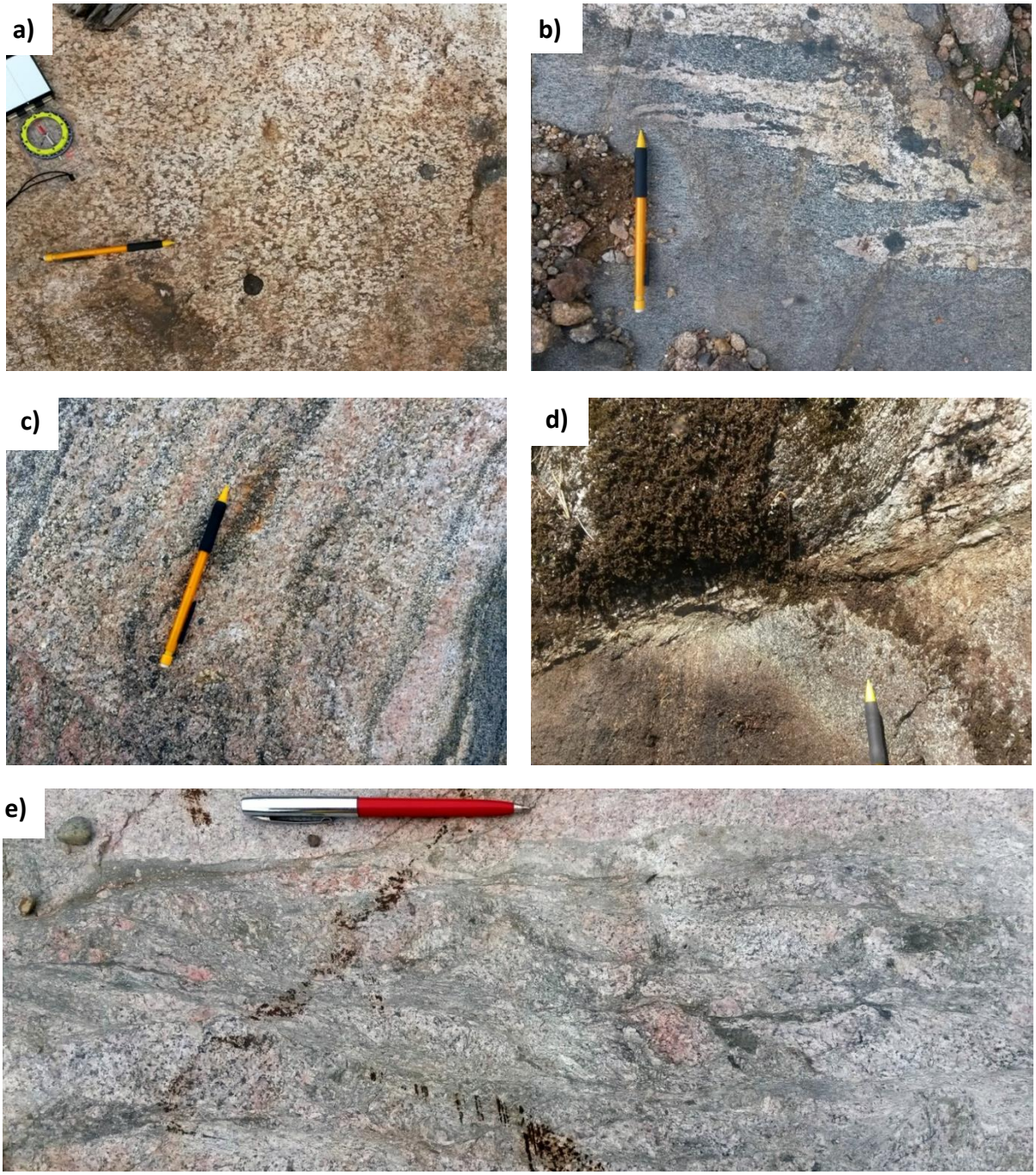

Figure 5.1.11: Field Examples of Ductile Structures

a - Weak igneous flow foliation in granite defined by aligned feldspar phenocrysts. View to the north, pencil for scale indicates strike of fabric (Station 17IL0079).

b - Well developed tectonic foliation in amphibolite gneiss. View to the north, pencil for scale (Station 17IL0078).

c - Gneissic layering in a granite gneiss xenolith. View to the west, pencil for scale (Station 17IL0078)

d - Ductile shear zone showing dextral drag of foliation. View to the southwest, pencil for scale (Station 17IL0052).

e - Brittle-ductile dextral shear zone exhibiting an anastomosing ductile fabric and associated cataclasite. Plan view to the west, pen for scale (17IL0086).

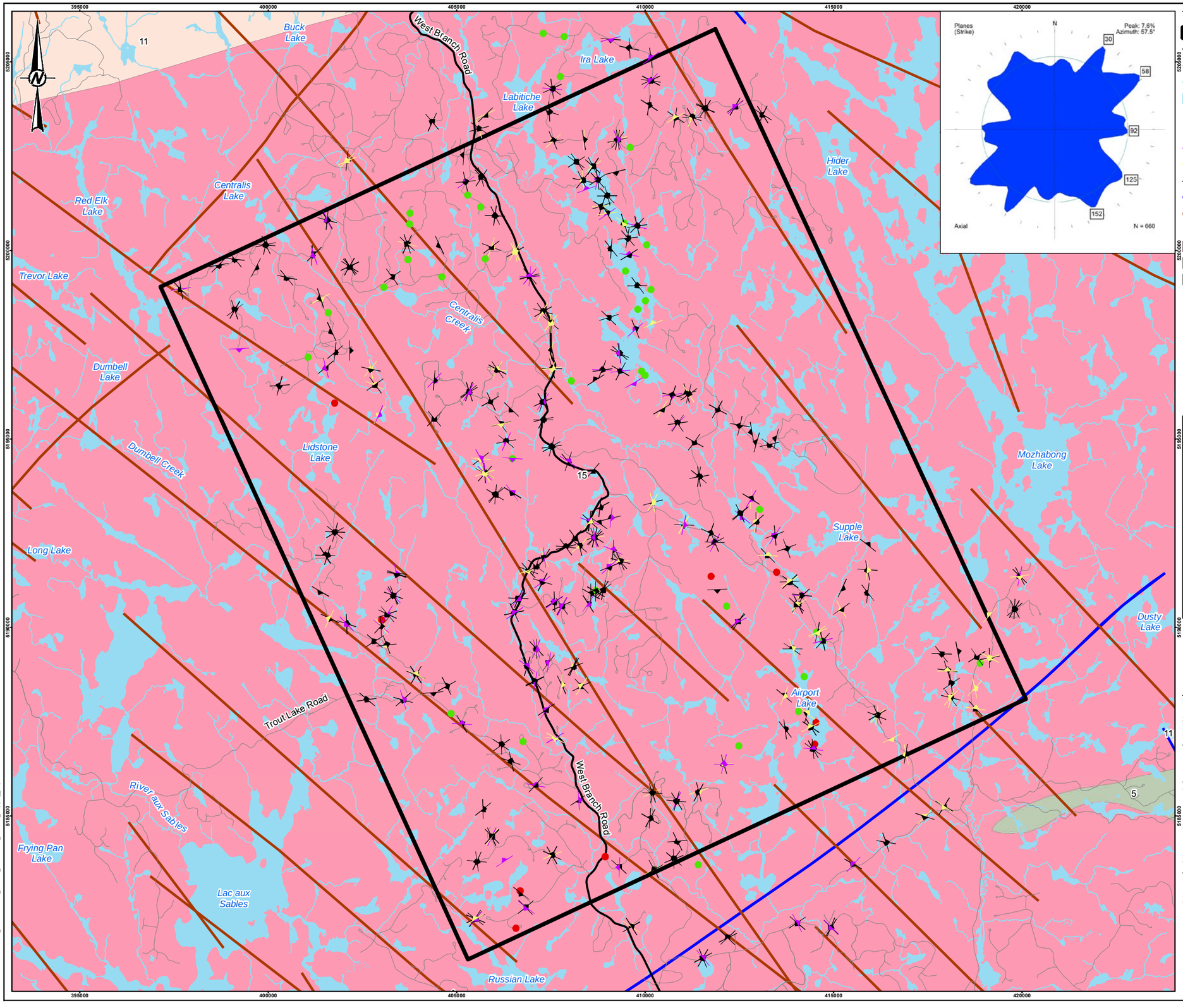

LEGEND

- Withdrawal Area
- Main Road
- Local Road
- Watercourse
- Waterbody
- Outcrop (37)
- Overburden (9)
- Sub horizontal joint: 0° - 24° (87)
- Intermediate joint: 25° - 65° (102)
- Sub vertical joint: 66° - 90° (471)
- Geologic Fault
- OGS Mapped Dyke

Bedrock Geology

- 15 Massive granodiorite to granite
- 11 Gneissic tonalite suite
- 5 Mafic to intermediate metavolcanic rocks

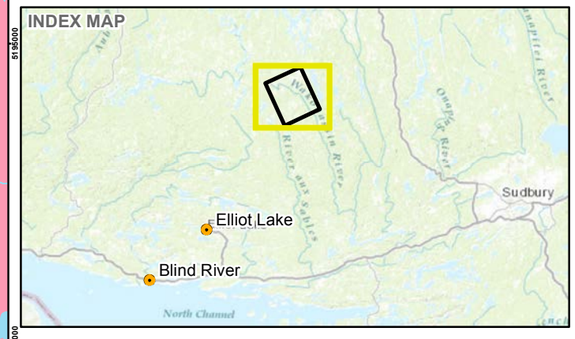

0 4 8

1:100,000 KILOMETRES

REFERENCE(S)

1. LIO (2017).
2. BEDROCK GEOLOGY, MRD126 REV-1, OGS (2011).
3. PRODUCED BY GOLDER ASSOCIATES LTD UNDER LICENCE FROM ONTARIO MINISTRY OF NATURAL RESOURCES AND FORESTRY, © QUEENS PRINTER 2017
4. PROJECTION: TRANSVERSE MERCATOR DATUM: NAD 83 COORDINATE SYSTEM: UTM ZONE 17

CLIENT
NWMO
BLIND RIVER, ELLIOT LAKE AND AREA, ONTARIO

PROJECT
BLIND RIVER, ELLIOT LAKE AND AREA GEOLOGICAL MAPPING REPORT

TITLE
WITHDRAWAL AREA - JOINTS

CONSULTANT
Golder Associates

YYYY-MM-DD	2017-11-23
DESIGNED	JB
PREPARED	JB
REVIEWED	CM
APPROVED	GWS

PROJECT NO. 1651985 | CONTROL | REV. | FIGURE **5.1.12**

IF THIS MEASUREMENT DOES NOT MATCH WHAT IS SHOWN, THE SHEET SIZE HAS BEEN MODIFIED FROM: 25mm 0

S:\Clients\NWMO\Ontario\99_PROJ\1651985_NOH40_PROD\0003_Detailed_Mapping_Report\1651985-0003-HS-0009.mxd

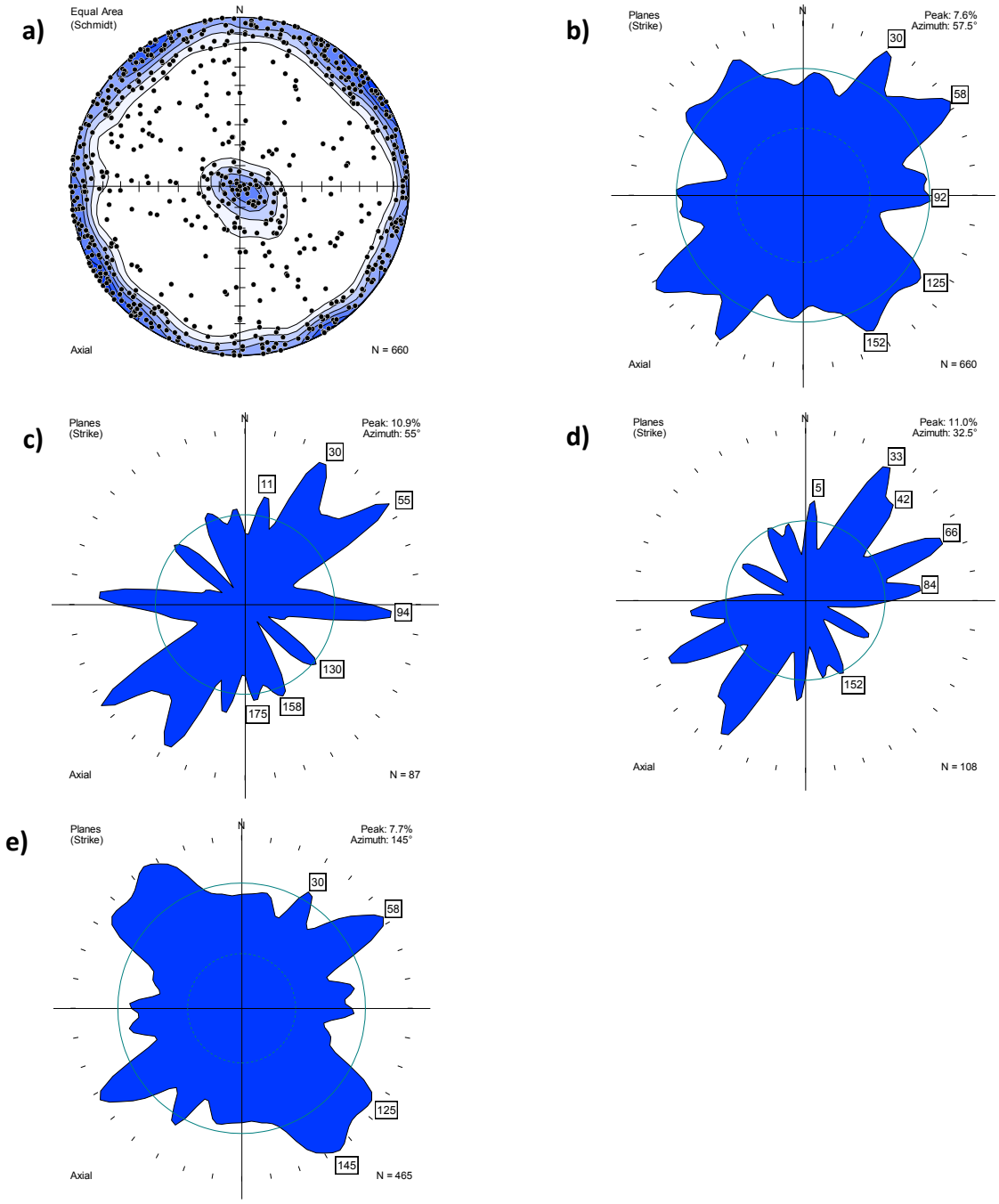

Figure 5.1.13: Joint Orientation Data and Joint Spacing Summary

a - All joint data displayed as equal area lower hemisphere stereonet plot of poles to joints (N=660). Contours show multiples of the standard deviation S above the expectant count E calculated using Gaussian K-100.

b - All joint data displayed as rose diagram of trends of joint planes (N=660). Bins for rose diagrams are 10°.

c - Shallow-dipping joints (<25° dip) displayed as rose diagram of trends of joint planes (N=87). Bins for rose diagrams are 10°.
d - Moderately-dipping joints (25°-65°) displayed as rose diagram of trends of joint planes (N=108). Bins for rose diagrams are 10°.
e - Steep joints (>65° dip) displayed as rose diagram of trends of joint planes (N=465). Bins for rose diagrams are 10°.

f)

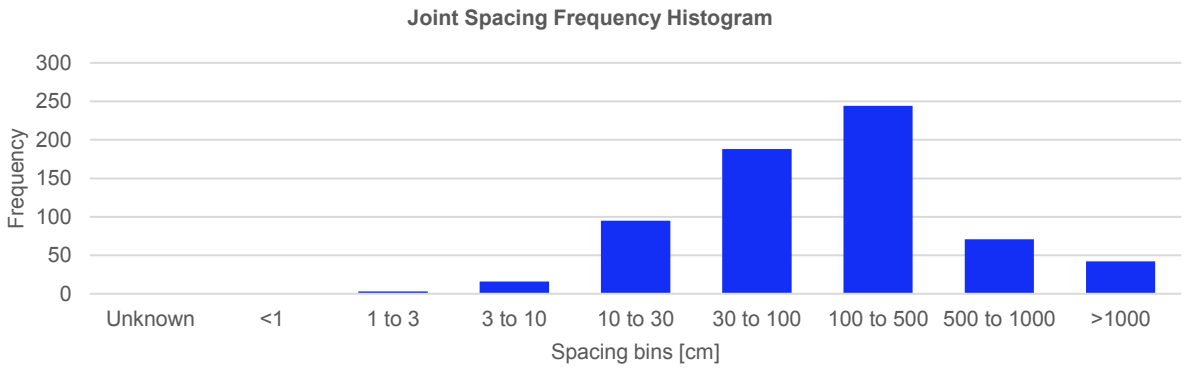

g)

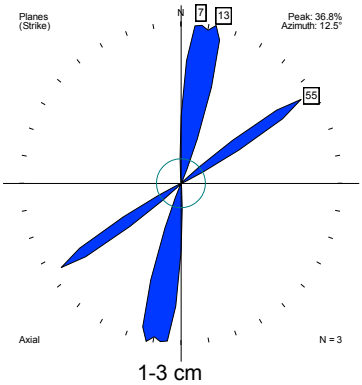

1-3 cm

h)

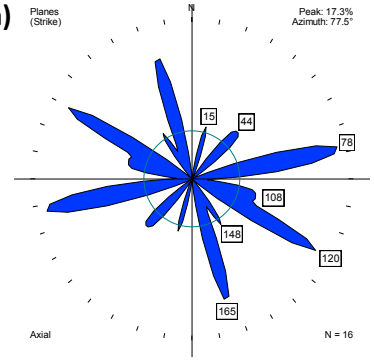

3-10 cm

i)

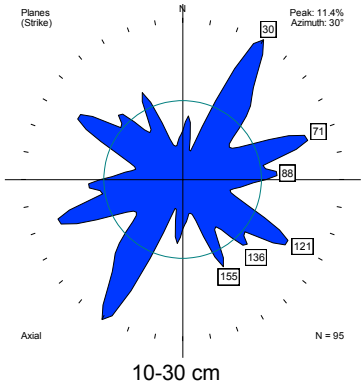

10-30 cm

j)

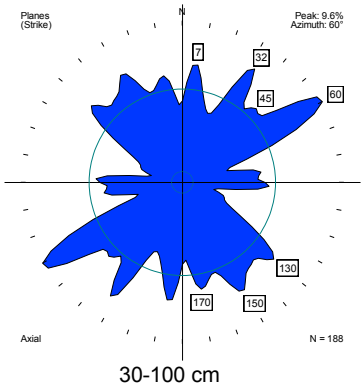

30-100 cm

k)

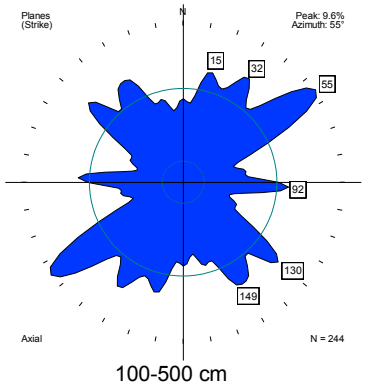

100-500 cm

l)

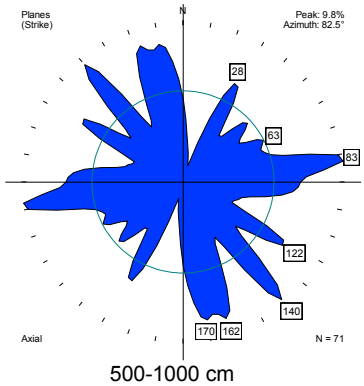

500-1000 cm

m)

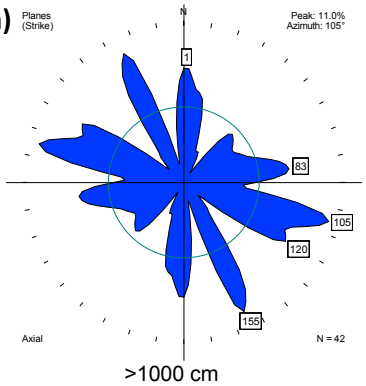

>1000 cm

n)

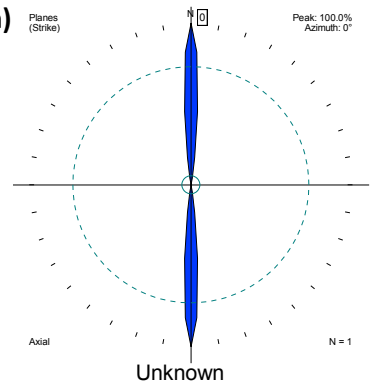

Unknown

Figure 5.1.13 (Cont'd): Joint Orientation Data and Joint Spacing Summary

f - Joint spacing histograms showing frequency distribution of all joint spacing classes.
g - Joint data with spacing 1-3 cm displayed as rose diagram of trends of joint planes (N=3). Bins for rose diagrams are 10°.
h - Joint data with spacing 3-10 cm displayed as rose diagram of trends of joint planes (N=16). Bins for rose diagrams are 10°.
i - Joint data with spacing 10-30 cm displayed as rose diagram of trends of joint planes (N=95). Bins for rose diagrams are 10°.
j - Joint data with spacing 30-100 cm displayed as rose diagram of trends of joint planes (N=188). Bins for rose diagrams are 10°.
k - Joint data with spacing 100-500 cm displayed as rose diagram of trends of joint planes (N=244). Bins for rose diagrams are 10°.
l - Joint data with spacing 500-1000 cm displayed as rose diagram of trends of joint planes (N=71). Bins for rose diagrams are 10°.
m - Joint data with spacing >1000 cm displayed as rose diagram of trends of joint planes (N=42). Bins for rose diagrams are 10°.
n - Joint data with unknown spacing displayed as rose diagram of trends of joint planes (N=1). Bins for rose diagrams are 10°.

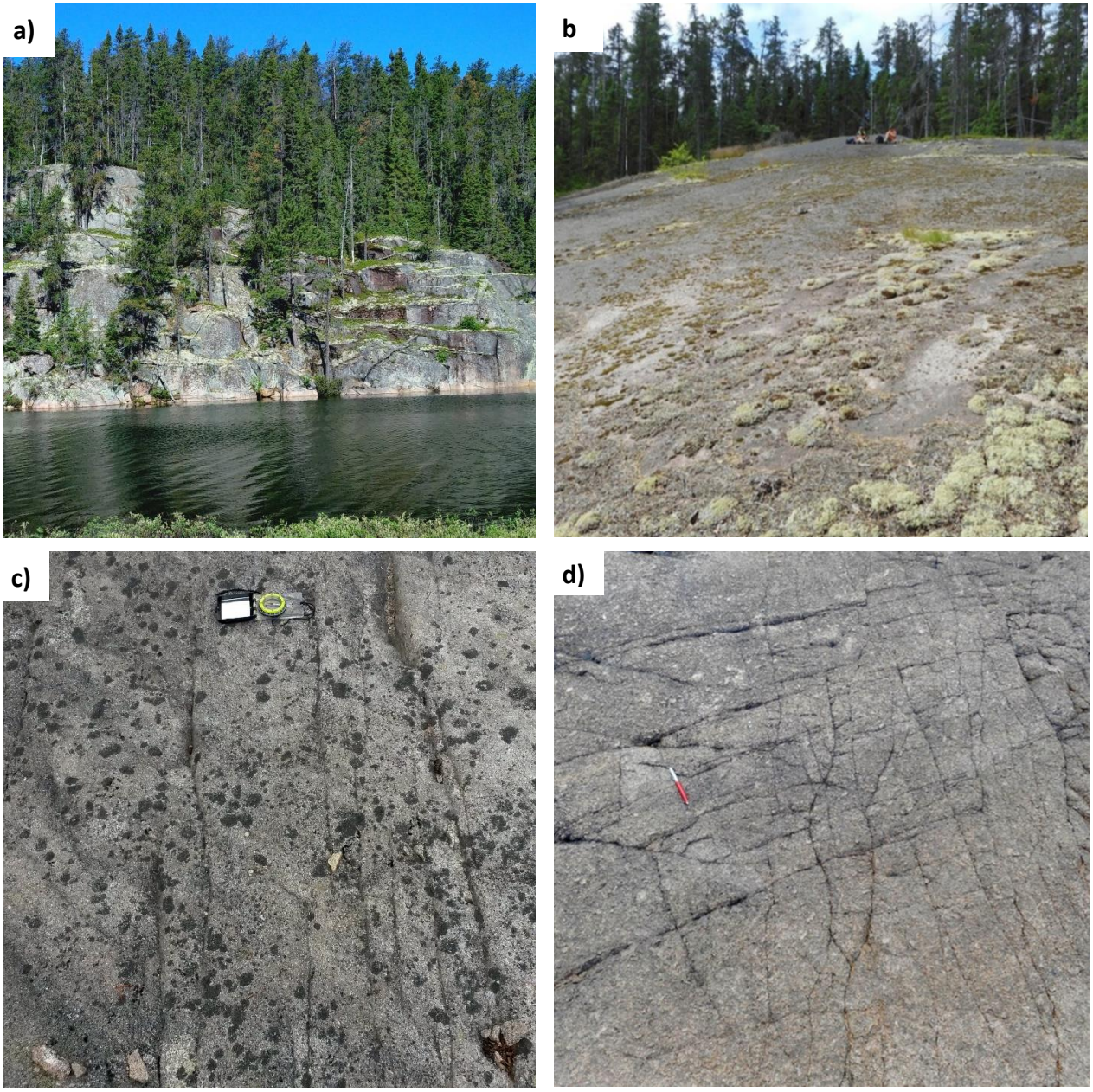

Figure 5.1.14: Field Examples of Joints

a - Example of easterly-dipping subhorizontal joints with a spacing of several metres forming steps on the bedrock outcrop. View to the east (Station 300m SE of 17TC0023).

b - Example of >1000 cm joint spacing, showing absence of fractures over several tens of metres of exposed bedrock. View to the west, person for scale (Station 17IL0121).

c - Example of 3-10 cm joint spacing. View to the east, compass for scale (Station 17IL0088).

d - Example of multiple intersecting joint sets in granite. View to the south, pen for scale (Station 17IL0129).

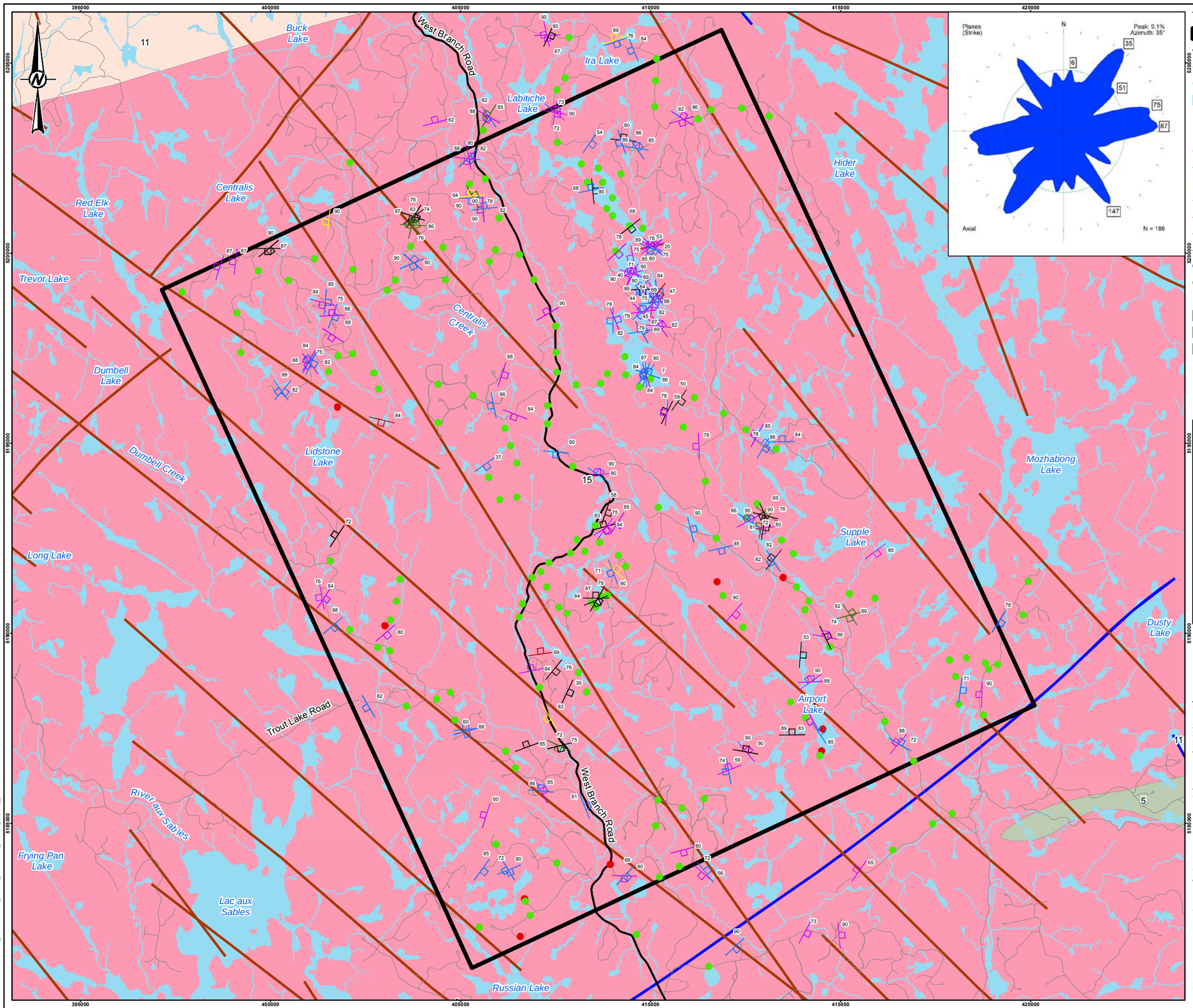

LEGEND

- Withdrawal Area
- Main Road
- Local Road
- Watercourse
- Waterbody
- Outcrop (157)
- Overburden (9)
- Fault - Dextral (73)
- Fault - Sinistral (63)
- Fault - Dip slip (5)
- Fault - Normal (1)
- Fault - Reverse (4)
- Fault - Strike Slip (10)
- Fault - Unknown slip (30)
- Geologic Fault
- OGS Mapped Dyke

Bedrock Geology

- 15 Massive granodiorite to granite
- 11 Gneissic tonalite suite
- 5 Mafic to intermediate metavolcanic rocks

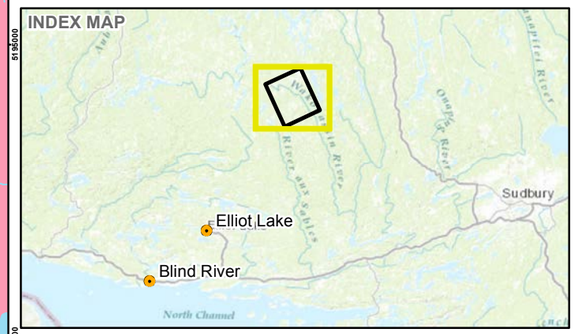

0 4 8

1:100,000 KILOMETRES

REFERENCE(S)

1. LIO (2017).
2. BEDROCK GEOLOGY, MRD126 REV-1, OGS (2011).
3. PRODUCED BY GOLDER ASSOCIATES LTD UNDER LICENCE FROM ONTARIO MINISTRY OF NATURAL RESOURCES AND FORESTRY, © QUEENS PRINTER 2017
4. PROJECTION: TRANSVERSE MERCATOR DATUM: NAD 83 COORDINATE SYSTEM: UTM ZONE 17

CLIENT
NWMO
BLIND RIVER, ELLIOT LAKE AND AREA, ONTARIO

PROJECT
BLIND RIVER, ELLIOT LAKE AND AREA GEOLOGICAL MAPPING REPORT

TITLE
WITHDRAWAL AREA - FAULTS

CONSULTANT
Golder Associates

YYYY-MM-DD	2017-11-23
DESIGNED	JB
PREPARED	JB
REVIEWED	CM
APPROVED	GWS

PROJECT NO. 1651985 | CONTROL | REV. | FIGURE **5.1.15**

S:\Clients\NWMO\Ontario\99_PROJ\1651985_NOH140_PROD\D0003_Data\ed_Mapping_Report\1651985-0003-HS-0010.mxd

IF THIS MEASUREMENT DOES NOT MATCH WHAT IS SHOWN, THE SHEET SIZE HAS BEEN MODIFIED FROM:

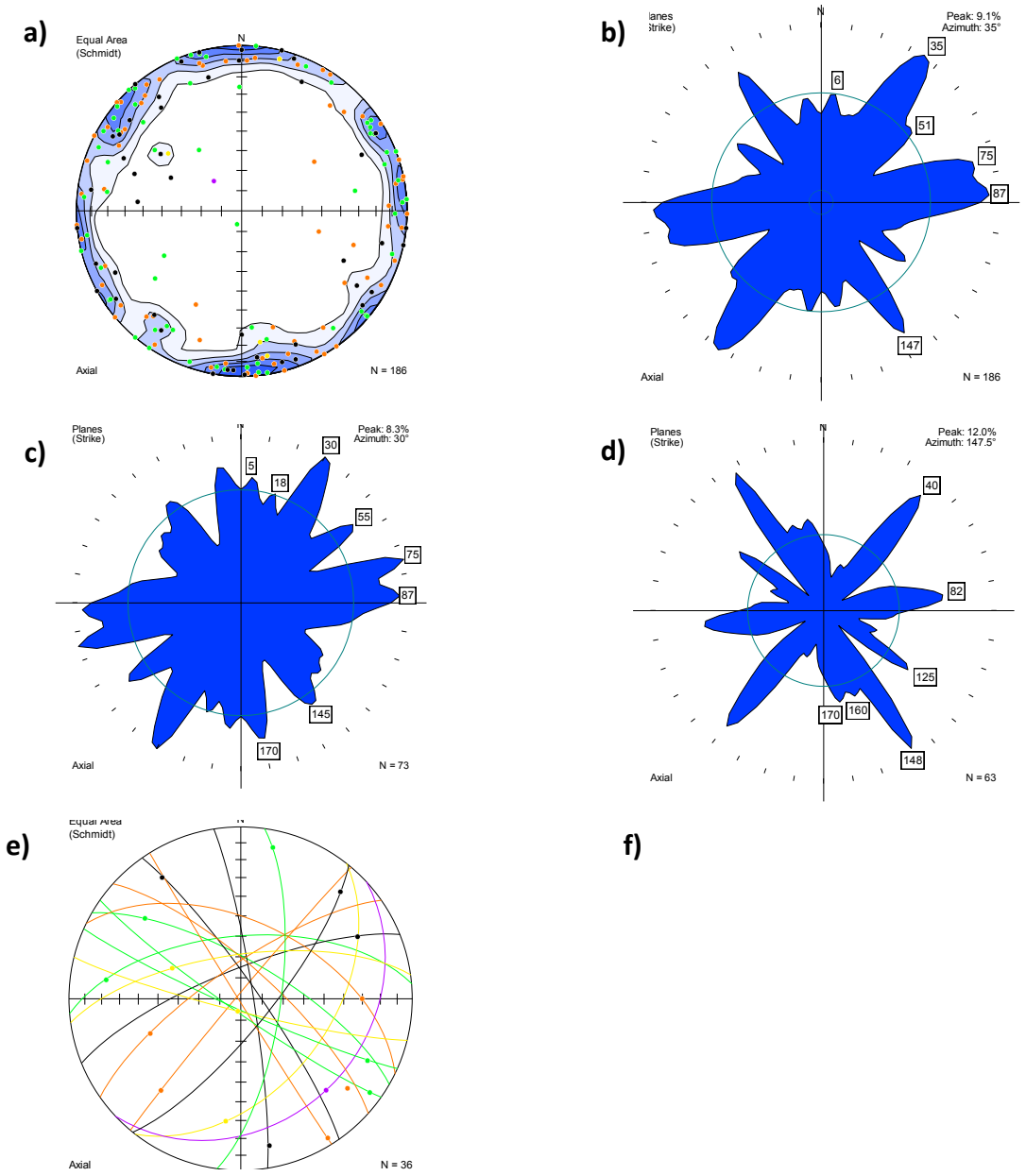

Figure 5.11.16: Fault Orientation Data

a - All fault data displayed as equal area lower hemisphere stereonet plot of poles to fault planes. Dextral faults: orange circles (N=73). Sinistral faults: green circles (N=63). Reverse faults: purple circles (N=4). Normal faults: yellow circles (N=1). Faults with unknown slip: black circles (N=45). Contours show multiples of the standard deviation S above the expectant count E calculated using Gaussian K-100.

b - All fault data displayed as rose diagram of trends of fault planes (N=186). Bins for rose diagrams are 10°.

c - Dextral fault data displayed as rose diagram of trends of fault planes (N=73). Bins for rose diagrams are 10°.

d - Sinistral fault data displayed as rose diagram of trends of fault planes (N=63). Bins for rose diagrams are 10°.
e - Faults displayed as great circles (N=18) and slickenline lineations displayed as points by their pitch on the corresponding fault plane (N=18). Dextral faults: orange lines (N=5). Sinistral faults: green lines (N=6). Reverse faults: yellow lines (N=4). Normal faults: purple line (N=1). Unknown slip: black lines (N=3).

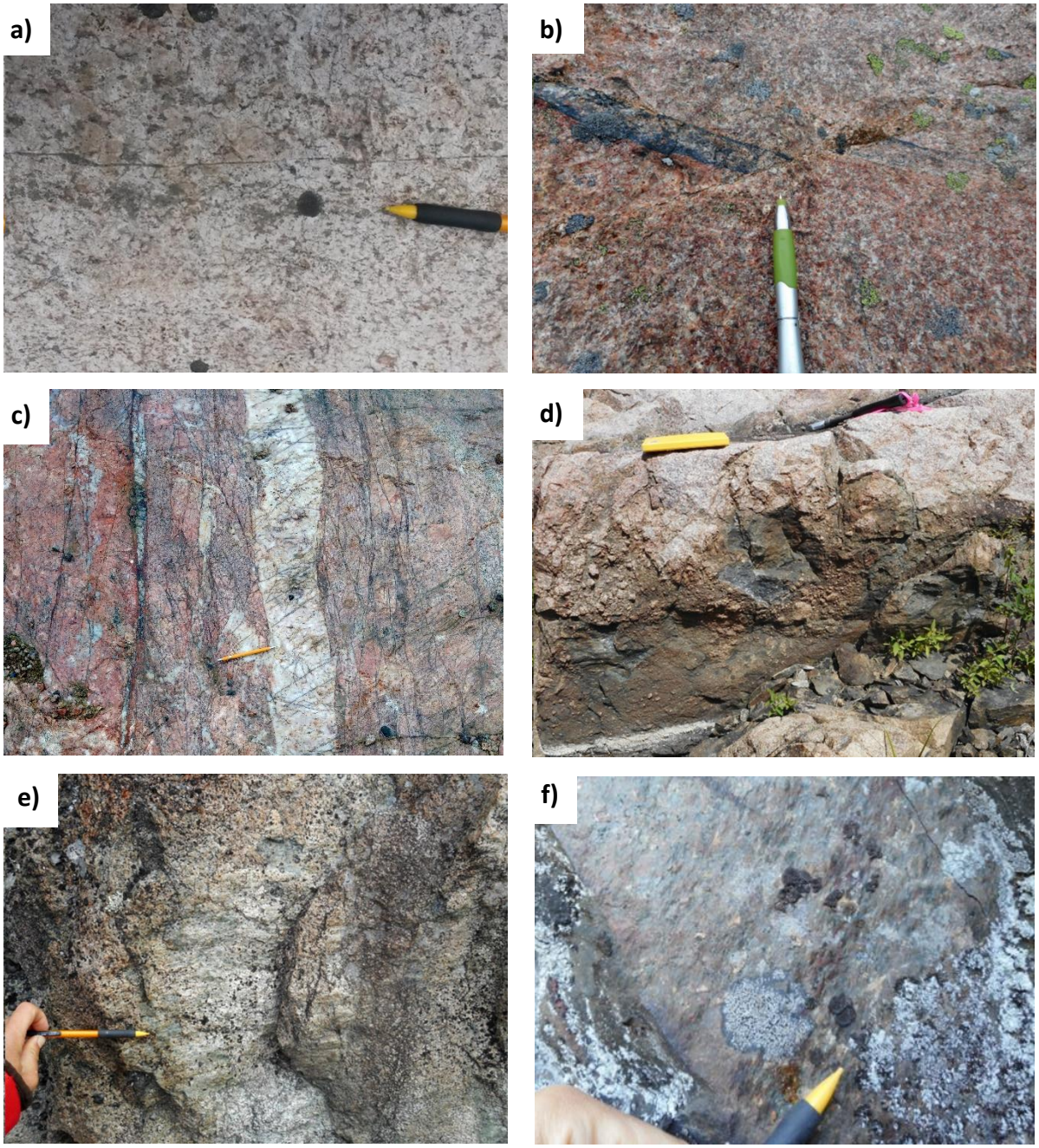

Figure 5.1.17: Field Examples of Faults

a – Dextral extensional jog in a mm-wide chloritic fault oriented 268/88. View to the north, pencil for scale (17IL0079).

b – Sinistral offset of a magnetite vein on a thin fault oriented 055/37. View to the northeast, pen for scale (17IL0125).

c – Broad brittle fault zone with quartz veins oriented 089/64 and hematite staining. View to the north, pencil for scale (Station 17IL0112).

d – Breccia with angular clasts of granite host rock in a dark aphanitic matric forming core of fault oriented 114/85. View to the northeast, hammer for scale (Station 17IL0163AP06).
e – Chlorite slickenlines plunging 5° to the southeast (towards the right in the photograph) on a slip surface of fault surface oriented 148/89. View to the northeast, pencil for scale indicating slip direction (Station 17IL0160).
f – Slip surface of an oblique-reverse fault oriented 262/69 in a mafic dyke. View to the east, pencil for scale indicating slip direction (Station 17IL0172).

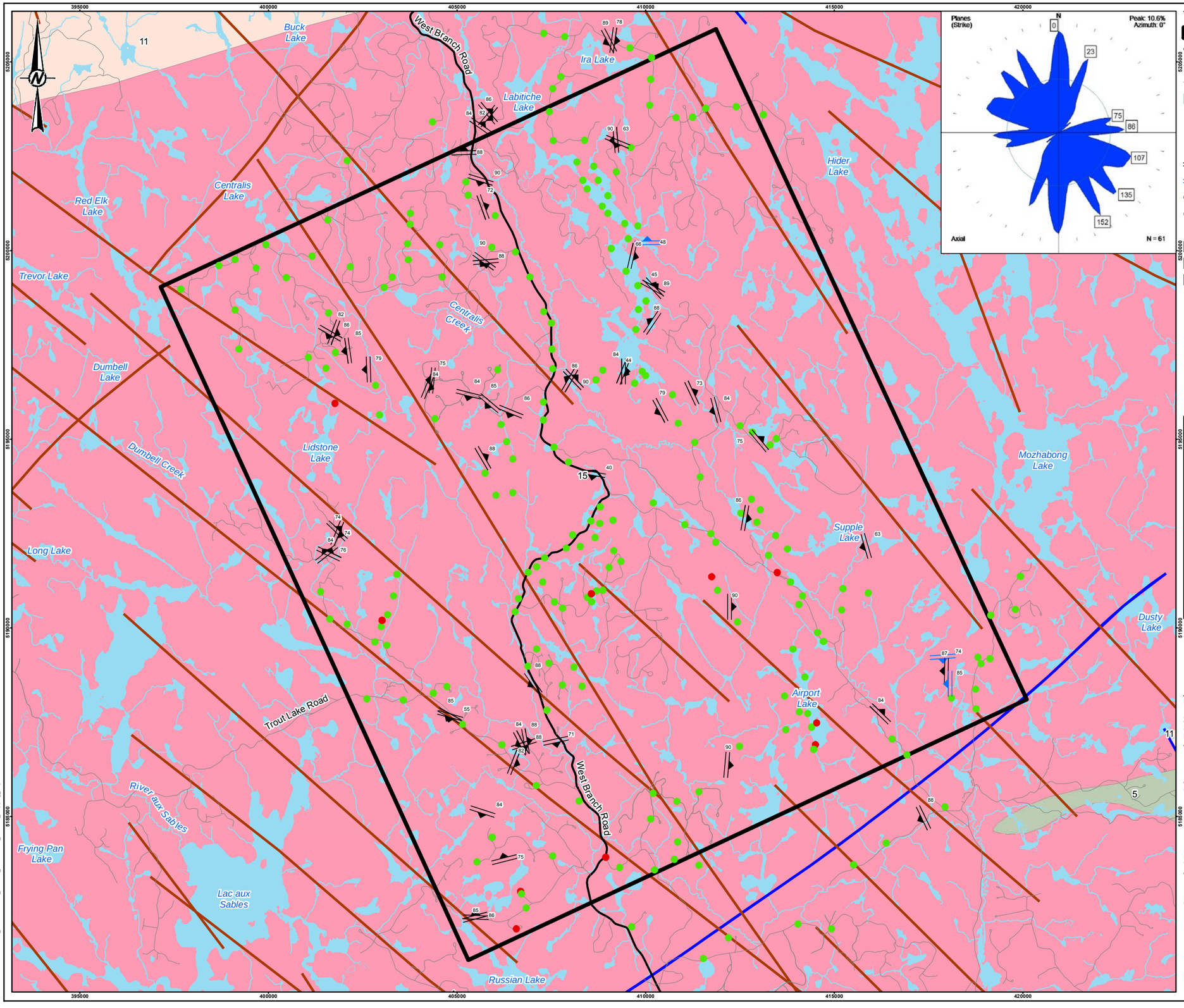

LEGEND

- Withdrawal Area
- Main Road
- Local Road
- Watercourse
- Waterbody
- Outcrop (208)
- Overburden (10)

Vein

- Extension (58)
- Shear Vein (3)
- Geologic Fault
- OGS Mapped Dyke

Bedrock Geology

- 15 Massive granodiorite to granite
- 11 Gneissic tonalite suite
- 5 Mafic to intermediate metavolcanic rocks

INDEX MAP

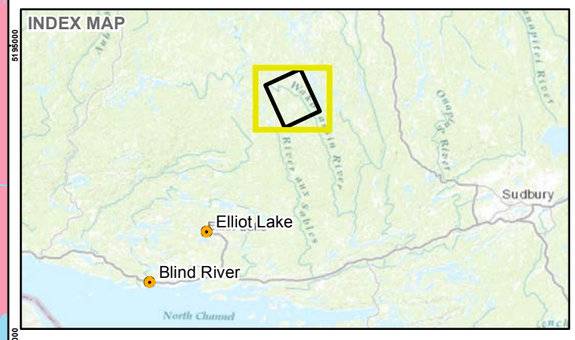

0 4 8

1:100,000 KILOMETRES

REFERENCE(S)

1. LIO (2017).
2. BEDROCK GEOLOGY, MRD126 REV-1, OGS (2011).
3. PRODUCED BY GOLDER ASSOCIATES LTD UNDER LICENCE FROM ONTARIO MINISTRY OF NATURAL RESOURCES AND FORESTRY, © QUEENS PRINTER 2017
4. PROJECTION: TRANSVERSE MERCATOR DATUM: NAD 83 COORDINATE SYSTEM: UTM ZONE 17

CLIENT
NWMO
BLIND RIVER, ELLIOT LAKE AND AREA, ONTARIO

PROJECT
BLIND RIVER, ELLIOT LAKE AND AREA GEOLOGICAL MAPPING REPORT

TITLE
WITHDRAWAL AREA - VEINS

CONSULTANT
Golder Associates

YYYY-MM-DD	2017-11-23
DESIGNED	JB
PREPARED	JB
REVIEWED	CM
APPROVED	GWS

PROJECT NO. 1651985 | CONTROL | REV. | FIGURE **5.1.18**

S:\Clients\NWMO\Ontario\99_PRO\1651985_NOH40_PRO\0003_Detailed_Mapping_Report\1651985-0003-HS-0011.mxd

IF THIS MEASUREMENT DOES NOT MATCH WHAT IS SHOWN, THE SHEET SIZE HAS BEEN MODIFIED FROM:

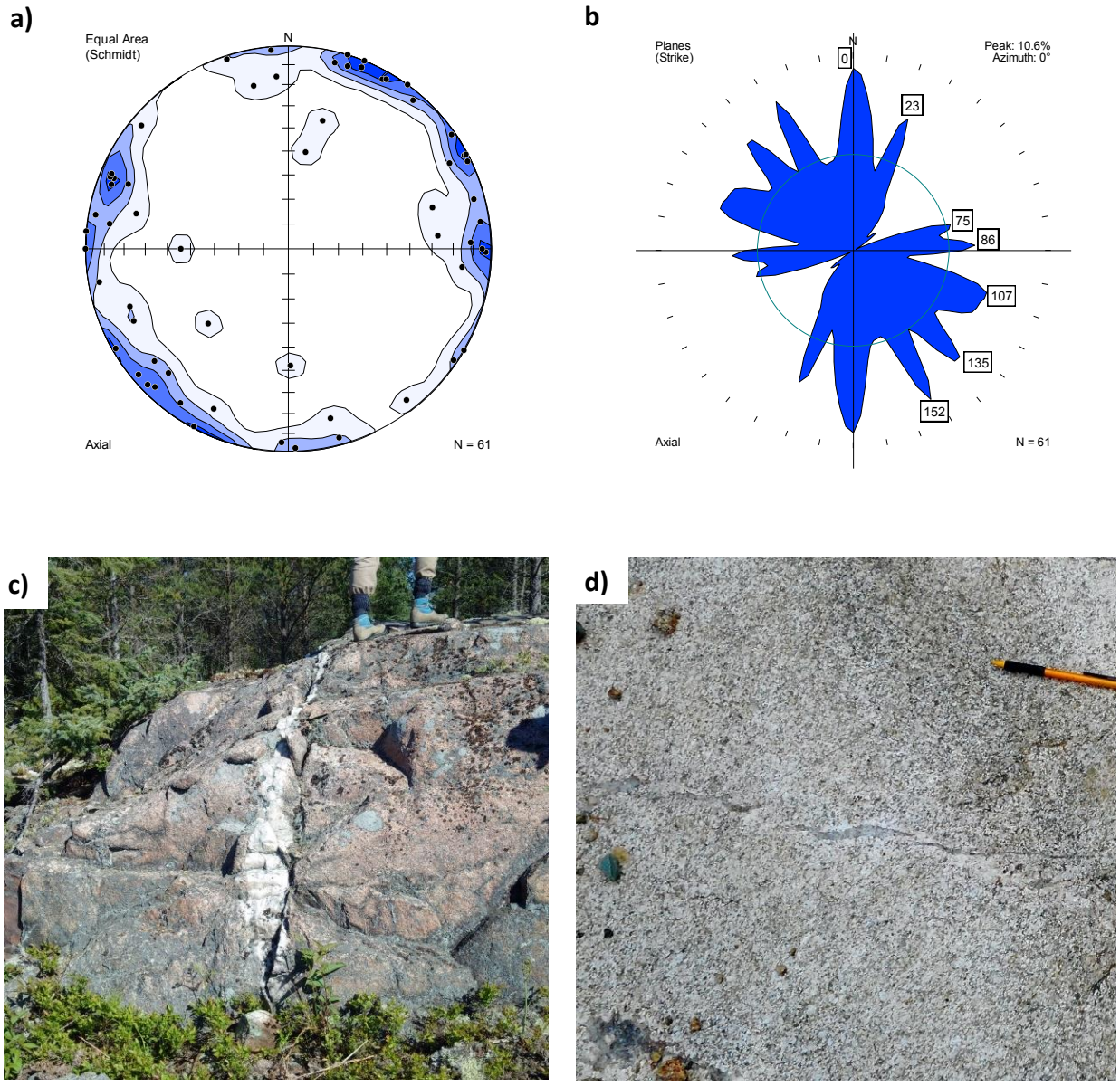

Figure 5.1.19: Vein Orientation Data and Field Examples

a - All vein displayed as equal area lower hemisphere stereonet plot of poles to veins (N=61). Contours show multiples of the standard deviation S above the expectant count E calculated using Gaussian K-100.

b - All vein data displayed as rose diagram of trends of veins (N=61). Bins for rose diagrams are 10°.

c - Photo of a tens of centimetres wide extensional quartz vein. View to the northwest, person for scale (Station 17TC0009).

d - Photo of a series of several millimetres wide en echelon, shear-related, quartz veins. View to the southeast, pencil for scale (Station 17IL0115).

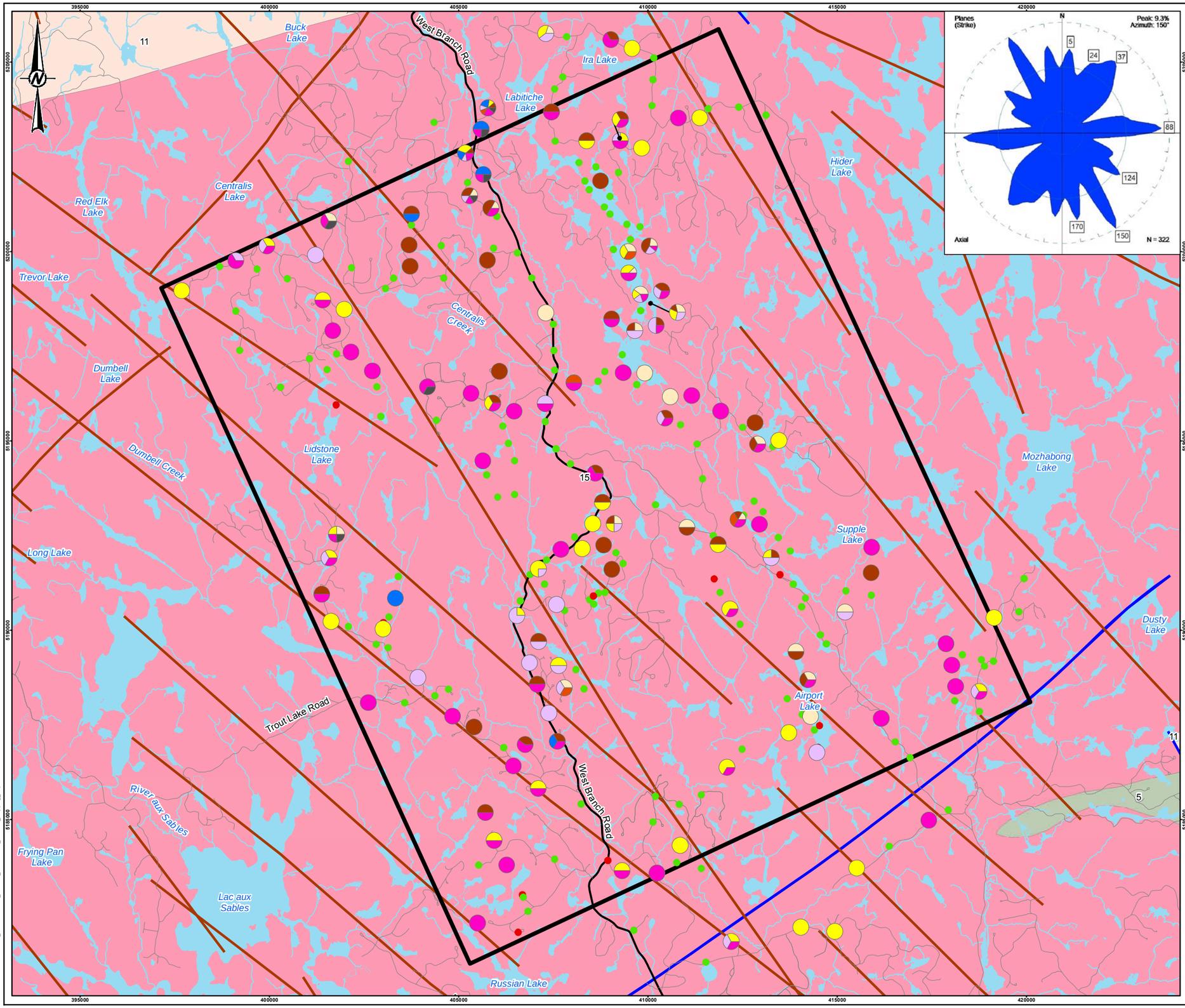

LEGEND

- Withdrawal Area
- Main Road
- Local Road
- Watercourse
- Waterbody
- Outcrop (140)
- Overburden (10)
- Geologic Fault
- OGS Mapped Dyke

Secondary Minerals and Alteration

- Cataclasite (32)
- Chlorite (56)
- Epidote (62)
- Feldspar (Plagioclase + K-feldspar) (12)
- Hematite (45)
- Magnetite (7)
- Quartz (91)
- Other (15)

Bedrock Geology

- 15 Massive granodiorite to granite
- 11 Gneissic tonalite suite
- 5 Mafic to intermediate metavolcanic rocks

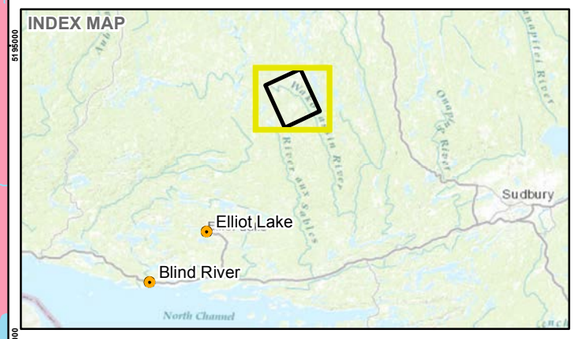

0 4 8

1:100,000 KILOMETRES

REFERENCE(S)

1. LIO (2017).
2. BEDROCK GEOLOGY, MRD126 REV-1, OGS (2011).
3. PRODUCED BY GOLDER ASSOCIATES LTD UNDER LICENCE FROM ONTARIO MINISTRY OF NATURAL RESOURCES AND FORESTRY, © QUEENS PRINTER 2017.
4. PROJECTION: TRANSVERSE MERCATOR DATUM: NAD 83 COORDINATE SYSTEM: UTM ZONE 17

CLIENT
NWMO
BLIND RIVER, ELLIOT LAKE AND AREA, ONTARIO

PROJECT
BLIND RIVER, ELLIOT LAKE AND AREA GEOLOGICAL MAPPING REPORT

TITLE
WITHDRAWAL AREA - SECONDARY MINERAL INFILL AND ALTERATION

CONSULTANT
Golder Associates

YYYY-MM-DD	2017-11-23
DESIGNED	JB
PREPARED	JB
REVIEWED	CM
APPROVED	GWS

PROJECT NO. 1651985 CONTROL REV. FIGURE **5.1.20**

IF THIS MEASUREMENT DOES NOT MATCH WHAT IS SHOWN, THE SHEET SIZE HAS BEEN MODIFIED FROM: 25mm

S:\Clients\NWMO\Ontario\99_PRO\1651985_NOH40_PRO\0003_Detailed_Mapping_Report\1651985-0003-HS-0012.mxd

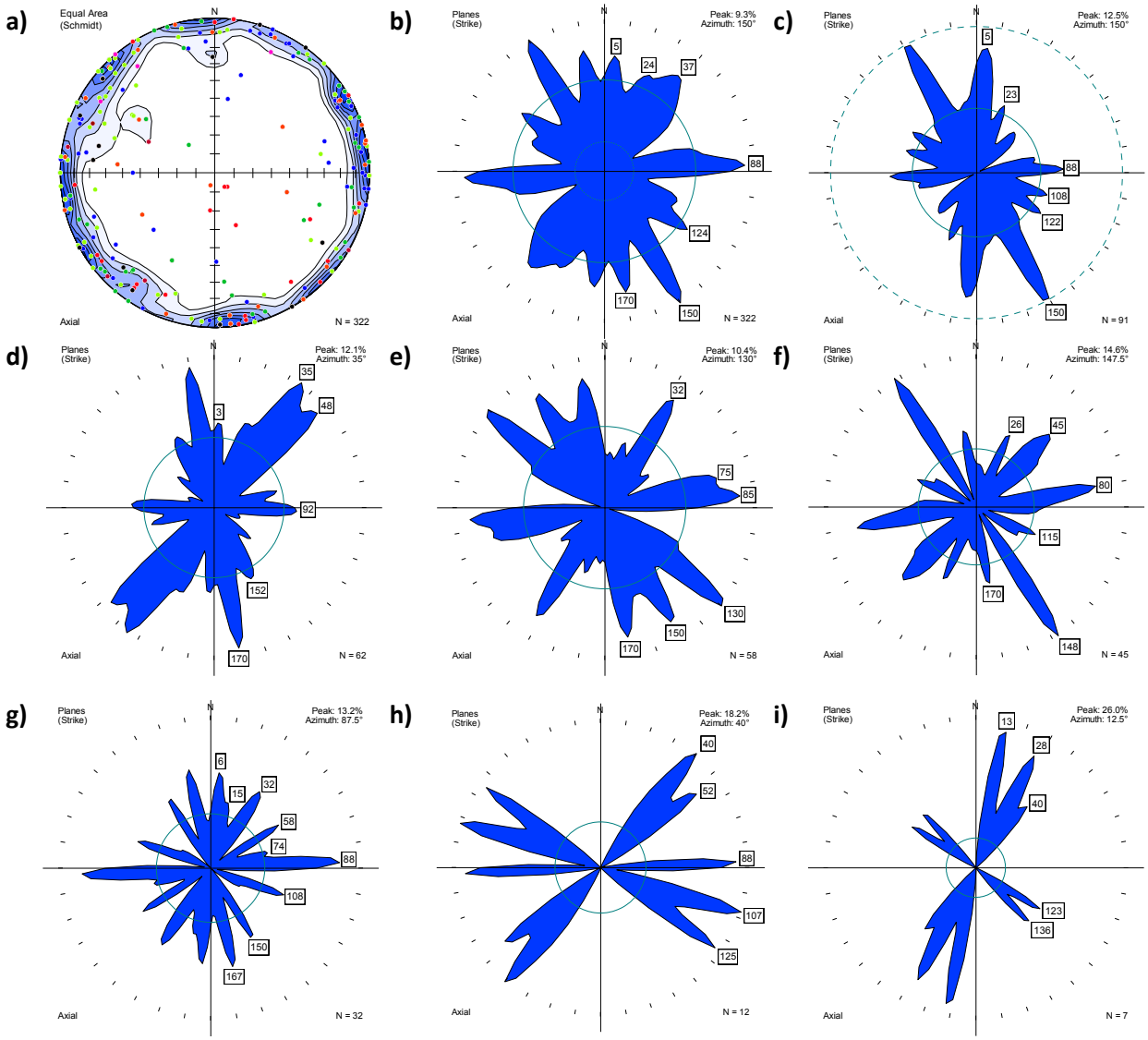

Figure 5.1.21: Secondary Minerals and Alteration Orientation Data

a - All mineral infill data displayed as equal area lower hemisphere stereonet plot of poles to joints, faults, or veins (N=322). Quartz infill: blue (N=91). Epidote infill: light green (N=62). Chlorite infill: dark green (N=58). Hematite infill: red (N=45). Cataclasite infill: orange (N=32). Feldspar infill: pink (N=12). Magnetite infill: dark red (N=7). Other infill (biotite, carbonate, pseudotachylite, pyrite, gouge, breccia, unknown): black (N=15). Contours show multiples of the standard deviation S above the expectant count E calculated using Gaussian K-100.

b - All mineral infill data displayed as rose diagram of trends of joints, faults, or veins (N=321). Bins for rose diagrams are 10°.

c - Quartz infill data displayed as rose diagram of trends of joints, faults, or veins (N=91). Bins for rose diagrams are 10°.

d - Epidote infill data displayed as rose diagram of trends of joints, faults, or veins (N=62). Bins for rose diagrams are 10°.

e - Chlorite infill data displayed as rose diagram of trends of joints, faults, or veins (N=58). Bins for rose diagrams are 10°.
f - Hematite infill data displayed as rose diagram of trends of joints, faults, or veins (N=45). Bins for rose diagrams are 10°.
g - Cataclasite infill data displayed as rose diagram of trends of joints, faults, or veins (N=32). Bins for rose diagrams are 10°.
h - Feldspar infill data displayed as rose diagram of trends of joints, faults, or veins (N=12). Bins for rose diagrams are 10°.
e - Chlorite infill data displayed as rose diagram of trends of joints, faults, or veins (N=58). Bins for rose diagrams are 10°.
f - Hematite infill data displayed as rose diagram of trends of joints, faults, or veins (N=45). Bins for rose diagrams are 10°.
g - Cataclasite infill data displayed as rose diagram of trends of joints, faults, or veins (N=32). Bins for rose diagrams are 10°.
h - Feldspar infill data displayed as rose diagram of trends of joints, faults, or veins (N=12). Bins for rose diagrams are 10°.
i - Magnetite infill data displayed as rose diagram of trends of joints, faults, or veins (N=7). Bins for rose diagrams are 10°.

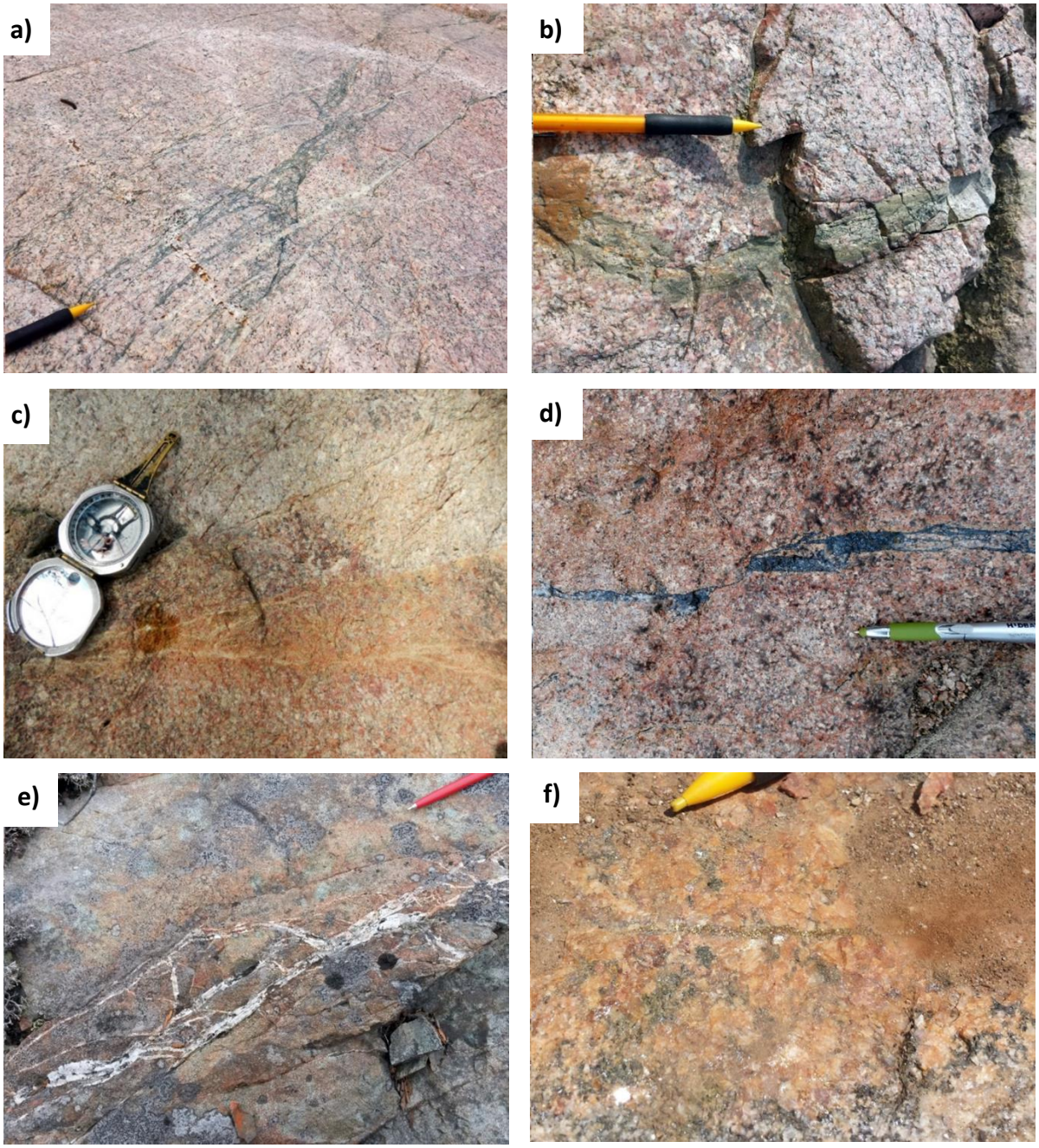

Figure 5.1.22: Field Examples of Secondary Minerals and Alteration

a - Chlorite infill on brittle faults overprinted by quartz veins. View to the southwest, pencil for scale (Station 17IL0019).

b - Epidote-filled shear zone. View to the southwest, pencil for scale (Station 17IL0019).

c - Hematite alteration forms a several cm-scale wide halo surrounding a shear zone. View to the northwest, compass for scale (Station17TC0140).

d - Magnetite infill in veins. View to the north, pencil or scale (Station 17IL0125).

e - Calcite veins forming a network in a mafic dyke. View to the south, pen for scale (Station 17IL0098).

f - Thin pyrite vein in granite. View to the southeast, pencil for scale (Station 17IL0039).

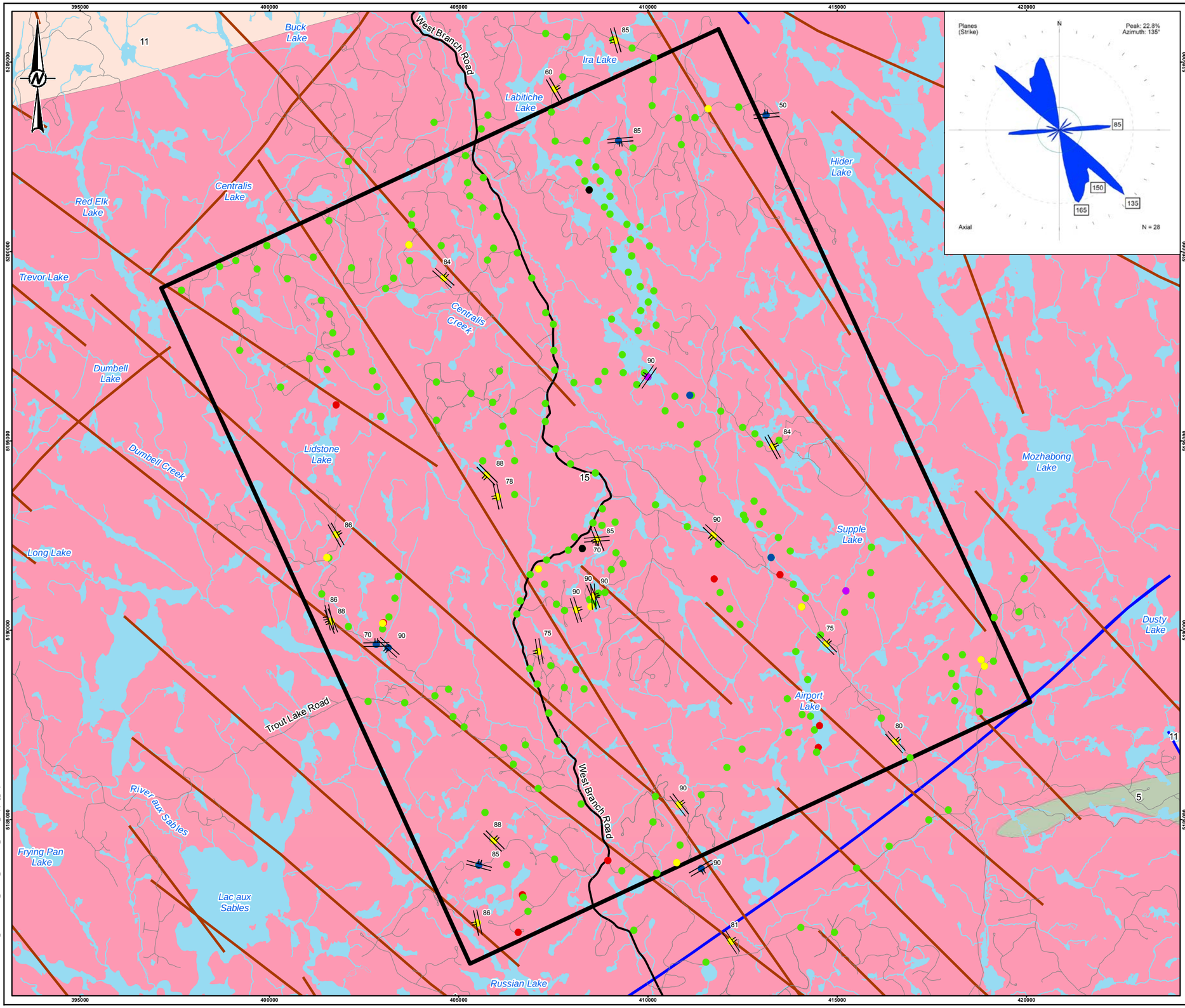

LEGEND

- Withdrawal Area
- Main Road
- Local Road
- Watercourse
- Waterbody
- Outcrop (225)
- Overburden (10)
- Breccia Dykes (2)
- Mafic Dyke - Structural (28)

Mafic Dyke Lithology

- Matachewan (29)
- Sudbury (2)
- Other (2)
- Geologic Fault
- OGS Mapped Dyke

Bedrock Geology

- 15 Massive granodiorite to granite
- 11 Gneissic tonalite suite
- 5 Mafic to intermediate metavolcanic rocks

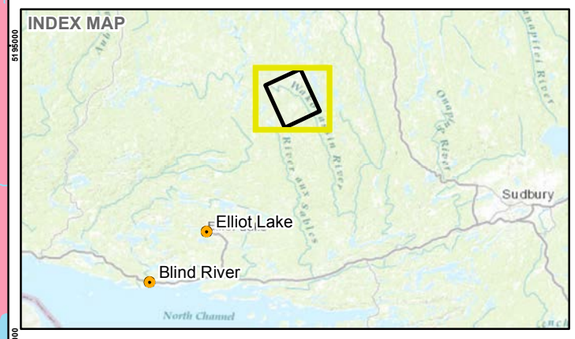

0 4 8

1:100,000 KILOMETRES

REFERENCE(S)

1. LIO (2017).
2. BEDROCK GEOLOGY, MRD126 REV-1, OGS (2011).
3. PRODUCED BY GOLDER ASSOCIATES LTD UNDER LICENCE FROM ONTARIO MINISTRY OF NATURAL RESOURCES AND FORESTRY, © QUEENS PRINTER 2017
4. PROJECTION: TRANSVERSE MERCATOR DATUM: NAD 83 COORDINATE SYSTEM: UTM ZONE 17

CLIENT
NWMO
BLIND RIVER, ELLIOT LAKE AND AREA, ONTARIO

PROJECT
BLIND RIVER, ELLIOT LAKE AND AREA GEOLOGICAL MAPPING REPORT

TITLE
WITHDRAWAL AREA - MAFIC DYKES

CONSULTANT
Golder Associates

YYYY-MM-DD	2017-11-23
DESIGNED	JB
PREPARED	JB
REVIEWED	CM
APPROVED	GWS

PROJECT NO. 1651985 CONTROL REV. FIGURE **5.2.1.1**

IF THIS MEASUREMENT DOES NOT MATCH WHAT IS SHOWN, THE SHEET SIZE HAS BEEN MODIFIED FROM: 25mm

S:\Clients\NWMO\Ontario\99_PRO\1651985_NOH40_PRO\0003_Detailed_Mapping_Report\1651985-0003-HS-0005.mxd

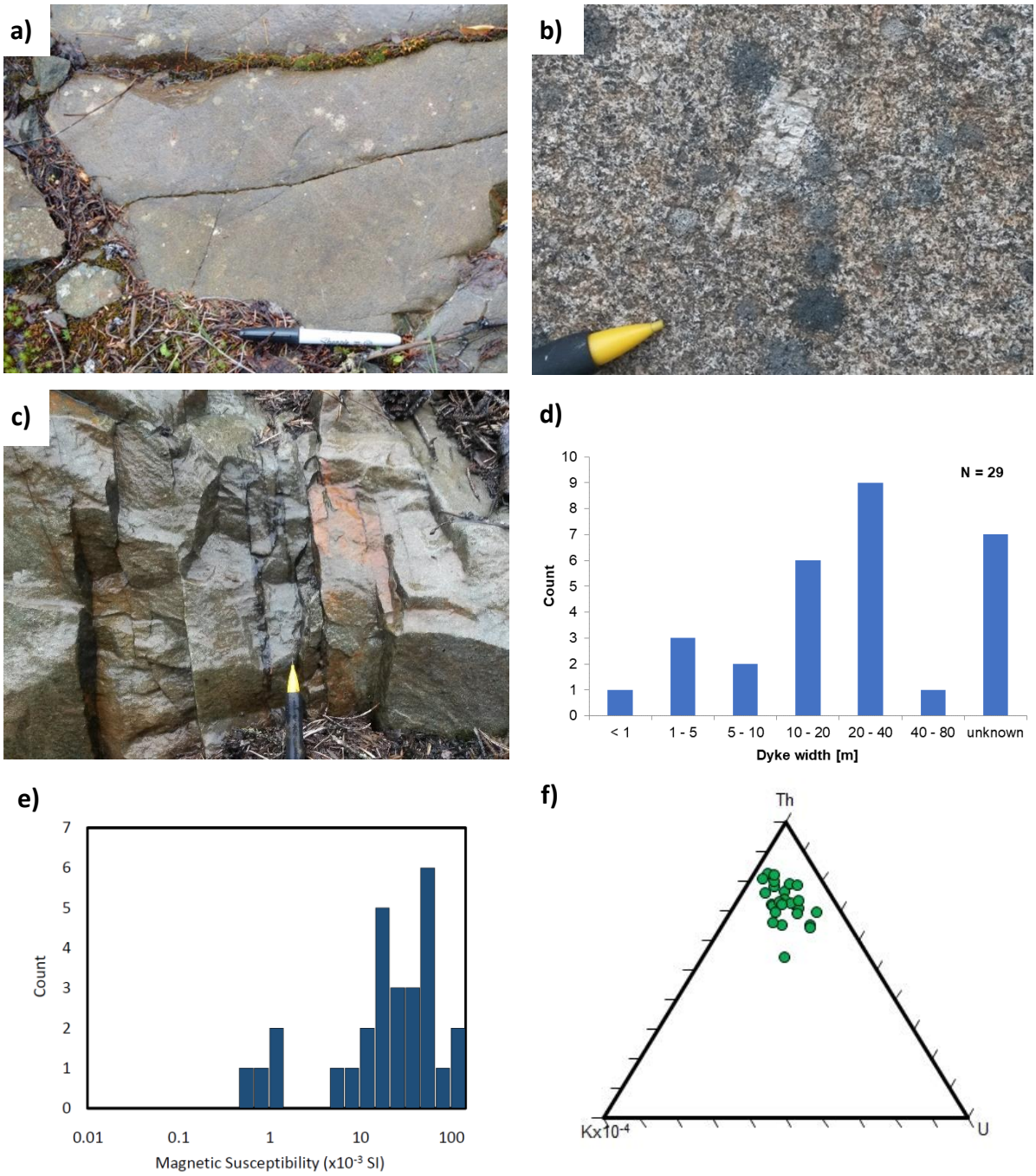

Figure 5.2.1.2: Matachewan Dykes – General Properties

a - Outcrop photo of a diabase dyke of the Matachewan dyke swarm. View to the northwest, pen for scale (Station 17TC0066).

b - Photo of a very coarse plagioclase phenocryst in a medium grained matrix, typical of dykes of the Matachewan swarm. View to the northeast, pencil for scale (Station 17IL0097).

c - Centimeter-scale joint spacing within a Matachewan dyke. View to the east, pencil for scale (Station 17IL0074).
d - Histogram showing frequency distribution of Matachewan dyke width (N=29).
e - Logarithmic plot of magnetic susceptibility for Matachewan mafic dykes (N= 28).
f - Ternary plot of gamma ray spectrometer data for Matachewan mafic dykes (N=27).

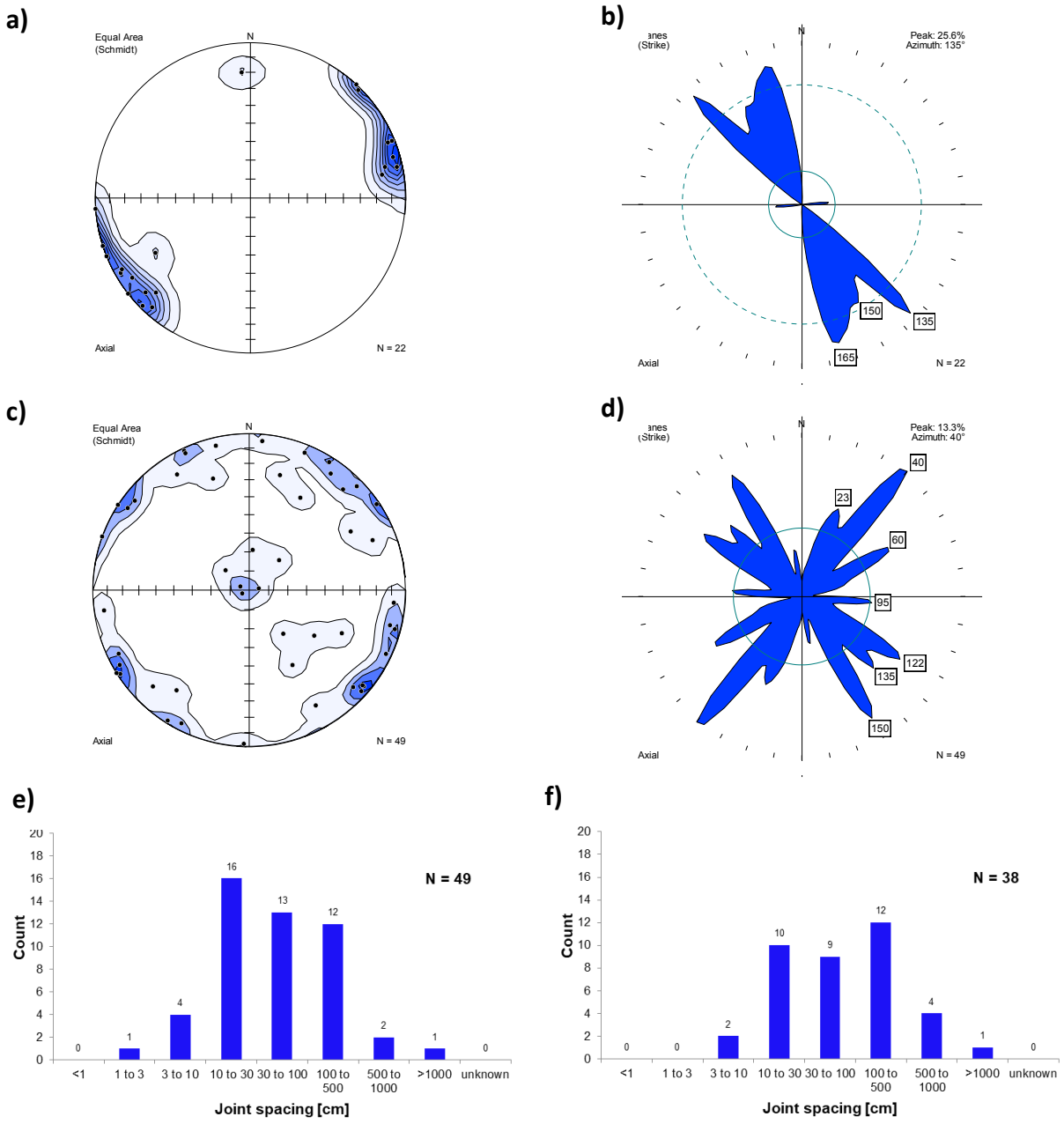

Figure 5.2.1.3: Matachewan Dykes – Structures

a - All mapped Matachewan dyke contact orientations displayed as equal area lower hemisphere stereonet of poles to planes (N=22).

b - All mapped Matachewan dyke contact orientations displayed as rose diagram of trends of planes with orientation of all peaks greater than the expected value E (N=22).

c - All joints measured in Matachewan dykes displayed as equal area lower hemisphere stereonet plot of poles to planes (N=49).

d - All joints measured in Matachewan dykes displayed as rose diagram of trends of planes with orientation of all peaks greater than the expected value E (N=49).
e - Histogram showing frequency distribution of joint spacing in Matachewan dykes (N=49).
f - Histogram showing frequency distribution of joint spacing in host rocks adjacent to Matachewan dykes (N=38).

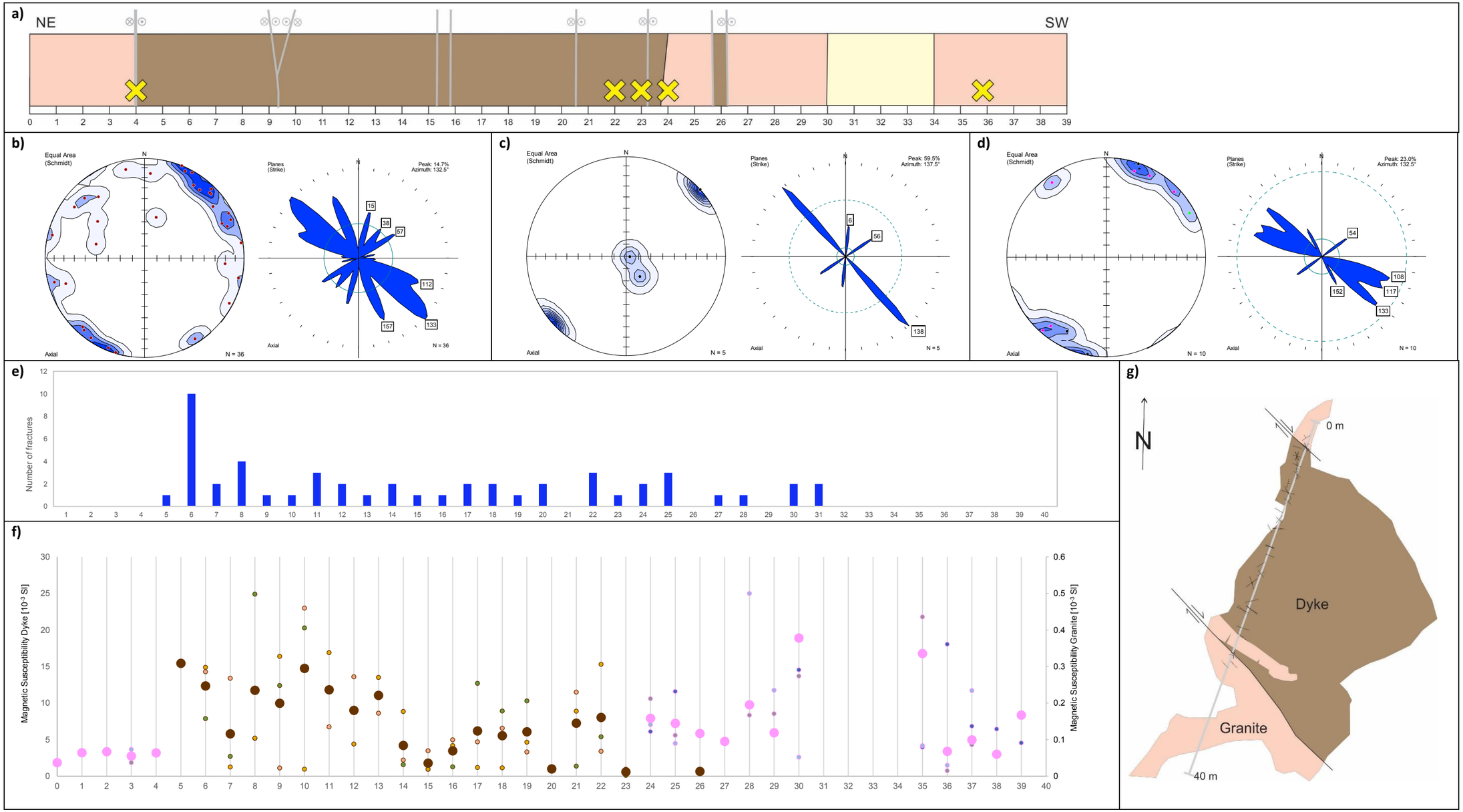
a)
NE
SW
b)
Equal Area (Schmidt)
Axial
N = 36
Planes (Strike)
Peak: 14.7%
Azimuth: 132.5°
c)
N = 5
Peak: 59.5%
Azimuth: 137.5°
d)
N = 10
Peak: 23.0%
Azimuth: 132.5°
e)
Number of fractures
f)
Magnetic Susceptibility Dyke [10⁻³ SI]
Magnetic Susceptibility Granite [10⁻³ SI]
g)
N
0 m
Dyke
Granite
40 m

Figure 5.2.1.4: Matachewan Dyke Scanline – Lithology, Joints, Fracture Frequency, and Magnetic Susceptibility

a - Simplified NE-SW profile of 40 m long scanline across a 20-m wide mafic dyke (shown in brown) within granite (pink) bedrock. One 4 m section of the profile is covered by vegetation and overburden (pale yellow). Both the southwestern and the northeastern contacts of the mafic dyke against the granite are exposed and oriented 108/89 and 311/87, respectively. Yellow crosses indicate photograph locations for Figure 5.4.4. Mapped fractures are indicated by grey lines. Strike-slip dextral faults are specified with x- and dot-filled circles indicating relative motion of bedrock on either side of fault away from reader and towards reader, respectively.
b - Joint data for the mafic dyke displayed as equal area lower hemisphere stereonet plot of poles to joints as well as rose diagrams (N=36). Contours show multiples of the standard deviation S above the expectant count E calculated using Gaussian K-100. Bins for rose diagrams are 10°.
c - Joint data for the granite bedrock displayed as equal area lower hemisphere stereonet plot of poles to joints as well as rose diagrams (N=5). Contours show multiples of the standard deviation S above the expectant count E calculated using Gaussian K-100. Bins for rose diagrams are 10°.
d - Fault data displayed as equal area lower hemisphere stereonet plot of poles to faults as well as rose diagrams for the granite bedrock (N=10). Dextral faults: pink circles (N=6). Sinistral faults: green circles (N=1). Faults with unknown slip: black circles (N=3). Contours show multiples of the standard deviation S above the expectant count E calculated using Gaussian K-100. Bins for rose diagrams are 10°.
e - Fracture frequency chart showing number of fractures per 1 m interval.
f - Magnetic Susceptibility measurements at 1 m intervals along the scanline profile. Large circles represent the average of three sets of five measurements, taken on the west side, east side, and center (small circle symbols) of the scanline profile. Pink circles denote measurements taken in the granite host rock while brown circles denote a measurement taken in the dyke. The left axis shows dyke magnetic susceptibility values in 10^{-3} SI, right axis shows granite magnetic susceptibility values in 10^{-3} SI.
g - Simplified sketch map of the outcrop exposure showing the contacts of the mafic dyke with the granite bedrock as well as all measured fractures along the scanline. The location of the scanline is shown by the grey line.

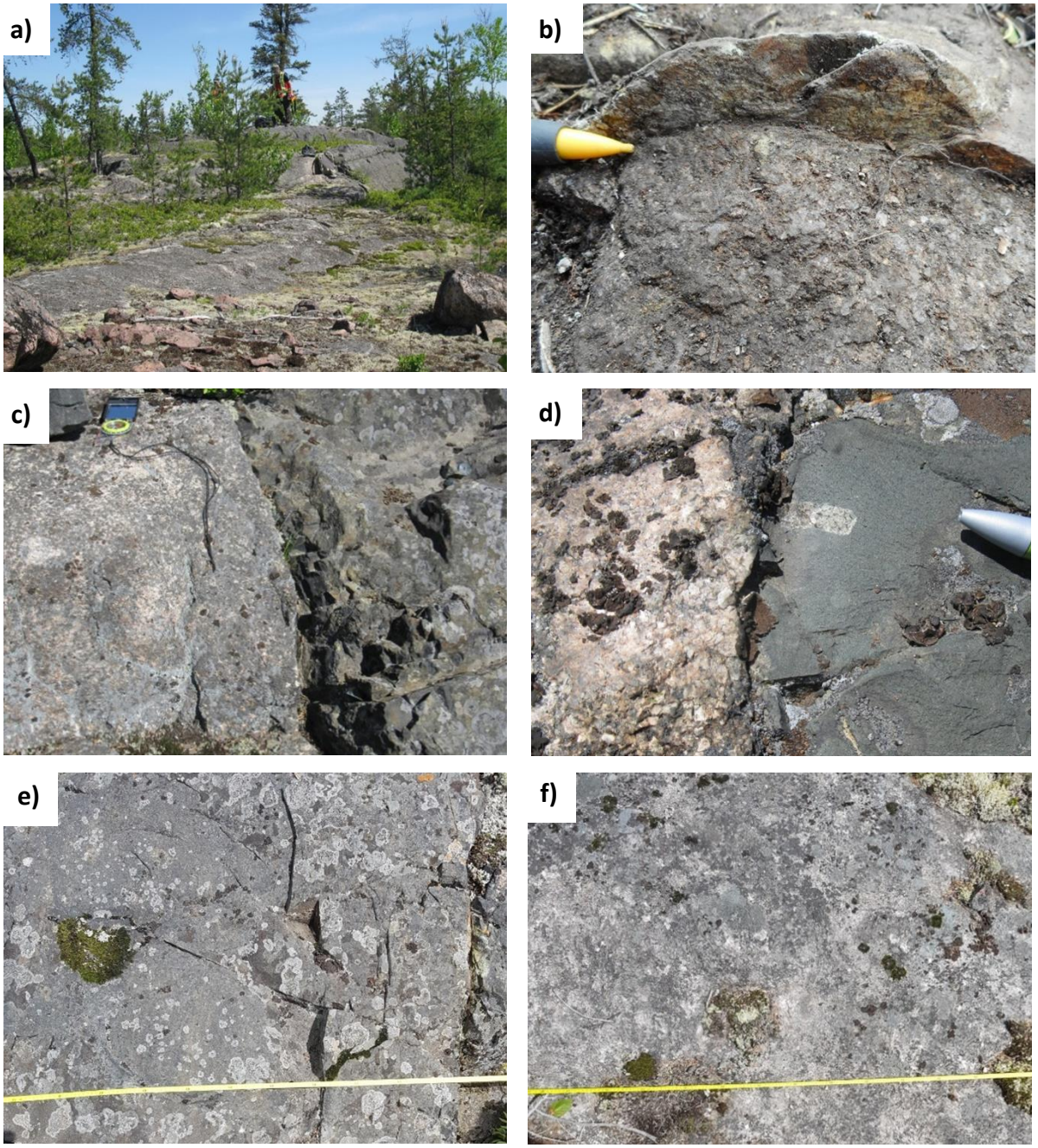

Figure 5.2.1.5: Matachewan Dyke Scanline – Field Examples

a - Scanline overview. View to the southwest, person for scale.

b - Northeastern dyke contact. Slickenlines plunging shallowly to the northwest. View to the southwest, pencil for scale. Location is at 4 m along scanline.

c - Southwestern dyke contact. View to the north, compass for scale. Location is 23 m along scanline.

d - Feldspar phenocryst near contact between mafic dyke and granite. Irregular dyke contact. View to the southeast, pen for scale. Location is 24 m along scanline.

e - Joints in dyke oriented parallel and orthogonal to contact with granite. View to the southeast, measuring tape for scale. Location is 22 m along scanline.
f - Absence of fractures in granite southwest of the dyke contact. View to the southeast, measuring tape for scale. Location is 36 m along scanline.

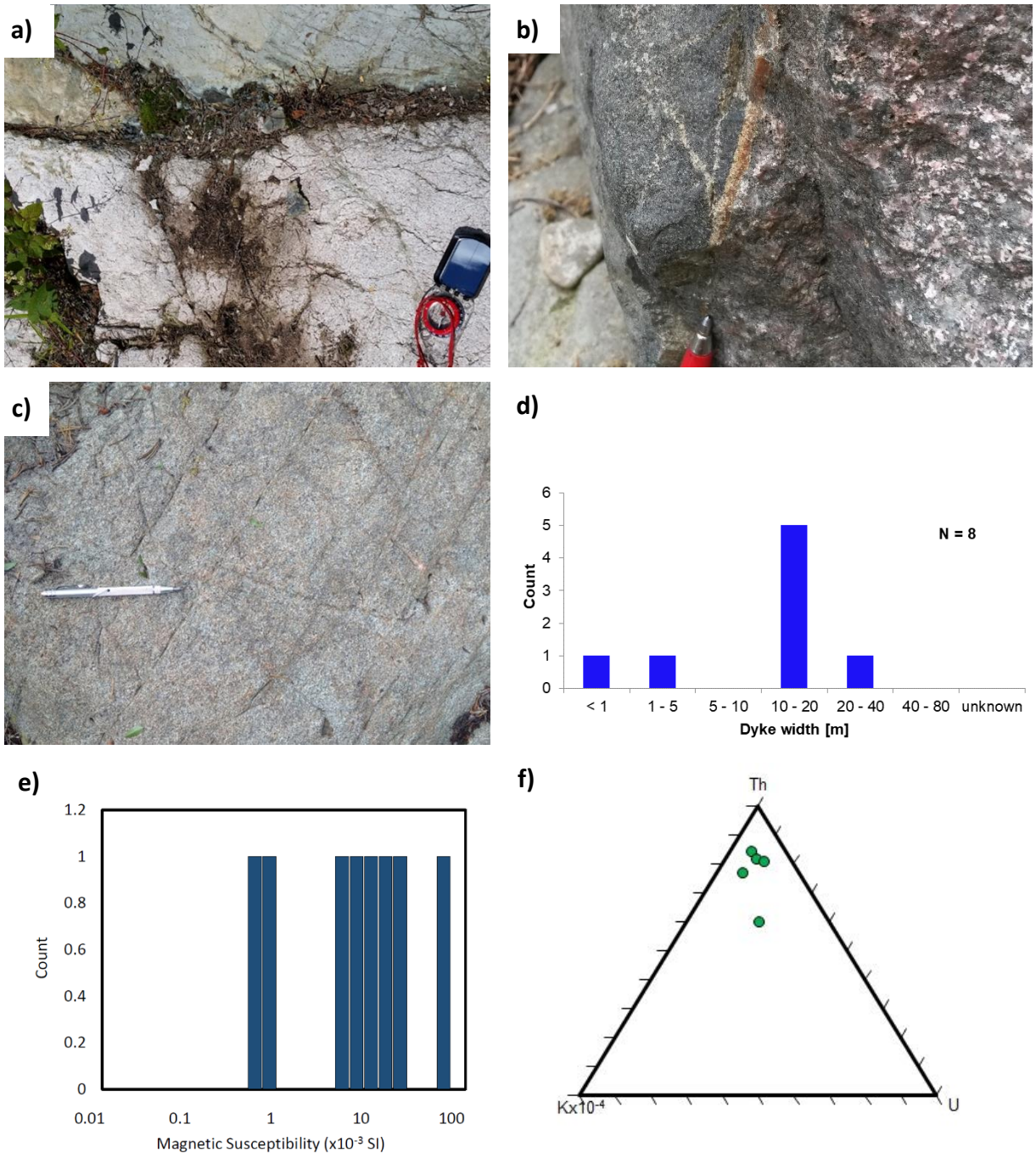

Figure 5.2.1.6: Sudbury Dykes – General Properties

a - Outcrop photo of a diabase All dyke of the Sudbury swarm in contact with the granite host rock. View to the north, compass for scale (Station 17TC0085).

b - Photo of a hematite vein at the contact between a Sudbury dyke and the granite host rock View to the west, pen for scale (Station 17IL0084).

c - Typical diabase texture and brownish weathering of a Sudbury dyke. View to the west, pen for scale (Station 17IL0140).
d - Histogram showing frequency distribution of Sudbury dyke width (N=8).
e - Logarithmic plot of magnetic susceptibility for Sudbury dykes (N= 8).
f - Ternary plot of gamma ray spectrometer data for Sudbury dykes (N=5).

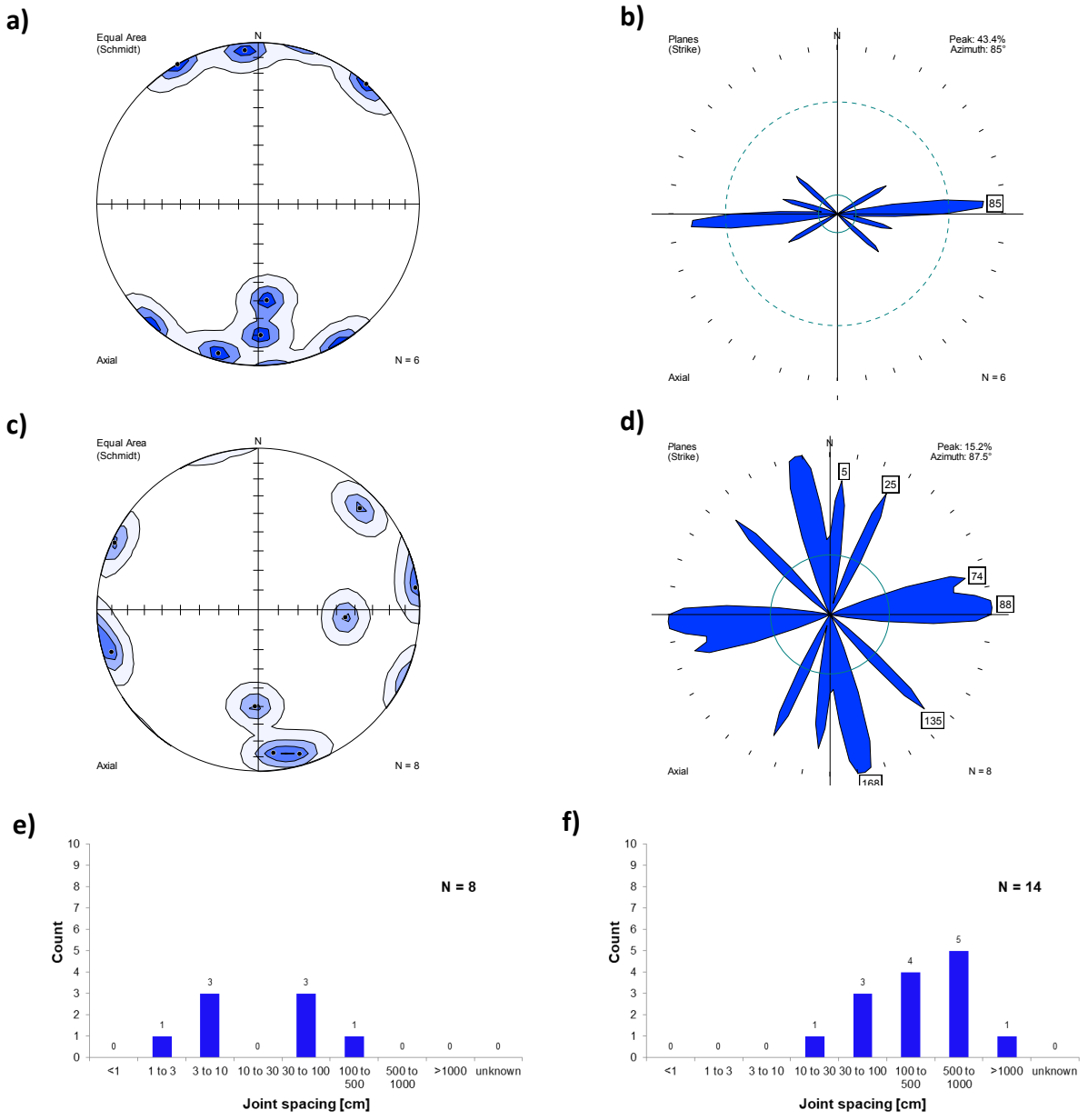

Figure 5.2.1.7: Sudbury Dykes – Structures

a – All mapped Sudbury dyke contact orientations displayed as equal area lower hemisphere stereonet plot of poles to contact planes (N=6).

b - All mapped Sudbury dyke contact orientations displayed as rose diagram of trends of planes with orientation of all peaks greater than the expected value E (N=6).

c - All joints measured in Sudbury dykes displayed as equal area lower hemisphere stereonet plot of poles to planes (N=8).

d - All joints measured in Sudbury dykes displayed as rose diagram of trends of planes with orientation of all peaks greater than the expected value E (N=8).

e - Histogram showing frequency distribution of joint spacing in Sudbury dykes (N=8).

f - Histogram showing frequency distribution of joint spacing in host rocks adjacent to Sudbury dykes (N=14).

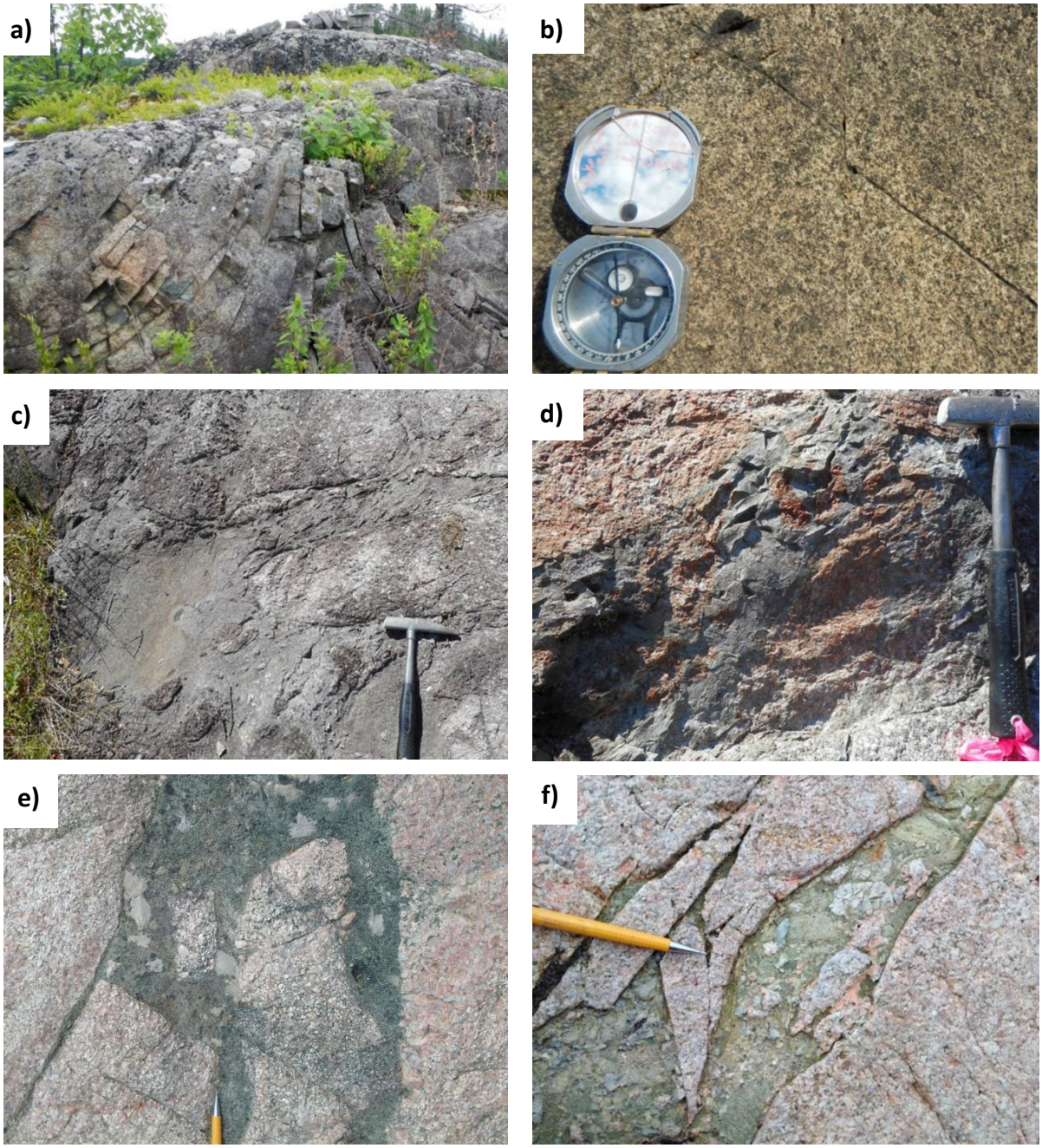

Figure 5.2.1.8: Other Mafic Dykes – Field Examples

a - Outcrop photo of a dyke (likely part of the Biscotasing swarm) showing folded joints forming two synforms. View to the north, compass for scale (Station 17TC0140).

b - Close up of a dyke, likely part of the Biscotasing swarm. View to the north, compass for scale (Station 17TC0140).

c - Outcrop photo of a brecciated dyke, likely part of the North Channel dyke swarm, with rounded granite host rock clasts in dyke matrix. View to the northwest, pen for scale (Station 17IL0150).

d - Close up photo of granite clasts in dyke (interpreted to be part of the North Channel dyke swarm) matrix. View to the northeast, hammer for scale (Station 17IL0150).
e - Close up photo of diatreme breccia showing irregular geometry and allochthonous clasts. View to the north, pen for scale (Station 17TC0115).
f - Close up photo of diatreme breccia showing variability in clast composition and fragmented granite host rock in an epidotized matrix. View to the northwest, pencil for scale (Station 17TC0067).

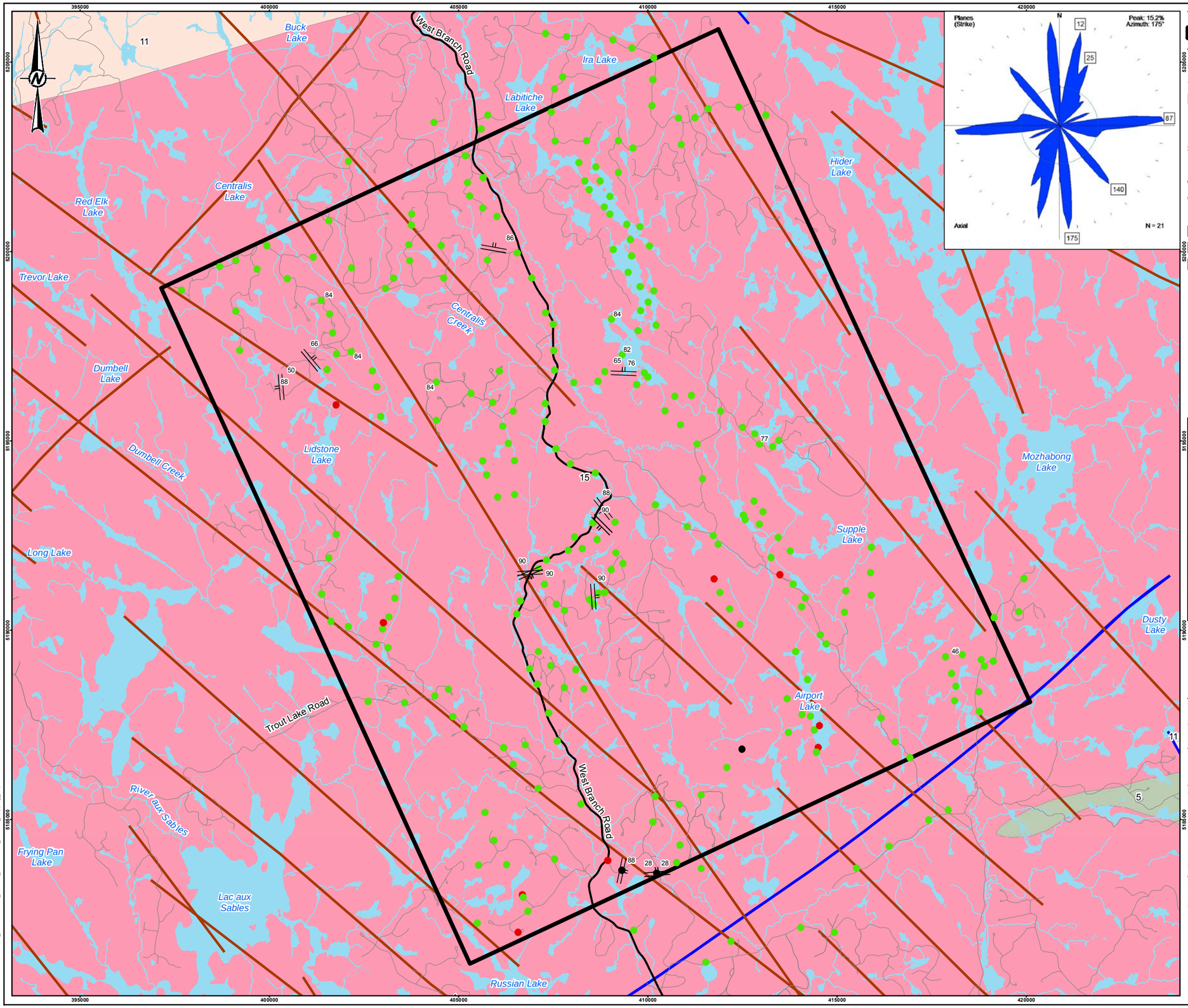

LEGEND

- Withdrawal Area
- Main Road
- Local Road
- Watercourse
- Waterbody
- Outcrop (251)
- Overburden (10)
- Felsic Dyke - Structural (21)
- Felsic Dyke - Lithology (3)
- Geologic Fault
- OGS Mapped Dyke

Bedrock Geology

- 15 Massive granodiorite to granite
- 11 Gneissic tonalite suite
- 5 Mafic to intermediate metavolcanic rocks

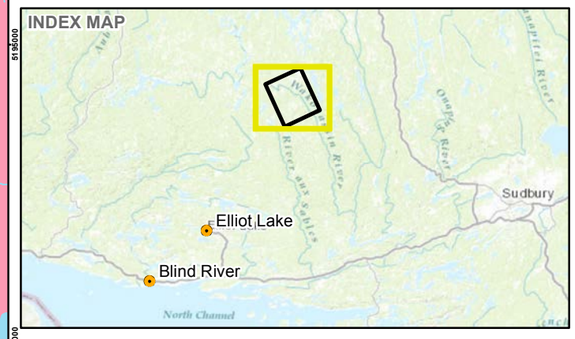

0 4 8

1:100,000 KILOMETRES

REFERENCE(S)

1. LIO (2017).
2. BEDROCK GEOLOGY, MRD126 REV-1, OGS (2011).
3. PRODUCED BY GOLDER ASSOCIATES LTD UNDER LICENCE FROM ONTARIO MINISTRY OF NATURAL RESOURCES AND FORESTRY, © QUEENS PRINTER 2017
4. PROJECTION: TRANSVERSE MERCATOR DATUM: NAD 83 COORDINATE SYSTEM: UTM ZONE 17

CLIENT
NWMO
BLIND RIVER, ELLIOT LAKE AND AREA, ONTARIO

PROJECT
BLIND RIVER, ELLIOT LAKE AND AREA GEOLOGICAL MAPPING REPORT

TITLE
WITHDRAWAL AREA - FELSIC DYKES

CONSULTANT
Golder Associates

YYYY-MM-DD	2017-11-23
DESIGNED	JB
PREPARED	JB
REVIEWED	CM
APPROVED	GWS

PROJECT NO. 1651985 CONTROL REV. FIGURE **5.2.2.1**

IF THIS MEASUREMENT DOES NOT MATCH WHAT IS SHOWN, THE SHEET SIZE HAS BEEN MODIFIED FROM: 25mm

S:\Clients\NWMO\Ontario\99_PRO\1651985_NOH40_PRO\0003_Detailed_Mapping_Report\1651985-0003-HS-0006.mxd

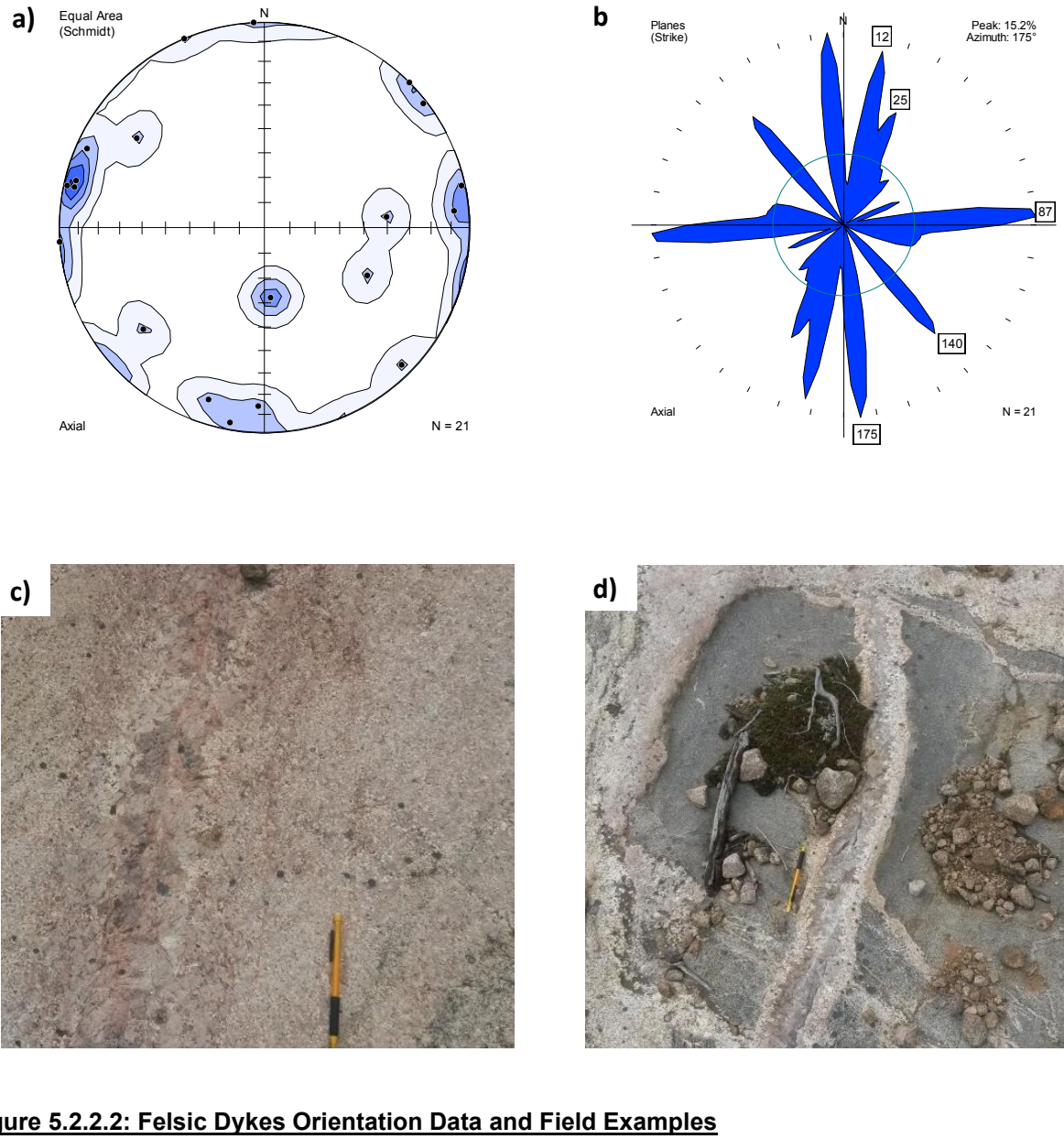

Figure 5.2.2.2: Felsic Dykes Orientation Data and Field Examples

a - All dyke contact data displayed as equal area lower hemisphere stereonet plot of poles to contact planes (N=21). Contours show multiples of the standard deviation S above the expectant count E calculated using Gaussian K-100.

b - All dyke contact data displayed as rose diagram of trends of dyke contacts (N=21). Bins for rose diagrams are 10°.

c - Outcrop-scale photo of a pegmatite dyke in granite. View to the south, pencil for scale (Station 17IL0078).

d - Photo of pegmatite dyke crosscutting amphibolite gneiss xenolith and along xenolith margin. View to the south, pencil for scale (Station 17IL0078)

APPENDIX A

Supporting Tables from the Work Plan

Table A.1: Source Data Descriptions

Source Data	Format/file name
NOH_Base_Map.gdb	NOH_Utility_Lines
	NOH_Domestic_Waste_Sites
	NOH_Waste_Water_Treatment_Plant
	NOH_Airport
	NOH_Transmission_Lines
	NOH_Wooded_Area
	NOH_Community
	NOH_Indian_Reserve
	NOH_Municipal_Lower_Tier
	NOH_Railway
	NOH_Roads
	NOH_US_States_Boundary
	NOH_Provincial_Boundary
NOH_Base_Map_docs.pdf	*Supporting documents for NOH_Base_Map gdb*
NOH_Bedrock_Geology.gdb	NOH_Cross_Section
	NOH_Detailed_Geology_Outlines
	NOH_Exclusion_Area_Finer_Analysis
	NOH_Fold_Synform_Inclined_Axial_Plane
	NOH_Faults
	NOH_Major_Batholiths_Dissolved_Outline
	NOH_Major_Fold_Anticline
	NOH_Major_Fold_Syncline
	NOH_Dyke
	NOH_Regional_Cross_Section_Southern_Province
	NOH_Additional_Mapped_Faults
	NOH_Bedrock_Geology
	NOH_Faults_Regional
	NOH_Geological_Provinces_Canada
	NOH_Iron_Formation
	NOH_Kapuskasing_Structures
	NOH_Limit_Exposed_Archean
	NOH_Dyke
	NOH_Superior_Province

Source Data	Format/file name
	NOH_Faults_M2670
NOH_Bedrock_Geology_docs.pdf	*Supporting documents for NOH_Bedrock_Geology.gdb*
NOH_Bedrock_Geology_lyr.zip	NOH_Bedrock_Geology.lyr
	NOH_Bedrock_Geology_Regional.lyr
NOH_Natural_Resource_Potential.gdb	NOH_Active_Mining_Claims
	NOH_Crown_Reserves
	NOH_Mineral_Occurrences
	NOH_Aggregate_Site
NOH_Natural_Resource_Potential_docs.pdf	*Supporting documents for NOH_Natural_Resource_Potential.gdb*
NOH_Protected_Area.gdb	NOH_Conservation_Reserves
	NOH_Crown_Land_NonFreehold_Dispositions
	NOH_Crown_Land_Unpatented
	NOH_Crown_Leased_Land
	NOH_Significant_Ecologial_Area
	NOH_Forest_Management_Unit
	NOH_CLUPA_Primary_Landuse
	Land_Ownership_Private_Land
	NOH_Municipal_Park
	NOH_Fish_Management_Zone
	NOH_Natural_Heritage_Value_Area
	NOH_Provincial_Park
	NOH_Provincial_Park_Additions
NOH_Protected_Areas_docs.pdf	*Supporting documents for NOH_Natural_Resource_Potential.gdb*
NOH_Quaternary_Geology.gdb	NOH_Quaternary_Features
	NOH_Dunes
	NOH_Overburden_Surficial_Geology
	NOH_Quaternary_Geology

Source Data	Format/file name
NOH_Quaternary_Geology_docs.pdf	*Supporting documents for NOH_Quaternary_Geology.gdb*
NOH_Quaternary_Geology_MRD160_Landform_metadata.pdf	*Supporting documents for NOH_Quaternary_Geology.gdb (MRD160_Landforms)*
NOH_Quaternary_Geology_lyr.zip	NOH_Overburden_Surficial_Geology.lyr
	NOH_Quaternary_Geology.lyr
NOH_Water.gdb	NOH_Waterbody
	NOH_Lake_Depth
	NOH_Watercourse
	NOH_Wetland
	NOH_Watershed_Interpreted
	NOH_Watershed_Quaternary
	NOH_Watershed_Outflow
	NOH_Watershed_Tertiary
	NOH_Surface_Water_Flow
NOH_Water_docs.pdf	*Supporting documents for NOH_Water.gdb*
NOH_Wells.gdb	NOH_East_Bull_Lake_Drillholes
	NOH_OGS_Drillholes
	NOH_Water_Wells
NOH_Wells_docs.pdf	*Supporting documents for NOH_Wells.gdb*
NOH_Topography.gdb	NOH_DEM_Hillshade_045_45
	NOH_DEM_Hillshade_315_45
	NOH_DEM_Elevation
	NOH_DEM_Slope
	NOH_DEM_Slope_density
	NOH_DEM_Relief_20km_departure
	NOH_DEM_Relief_2km_departure
	NOH_DEM_Relief_250m_range
NOH_Topography_docs.pdf	*Supporting documents for NOH_Topography.gdb*
NOH Geophysics Grids	NorthOfHuron_P2AirborneGeophysics_250m_DEM.grd

Source Data	Format/file name
	NorthOfHuron_P2AirborneGeophysics_250m_MAGRTP.grd
	NorthOfHuron_P2AirborneGeophysics_250m_1VDRTP.grd
	NorthOfHuron_P2AirborneGeophysics_25m_MAGRTP.grd
	NorthOfHuron_P2AirborneGeophysics_25m_DEM.grd
	NorthOfHuron_P2AirborneGeophysics_25m_1VDRTP.grd
NOH withdrawal areas	NorthOfHuron_WithdrawalAreas_r2.shp
NOH Predicted Outcrops	NorthOfHuron_OutcropInterpreted_r1.shp
FRI Imagery Tile Index (46 tiles)	NorthOfHuron_TileIndexFRI_r1_subset.shp

Table A.2: Equipment Requirements

Equipment	Calibration Required
Compass (Brunton Pocket Transit or similar)	Y – Check magnetic declination setting daily
Handheld GPS	Y – Check against fixed calibration location
iPad field data collector w/GPS	Y – Check against hand held GPS
iPad with ArcPad software	Y – Daily check of uploaded data against hard copy maps
Magnetic Susceptibility Meter (KT-20)	Y – Calibrated by supplier before rental and upon return from rental period / daily check of reading at a reference rock outcrop. Certificate of Calibration to be provided by supplier and provided to NWMO.
Gamma Spectrometer (RS-125 or equivalent)	Y – Calibrated by supplier before rental and upon return from rental period. Certificate of Calibration to be provided by supplier and provided to NWMO.
Notebook and Pen	N
Digital Camera	N
Geological Hammer	N
Sample Bags	N
Personal Protective Equipment	N

Table A.3: Task Allocation

Task	Responsibility
Daily safety briefing	Project Field Manager
Daily equipment calibration with entries in notebook and digital database	Engineering Geologist, Structural Geologist
Host rock lithology characterization	Structural Geologist
Host rock structural characterization	Structural Geologist
Digital photographs	Structural Geologist
Fracture characterization	Engineering Geologist
Lineament observation/assessment	Structural Geologist
Data input into ArcPad	Structural Geologist/Engineering Geologist
Manual (pencil and paper) note transcription	Structural Geologist/Engineering Geologist
Magnetic susceptibility measurements	Engineering Geologist
Gamma measurements	Structural Geologist
Rock strength assessment - Hammer test	Engineering Geologist
Bedrock overburden assessment	Engineering Geologist
Sample collection (if necessary)	Structural Geologist
Surface constraint assessment	Engineering Geologist
Identification of potential detailed mapping areas	Structural Geologist
Daily log write-up and transmittal	Engineering Geologist
Daily data back-up (and back-up for the back-up)	Structural Geologist (GIS Analyst)
Planning the next day traverse	Structural Geologist (Team Lead)

Table A.4: Key Geological Attributes to be characterized during Detailed Outcrop Mapping

General Attributes	Characterization Method(s)
Station Location	Geo-locate exposed bedrock observation locations using GPS Take representative digital photograph of outcrop area
Bedrock exposure and overburden thickness	Visually inspect the distribution and thickness of overburden vs. exposed bedrock during the daily traverse (in comparison to existing understanding)
Surface Constraints	Visually identify and geo-locate any surface constraints that would create challenges for further geological characterization activities (e.g., bridge wash-outs, poorly or unmaintained logging roads, beaver dams, steep and deep (impassable) valleys, etc.) Visually identify access issues in areas without mapped roads or navigable waterways
Geological Attributes	**Characterization Method(s)**
Lithology	Visually inspect weathered and fresh rock surfaces for identification of major and minor lithological units and their constituent colour, primary minerals (e.g., granitic rocks have varying proportions of quartz, K-feldspar and plagioclase plus other minerals including micas, hornblende, etc.), grain size, texture, etc. Name the lithological unit(s) in terms of relative abundance at the outcrop scale Collect a representative sample(s) of the dominant lithological unit(s) at each outcrop (will require use of hammer and chisel only; fist-sized piece with both weathered and fresh surface) Take digital photographs of representative lithological unit(s) across the area of interest [documentation will include (at a minimum), file name, scale, GPS coordinates, direction of view and description of the photo.]
Primary and Ductile Structure	Observe and document the bedrock structural features (e.g., bedding, foliations, lineations, folds and shear zones) Take digital photographs/make field sketches of representative key structural features Measure and document (by hand with compass-clinometer and subsequent digital and manual entry) Strike and dip of planar structures Trend and plunge of linear structures Orientations of fold hinge lines and axial surfaces
Geophysical and Geomechanical Character	Record 5 magnetic susceptibility measurements for each identified lithological unit (will require use of magnetic susceptibility meter, e.g., KT10 or KT20) Undertake gamma ray readings for each identified lithological unit using a gamma ray spectrometer (RS-125 or equivalent) Undertake field rock strength test on representative lithologies at each station and in spatial relation to identified structural features (i.e. lineaments, fracture zones, dykes)

General Attributes	Characterization Method(s)
Fracture Characteristics	Visually inspect the rock surface for identification of systematic fracture sets Characterize fracture sets by type (joints, faults, veins, altered wallrock around fractures) Measure and document (by hand with compass-clinometer and subsequent digital and manual entry): ■ Strike and dip of planar structures ■ Trend and plunge of linear structures on fracture planes ■ Fracture mineral filling ■ Abutting, cross-cutting and intersection (relative age) relationships ■ between fracture sets ■ Displacement (strike separations and dip separations if visible) ■ Fracture surface ornamentation ■ Fracture set spacing Undertake block size analysis based on outcrop fracture geometry and spacing Take representative digital photograph(s) as needed to show key fracture characteristics, for example cross-cutting relationships, damage zone width, alteration, mineral infill
Dyke Characteristics	Visually inspect dyke for characteristic features (e.g., mineralogy, colour) Collect a representative sample of each dyke type Take representative digital photograph of dyke, including contact relationship with bedrock, if exposed Document: ■ Internal structure (fractures) ■ Width ■ Orientation (strike and dip along bedrock contact) ■ Nature of bedrock contact (e.g., welded, fractured, sheared, altered, extent of damage, etc.)
Geophysical and Geomechanical Character	Record 5 magnetic susceptibility measurements for each identified dyke Undertake gamma ray readings for each identified dyke Undertake field rock strength test on each dyke

Notes:
1. Samples will be stored in bags numbered in accordance with the sample number generated in the database.
2. Effort will be made to characterize fractures of all dip magnitudes (including horizontal to shallow dipping features)
3. Strike and dip measurements follow Canadian right-hand-rule notation.
4. All observations will be recorded in digital format with manual (pen and paper) backup for most pertinent field observations only, unless required due to digital device failure.

APPENDIX B

Remote Predictive Bedrock Analysis

November 2017
Report No. 1651985 (3000)

Golder Associates

Remote Predictive Bedrock Analysis

Potential outcrop locations were identified through an automated object based image analysis (OBIA), filtered, and prioritized for use in planning and implementing the Phase 2 Geological Mapping in the Elliot Lake and Blind River area of Ontario. This work involved 2 main tasks: 1) automated OBIA and 2) manual filtering of OBIA results to produce an output of potential outcrop locations.

Object Based Image Analysis using eCognition

Automated OBIA was conducted using Trimble's eCognition 9.1 software for the two withdrawal areas identified for geological mapping in the Elliot Lake and Blind River area. Forest Resource Inventory (FRI) orthoimagery of the Elliot Lake and Blind River area, from 2009, was the primary dataset used in the analysis. FRI imagery is 4-band (red, green, blue, near infra-red) multi-resolution, 40 cm airborne imagery collected and used for forest resource purposes by the Ministry of Natural Resources.

A ruleset was developed in eCognition which initially employed multi-resolution segmentation to develop small image objects of almost pixel size. Through a series of iterative steps, the ruleset was refined and the small image objects were merged into larger more identifiable objects of distinct classes. Areas of water were classified first, followed by those areas that are spatially and spectrally similar to exposed bedrock, such as unpaved road surfaces, sand covered areas and brightly reflecting bogs. The remaining image objects were considered to most likely represent exposed outcrop and output as a distinct data set. This raw eCognition output provided a framework for remotely interpreting the location of probable bedrock outcrops in the four potentially suitable areas.

Filtering of OBIA results

It is understood that similarities in spectral response of areas of ground cover versus areas of exposed bedrock in the Elliot Lake and Blind River area results in instances of false positive exposed bedrock classification when classifying by means of OBIA. In order to use the remotely predicted outcrop data set in a meaningful way for detailed outcrop mapping an additional step of manually comparing the raw output, against the FRI imagery, was required.

The process to undertake this filtering was straightforward and involved examining the FRI imagery in areas where the eCognition output showed clusters of pixels locating possible exposed bedrock. The cluster area was visually evaluated in the FRI imagery and a determination by consensus of two or more individual interpreters was made as to whether the location in question did or did not likely represent actual exposed bedrock. If it was determined likely, then the location was outlined and defined as a unique polygon. This analysis produced a set of shapefiles of polygons representing interpreted priority outcrop locations, for both withdrawal areas in the Elliot Lake and Blind River area (see Figure 1.2 from main body of this report). The planning for the Phase 2 Geological Mapping activity in the Elliot Lake and Blind River Area is based upon these interpreted priority outcrop locations.

As a global, employee-owned organisation with over 50 years of experience, Golder Associates is driven by our purpose to engineer earth's development while preserving earth's integrity. We deliver solutions that help our clients achieve their sustainable development goals by providing a wide range of independent consulting, design and construction services in our specialist areas of earth, environment and energy.

For more information, visit golder.com

Africa	+ 27 11 254 4800
Asia	+ 86 21 6258 5522
Australasia	+ 61 3 8862 3500
Europe	+ 44 1628 851851
North America	+ 1 800 275 3281
South America	+ 56 2 2616 2000

solutions@golder.com
www.golder.com

Golder Associates Ltd.
6925 Century Avenue, Suite #100
Mississauga, Ontario, L5N 7K2
Canada
T: +1 (905) 567 4444

Golder Associates